

**Landslide hazard assessment
Hydro-meteorological thresholds in Rwanda**

Uwihirwe, J.

DOI

[10.4233/uuid:f5c3f45b-6862-4f8c-900a-fa4de4ce731e](https://doi.org/10.4233/uuid:f5c3f45b-6862-4f8c-900a-fa4de4ce731e)

Publication date

2023

Document Version

Final published version

Citation (APA)

Uwihirwe, J. (2023). *Landslide hazard assessment: Hydro-meteorological thresholds in Rwanda*. [Dissertation (TU Delft), Delft University of Technology]. <https://doi.org/10.4233/uuid:f5c3f45b-6862-4f8c-900a-fa4de4ce731e>

Important note

To cite this publication, please use the final published version (if applicable).
Please check the document version above.

Copyright

Other than for strictly personal use, it is not permitted to download, forward or distribute the text or part of it, without the consent of the author(s) and/or copyright holder(s), unless the work is under an open content license such as Creative Commons.

Takedown policy

Please contact us and provide details if you believe this document breaches copyrights.
We will remove access to the work immediately and investigate your claim.

**LANDSLIDE HAZARD ASSESSMENT: LANDSLIDE
HYDRO-METEOROLOGICAL THRESHOLDS IN
RWANDA**

LANDSLIDE HAZARD ASSESSMENT: LANDSLIDE HYDRO-METEOROLOGICAL THRESHOLDS IN RWANDA

Dissertation

for the purpose of obtaining the degree of doctor
at Delft University of Technology
by the authority of the Rector Magnificus, Prof.dr.ir. T.H.J.J. van der Hagen,
chair of the Board for Doctorates
to be defended publicly on Monday 23 January 2023 at 12:30 hours

by

Judith UWHIRWE

Master of Science in Physical Land Resources/Land Resources Engineering
Vrije Universiteit Brussel and Universiteit Gent, Belgium
Born in Muhanga, Rwanda

This dissertation has been approved by the promotor.

Composition of the doctoral committee:

Rector Magnificus
Dr. T. A. Bogaard
Dr. M. Hrachowitz

Chairperson
Delft University of Technology, promotor
Delft University of Technology, promotor

Independent members:

Dr. O. Dewitte
Prof. dr. G. Nyagatare
Dr. D.B. Kirschbaum
Prof.dr. C.J. van Westen
Prof.dr.ir. R. Uijlenhoet

Africa Museum, Belgium
University of Rwanda, Rwanda
NASA, USA
University of Twente, Netherlands
Delft University of Technology, Netherlands

Reserve member:

Prof.dr.ir. M. Bakker

Delft University of Technology, Netherlands



Keywords: Landslide, Hydro-geology, Hydro-Meteorology, Groundwater, Soil Moisture

Copyright © 2023 by J. Uwihirwe

ISBN: 978-94-6366-644-2

Printed by: Proefschrift-aio.nl

The photo on the cover page shows the landslide events in Karongi District, western Province. It was taken in September 2018.

An electronic version of this dissertation is available at
<http://repository.tudelft.nl/>

To my family

CONTENTS

Summary	xi
Samenvatting	xv
1 Introduction	1
1.1 Landslide hazard problems and opportunities for solutions	2
1.2 Research concepts and statistical approaches.	4
1.2.1 Landslide trigger-based thresholds	4
1.2.2 Landslide cause-trigger-based thresholds	4
1.2.3 Single variable and bilinear thresholds.	5
1.3 Research objective	6
1.4 Research outline	6
2 Study area description and landslide hazard experience	9
2.1 Geographic location	10
2.2 Climatic controls and variability	10
2.3 Topography and geomorphology	11
2.4 Hydro-geology and tectonic movements	12
2.5 Land use change and demographic pressure	13
2.6 Landslide events and characteristics	13
3 Hydro-geological and meteorological behaviours of typical landslide-prone hillslopes	17
3.1 Introduction	19
3.2 Karago hillslope.	20
3.3 Rwaza hillslope	20
3.4 Geotechnical analysis.	22
3.5 Hydro-meteorological processes and slope failure	22
3.6 Slope response to hydro-meteorological processes	24
3.7 Results and discussion	24
3.7.1 Geotechnical characteristics	24
3.7.2 Soil moisture dynamics and landslide occurrence	25
3.7.3 Groundwater fluctuations and landslide occurrence.	28
3.7.4 Surface displacement	28
3.7.5 Slope response to hydro-meteorological processes	31
3.8 Conclusion	33

4	Landslide precipitation thresholds in Rwanda	35
4.1	Introduction	37
4.2	Landslide data	37
4.2.1	Landslide inventory	37
4.2.2	Rainfall and representative rain gauges	38
4.3	Methodology	38
4.3.1	Definition of landslide rainfall conditions	38
4.3.2	Quantification of landslide explanatory precipitation variables	39
4.3.3	Threshold definition techniques	40
4.3.4	Hydro-meteorological/Cause-trigger-based thresholds definition	41
4.4	Results and discussion	42
4.4.1	Landslide explanatory rainfall variables and thresholds	42
4.4.2	Landslide trigger and trigger-cause based hydro-meteorological thresholds and implication for landslide prediction	46
4.5	Conclusion	50
5	Integration of observed and model-derived groundwater levels in landslide threshold models in northwestern Rwanda	51
5.1	Introduction	53
5.2	Study area	53
5.3	Groundwater modelling: data and methodology	55
5.3.1	Meteorological data and selection of landslide representative meteorological stations	55
5.3.2	Groundwater data and selection of landslide representative groundwater stations	55
5.3.3	Transfer function noise (TFN) time series model.	56
5.3.4	Groundwater modelling approach: Pastas	56
5.4	Regional landslide assessment: data and methodology	57
5.4.1	Landslide inventory	57
5.4.2	Definition of landslide hydrological and meteorological conditions	58
5.4.3	Quantification of landslide predictor variables.	58
5.4.4	Landslide threshold definition techniques	58
5.4.5	Single variable and bilinear threshold models and landslide predictive capabilities	59
5.5	Results and discussion	59
5.5.1	Regional groundwater modelling	59
5.5.2	Catchment standardised groundwater levels and landslide activities.	59
5.5.3	Landslide predictor variables and discriminatory power.	61
5.5.4	Comparative prediction power of single variable and bilinear threshold models.	63
5.5.5	Comparative analysis of the warning capabilities of landslide hydro-meteorological thresholds and precipitation based thresholds	65
5.5.6	Adaptability and limitation of the defined landslide threshold models	73

5.6	Conclusion	75
6	Potential of satellite derived hydro-meteorological information for landslide initiation thresholds in Rwanda	77
6.1	Introduction	79
6.2	Methods and data.	79
6.2.1	Landslide inventory	79
6.2.2	Precipitation products and performance evaluation	80
6.2.3	Soil moisture products and data acquisition	82
6.2.4	Landslide hazard assessment and thresholds definition	84
6.3	Results and discussion	87
6.3.1	Performance of satellite precipitation products	87
6.3.2	Mean soil moisture response to rainfall and landslide events	88
6.3.3	Single variable landslide meteorological and hydrological thresholds and prediction capabilities	89
6.3.4	Landslide hydro-meteorological thresholds and implication for warning	93
6.3.5	Prospective of the satellite-based hydro-meteorological thresholds, advances and limitations	98
6.4	Conclusion	100
7	Synthesis and Conclusions	103
7.1	Synthesis of research findings.	104
7.1.1	Hydro-geological and meteorological processes of the typical hillslopes prone to landslide in Rwanda.	104
7.1.2	Precipitation-related variables with the highest explanatory power and warning capability for landslide hazard in Rwanda	104
7.1.3	Asset of regional groundwater level information on landslide hazard assessment thresholds	105
7.1.4	Potential of satellite and model derived precipitation and soil moisture for landslide initiation thresholds in Rwanda	105
7.2	Comparative performance of the defined hydro-meteorological thresholds	106
7.2.1	Landslide hydro-meteorological thresholds at country scale.	106
7.2.2	Landslide hydro-meteorological thresholds at regional scale	106
7.2.3	Landslide hydro-meteorological thresholds at catchment scale	107
7.3	Capabilities and limitations of the defined bilinear hydro-meteorological thresholds and perspective for future research	107
	References	109
	Acknowledgements	121
	Curriculum Vitae	123
	List of Publications	125

SUMMARY

For the development of regional landslide early warning systems, empirical-statistical thresholds are of crucial importance. The thresholds indicate the meteorological and hydrological conditions initiating landslides and are an affordable approach towards reducing people's vulnerability to landslide hazards. This thesis defined different landslide hydro-meteorological thresholds in Rwanda and evaluated their predictive capabilities. Chapter 1 identifies the landslide problem to society, opportunities for possible solutions, overview of the previous research and knowledge gap. It defines the research concepts, research objectives and outlines.

Chapter 2 describes the study area and landslide hazards in Rwanda. It includes the geographic location, hydro-geology and tectonic movements, topography and geomorphology, climatic controls and variability, land use changes and population pressure, and involvement in landslide hazards occurrence. Chapter 3 provides an understanding of the hydro-geological and meteorological behaviours of the typical landslide prone hillslopes and possible implication for landslide initiation. Field and laboratory tests were conducted to quantify various geotechnical and hydrological parameters on two hillslopes in north-western Rwanda renowned to be prone to landslide hazards. The geotechnical characterization indicated instability conditions at the Karago hillslope and marginally stable conditions at the Rwaza hillslope. A strong correlation was found between surface displacement and depth to groundwater and thus stressing its role on landslide initiation. The role of rainfall was also significant with long lasting low intensity rainfall being more impactful than short and high intensity rainfall events. Rainfall was identified as a trigger of landslides in Karago and Rwaza and is of course also the source of other hydrological processes and stocks such as local and regional groundwater levels and soil moisture water content.

Following these insights, chapter 4 assessed the landslide hazard in Rwanda at national scale by using the landslide inventory that was made for this study and rainfall data in an empirical-statistical approach to identify the precipitation-related variables to explain landslide initiation. This chapter defines both rainfall thresholds referred to as landslide trigger and the antecedent precipitation index as a proxy for soil moisture content prior to landslide initiation referred to as landslide cause. Both precipitation and antecedent precipitation index were combined to define the hydro-meteorological thresholds. The findings indicated the rainfall event volume and the cumulative one day rainfall that coincide with the landslide day to be the most powerful explanatory factors to statistically describe the landslide triggering. The antecedent precipitation index, calculated over the 10 days prior to the landslide triggering, showed the highest explanatory power for the causal conditions prior to landslide initiation. The highest landslide prediction capability (in terms of predicted positive alarms) was found to be a single

rainfall variable; so a trigger-based threshold. However, at the same time this trigger-based threshold resulted in a high number of false alarms. Constraining this trigger-based threshold with a causal variable in a bilinear hydro-meteorological framework, improved the overall prediction capability by reducing the number of false alarms.

Chapter 5 aimed to improve the national scale landslide prediction capability by incorporating catchment specific hydrological information in empirical-statistical landslide threshold models. Specifically, this chapter tested the value of regional groundwater level information, as a proxy for water storage (i.e. wetness of the entire catchment), to improve landslide predictions. As this type of information is scarce in Rwanda, a parsimonious transfer function noise model was used to simulate and extend regional groundwater level time series to the same period covered by the Rwanda landslide inventory. The standardized groundwater levels modelled on a landslide day and the event rainfall volume were identified as the hydrological and meteorological variables with the highest discriminatory power to distinguish landslide from no landslide conditions and thus the dominant control on landslide occurrence in the studied region. Interestingly, using only regional groundwater levels (single variable threshold) gave the best prediction of landslide initiation (true positives) despite the resulting number of false alarms. Similarly, the single variable thresholds using rainfall event volume and rainfall intensity revealed also high predictive skill in terms of true positive landslide initiation predictions, however associated with quite high number of false alarms. Moreover, it was noticed that relying exclusively on single variable thresholds derived from precipitation data like rainfall event volume and rainfall intensity, could lead to biased results due to the fact that many landslides occur not only due to the trigger itself but rather a combination of both trigger and pre-event hydrological conditions. Contrarily, relying exclusively on single variable thresholds using groundwater levels, lead to unbiased landslide predictions as this considers the long-term antecedent wetness conditions until the day of landslide occurrence. Further combination of the groundwater level and precipitation to predict landslide initiation using bilinear hydro-meteorological thresholds reduced the number of false alarms at the expense of reduced number of true positive alarms. However, for Rwanda the bilinear hydro-meteorological threshold models using groundwater and rainfall information indicated higher landslide predictive skill than the classical rainfall intensity-duration threshold models.

The hydro-meteorological thresholds for Rwanda defined from both Chapter 4 and 5 relied on in-situ rain gauges and groundwater monitoring wells with the highest data accuracy but constrained by the coarse spatial resolution of the networks, and providing data at point scale. Chapter 6, tested the reliability of satellite derived precipitation and soil moisture content data as well as soil moisture content derived from a simple regional hydrological model as alternatives to the in-situ based information. Both precipitation and soil moisture content information were integrated in landslide threshold models and we evaluated their landslide predictive capabilities in Rwanda. Based on statistical indicators, the NASA GPM-based precipitation product IMERG showed the highest skill to reproduce the main spatiotemporal precipitation patterns. Similarly, the satellite and model derived soil moisture content time series broadly reproduce the most important

trends of the in-situ measured soil moisture content and show interesting potential for regional landslide hazard assessment. The root zone antecedent soil moisture content was found the most useful in landslide hazard assessment in the study area. The hydro-meteorological thresholds that incorporate the antecedent soil moisture from the root zone and the recent 3day cumulative rainfall over performed other threshold models and thus useful alternative for landslide hazard assessment and early warning system development in Rwanda.

Chapter 7 provides a synthesis of research findings, overall comparison of the defined hydro-meteorological thresholds, constraints and perspectives for future researchers for Rwanda landslide hazard assessment. The overall comparison of the defined hydro-meteorological thresholds for Rwanda shows that the consideration of the pre-wetting conditions of the terrain using either soil moisture or groundwater levels improves the landslide prediction as compared to the exclusive use of the classical precipitation thresholds. We concluded that the hydrological information, especially regional groundwater levels, was the most important landslide predictor, and therefor potentially useful for landslide hazard assessment in Rwanda. The landslide hydro-meteorological thresholds defined using satellite-based information performed somewhat less than using in-situ information but are still considered very useful for landslide early warning system development in data scarce areas like Rwanda.

SAMENVATTING

Voor de ontwikkeling van regionale waarschuwingssystemen voor aardverschuivingen zijn empirisch-statistische drempelwaarden van cruciaal belang. De drempelwaarden geven de meteorologische en hydrologische omstandigheden aan waarboven aardverschuivingen plaatsvinden en zijn een betaalbare methode om de kwetsbaarheid van mensen voor aardverschuivingen te verminderen. Dit proefschrift definieert verschillende hydro-meteorologische drempelwaarden voor aardverschuivingen in Rwanda en evalueert hun voorspellende vermogen. Hoofdstuk 1 identificeert het aardverschuivingsprobleem voor de samenleving, mogelijke oplossingen, overzicht van eerder onderzoek en kennishiaten. Het definieert de onderzoek concepten en doelstellingen.

Hoofdstuk 2 beschrijft het studiegebied en de aardverschuivingsgevaaren in Rwanda. Het omvat de geografische locatie, hydrogeologie en tektonische bewegingen, topografie en geomorfologie, klimatologische controles en variabiliteit, veranderingen in landgebruik en bevolkingsdruk, en de betrokkenheid van dit alles bij het optreden van aardverschuiving in Rwanda. Hoofdstuk 3 geeft inzicht in het hydro-geologische en meteorologische gedrag van typische hellingen die vatbaar zijn voor aardverschuivingen en mogelijke implicaties voor het initiëren van aardverschuivingen. Er werden veld- en laboratoriumtesten uitgevoerd om verschillende geotechnische en hydrologische parameters te kwantificeren op twee hellingen in het noordwesten van Rwanda die bekend staan om hun risico op aardverschuivingen. De geotechnische karakterisering wees op instabiliteit op de Karago-heuvels en marginaal stabiele omstandigheden op de Rwaza heuvels. Er werd een sterke correlatie gevonden tussen oppervlakteverplaatsing en diepte tot grondwater, wat de rol ervan bij het initiëren van aardverschuivingen benadrukt. De rol van regenval was ook significant, waarbij langdurige regenval met lage intensiteit meer impact had dan korte regenbuien met hoge intensiteit. Neerslag wordt geïdentificeerd als een trigger van aardverschuivingen in Karago en Rwaza en is natuurlijk ook de bron van andere hydrologische processen en waterberging, zoals lokaal en regionaal grondwater en bodemvochtgehaltes.

In navolging van deze inzichten wordt in hoofdstuk 4 het gevaar voor aardverschuivingen in Rwanda op nationale schaal beoordeeld. Hiervoor is gebruik gemaakt van de voor deze studie gemaakte aardverschuivingsinventaris en beschikbare neerslaggegevens. Vervolgens zijn empirisch-statistisch de neerslaggerelateerde variabelen geïdentificeerd die het begin van aardverschuivingen verklaren. Dit hoofdstuk definieert zowel de neerslagdrempels die aardverschuivingstriggers worden genoemd als de voorafgaande neerslagindex die als een proxy dient voor het bodemvochtgehalte voorafgaand aan de aardverschuiving. Zowel de neerslag- als de voorafgaande neerslagindex werden gecombineerd om de hydro-meteorologische drempels te definiëren. De bevindingen gaven aan dat zowel het volume van de regenvalgebeurtenis als de cumulatieve een-

daagse regenval die samenvalt met de dag van de aardverschuiving, de beste verklarende factoren zijn om de triggers van aardverschuivingen statistisch te beschrijven. De neerslagindex, berekend over de 10 dagen voorafgaand aan de aardverschuiving, bleek de de oorzakelijke omstandigheden voorafgaand aan de aardverschuiving het best te beschrijven. De beste voorspelling van aardverschuivingen (percentage positieve alarmen) werd genoteerd met behulp van slechts een enkele regenvalvariabele zonder de hydrologische condities voorafgaand aan de aardverschuiving mee te nemen. Tegelijkertijd resulteerde dit echter in een hoog aantal valse alarmen. Door de neerslag drempelwaarde te beperken tot hydrologisch nattere condities verbeterde het algehele voorspellingsvermogen doordat het aantal valse alarmen verminderde.

Hoofdstuk 5 had als doel het voorspellen van aardverschuivingen op nationale schaal te verbeteren door de stroomgebiedspecifieke hydrologische informatie op te nemen in empirisch-statistische modellen voor aardverschuivingsdrempels. Dit hoofdstuk test met name de waarde van regionale grondwaterstandinformatie, als een proxy voor waterberging (d.w.z. nattigheid van het gehele stroomgebied), om de voorspellingen van aardverschuivingen te verbeteren. Aangezien dit soort informatie schaars is in Rwanda, werd een eenvoudig statisch tijdserie model (Transfer Noise Model) gebruikt om regionale tijdreeksen van grondwaterstanden te simuleren en uit te breiden tot dezelfde periode die wordt bestreken door de Rwandese aardverschuiving database. De gemodelleerde regionale grondwaterstanden op de dag dat een aardverschuiving was opgetreden en de hoeveelheid regen op deze dag bleken de aardverschuivingen goed te kunnen voorspellen in de bestudeerde regio. Als alleen gemodelleerde regionale grondwaterstanden werden gebruikt, werd het optreden van aardverschuiving het best voorspeld (positieve alarmen) ondanks het aantal valse alarmen. Het toevoegen van neerslag als verklarende variabele verminderden de kans op vals alarm maar echter ten koste van een iets verminderd aantal goed voorspelde aardverschuivingen (positieve alarmen). Echter, deze gecombineerde hydro-meteorologische drempelwaarden op basis van regionale grondwater en neerslag zijn duidelijk beter in het voorspellen van aardverschuivingen dan de klassieke modellen die uitsluitend vertrouwen op neerslag.

De hydro-meteorologische drempelwaarden voor Rwanda, gedefinieerd in zowel hoofdstuk 4 als hoofdstuk 5, waren gebaseerd op in-situ regenmeters en grondwatermonitoringputten met hoge nauwkeurigheid maar beperkt door de grove ruimtelijke verdeling van de netwerken, en de puntschaalresolutie. Hoofdstuk 6 test de betrouwbaarheid van satelliet metingen van neerslag en bodemvocht en ook van bodemvocht zoals gemodelleerd met een eenvoudig regionaal hydrologisch model als alternatieven voor de in-situ gebaseerde informatie. Zowel informatie over neerslag als bodemvochtgehalte werd geïntegreerd in de modeldefinitie van aardverschuivingsdrempels en hun voorspellende vermogen voor aardverschuivingen in Rwanda werd geëvalueerd. Op basis van statistische indicatoren toonde het NASA GPM-gebaseerde neerslagproduct IMERG de grootste vaardigheid om de belangrijkste spatiotemporele neerslagpatronen te reproduceren. Evenzo bleken de tijdreeksen van de satelliet en het model afgeleide bodemvochtgehalten in grote lijnen overeen te komen met de in-situ gemeten bodemvochtgehalten en tonen ze interessante mogelijkheden voor regionale risicobeoordeling van aardverschui-

vingen. Het antecedent bodemvochtgehalte in de wortelzone bleek het meest bruikbaar bij de beoordeling van aardverschuivingsgevaar in het studiegebied. De hydro-meteorologische drempels die antecedent bodemvocht in de wortelzone combineert met de 3-daags cumulatieve neerslag bleek een nuttig alternatief voor regionale aardverschuivingsvoorspellingen in Rwanda.

Hoofdstuk 7 biedt een synthese van onderzoeksbevindingen, een algemene vergelijking van de gedefinieerde hydro-meteorologische drempelwaarden, beperkingen en perspectieven voor toekomstig onderzoek voor de risicobeoordeling van aardverschuivingen in Rwanda. De algehele vergelijking van de gedefinieerde hydro-meteorologische drempels laat zien dat het in aanmerking nemen van de mate van natheid van het terrein door middel van bodemvocht of grondwaterniveaus, de voorspelling van aardverschuivingen verbetert in vergelijking met het exclusieve gebruik van de klassieke neerslagdrempelwaarden. Geconcludeerd wordt dat de hydrologische informatie, met name regionale grondwaterstanden, de belangrijkste voorspellers van aardverschuivingen zijn, mogelijk nuttig voor de beoordeling van het gevaar van aardverschuivingen in Rwanda. De hydro-meteorologische drempels voor aardverschuivingen die zijn gedefinieerd met behulp van op satellieten gebaseerde informatie presteerden iets minder dan het gebruik van in-situ informatie, maar zijn nog steeds erg nuttig voor de ontwikkeling van systemen voor vroegtijdige waarschuwing voor aardverschuivingen in gebieden met schaarse gegevens, zoals Rwanda.

1

INTRODUCTION

Parts of this chapter are based on:

Uwihirwe, J., Hrachowitz, M., and Bogaard, T. (2020). *Landslide precipitation thresholds in Rwanda*. *Landslides* 17, 2469–2481, <https://doi.org/10.1007/s10346-020-01457-9>

Uwihirwe, J., Hrachowitz, M., and Bogaard, T. (2022). *Integration of observed and model derived groundwater levels in landslide threshold models in Rwanda*. *Nat. Hazards Earth Syst. Sci.*, 22, 1723–1742, <https://doi.org/10.5194/nhess-22-1723-2022>

Uwihirwe, J., Pavez R. A., Wanjala, H., Schellekens, J., Weiland, S.F., Markus Hrachowitz, M., and Bogaard, T. (2022). *The potential of satellite derived hydro-meteorological information for landslide initiation thresholds in Rwanda*. *Nat. Hazards Earth Syst. Sci.*, 22, 3641–3661, <https://doi.org/10.5194/nhess-22-3641-2022>

1.1. LANDSLIDE HAZARD PROBLEMS AND OPPORTUNITIES FOR SOLUTIONS

Water induced landslides are one of most prevalent hazards in mountainous regions of the world associated with rates of fatalities, injuries and economic loss globally (Froude and Petley, 2018; Haque et al., 2016; Kirschbaum et al., 2015; Petley, 2012). According to a recent estimate (Froude and Petley, 2018), precipitation-induced landslides were responsible for a global total of about 55000 deaths over the 13-year period from 2004 to 2016. In landslide-prone regions, much effort is therefore put on the implementation of prevention and protection measures to control the most sensitive factors. These measures include the slope stabilization approaches and landslide early warning systems (LEWS). Both reliable warning systems and sustainable slope stabilisation approaches require an understanding of the hydro-geological and meteorological behaviours of the hillslopes prone to failures including the failure mechanism, potential predisposing and triggering conditions and their respective thresholds. However, in many places, stabilisation approaches may be expensive in terms of financial and environmental limitations and hence early warning systems are adopted to timely inform the public about the landslides imminent dangers.

LEWS are defined as “set of capacities needed to generate and disseminate timely and meaningful landslide warning information to enable individuals, communities and organizations threatened by a hazard to act appropriately and in sufficient time to reduce the possibility of harm or loss” (UNISDR, 2009). LEWS are used as non-structural and cost effective mitigation approach adopted to minimize the landslides’ harms and fatalities (Calvello et al., 2020). However, global landslide research shows a bias in geographical distribution of landslide research and LEWS with a major gap in Africa (Kirschbaum et al., 2010, 2015; Gariano and Guzzetti, 2016; Guzzetti et al., 2020). According to Guzzetti et al. (2020), there is no LEWS in African countries despite the high number of fatal landslides recorded (Kirschbaum et al., 2015; Broeckx et al., 2018) and the high landslide susceptibility (Broeckx et al., 2018). The East African Rift (EAR) was identified as a major hotspot of hazardous landslides in Africa with high rate of population exposure (Depicker et al., 2020, 2021c; Monsieurs et al., 2018a). On the long term, this is due to the active continental rifting caused by the persistent divergence of the Victoria and Nubia microplates (Glerum et al., 2020) while on the short term it is controlled by the interactions of prolonged, intense rainstorms and hydro-geological processes.

Rwanda is among the tropical countries located in the East African Rift region, threatened by landslide hazards (Bizimana and Sönmez, 2015; Nsengiyumva et al., 2018; Nsengiyumva and Valentino, 2020). About 43% of its surface area is classified as moderate to very high susceptibility to landslide with about 49% of the total population exposed to landslide risks (Nsengiyumva et al., 2018). The long term landslide predisposing factors include its topographic nature, inherent geological and lithological units, weathering process, demographic pressure and related anthropogenic activities such as deforestation, expansion of agriculture, buildings and slope incision through roads construction activities (Bizimana and Sönmez, 2015; Moeyersons, 1989; Nsengiyumva et al., 2018; Valentino et al., 2021; Depicker et al., 2021c). Development of mining sites and connected feeder roads also change the nature of natural hillslope through excavation and

thus exacerbating landslide susceptibility and risks of slope failures. The urban expansion also forces the society to bring infrastructures like buildings and roads in hazardous areas that are naturally unstable (Valentino et al., 2021) and thus increasing the number of elements at landslide risks. In the past 15-year period from January 2006 to May 2021, the landslide inventory in Rwanda (Uwihirwe, 2021) indicated about 425 landslide victims (0.6% of the global landslide induced death) with about 2000 injuries. The lack of operational LEWS is one of the key causal factors of the landslide victims.

Empirical and physically based landslide threshold models are of crucial importance for LEWS development to reduce people's vulnerability to landslide hazard. Empirical-statistical threshold models indicate the meteorological and hydrological conditions initiating landslides. Physical, process-based models aim to understand and describe the dynamic processes responsible for landslide initiation. They typically combine slope stability and hydrological models in which dynamic hydrological processes are used to evaluate the slope failure probabilities (Anderson and Lloyd, 1991; Montgomery and Dietrich, 1994; Van Beek, 2002; Rosso et al., 2006; Kuriakose et al., 2009). However, physically based dynamic models require high resolution spatio-temporal data, which are largely unavailable in most of the areas worldwide. Applications of this type of models are thus highly limited to few regions with sufficient data and typically to local scales only (Aleotti, 2004).

Due to their less detailed data requirements, empirical-statistical models have been widely adopted to define the landslide early warning thresholds at local (Crozier, 1999; Prenner et al., 2018; Mirus et al., 2018b,a); regional (Martelloni et al., 2012; Roccati et al., 2018; Ciavolella et al., 2016); national (Robbins, 2016; Peruccacci et al., 2017; Rosi et al., 2016; Brunetti et al., 2010; Hong et al., 2017); and global scales (Caine, 1980; Guzzetti et al., 2008). The empirical-statistical models typically relate precipitation characteristics, such as antecedent precipitation, cumulative event precipitation, precipitation intensity and precipitation duration or combination thereof to the occurrence of landslides. Despite the considerably lower data requirements of empirical-statistical threshold models, landslide initiation thresholds remain poorly explored and defined throughout Africa (Gariano and Guzzetti, 2016). This is due to the lack of accurate and complete landslide inventories and insufficient spatio-temporal resolution of the available precipitation (Monsieurs et al., 2018c) and hydrological data. The development of a robust LEWS hinges on the availability of sufficient spatio-temporal resolution meteorological and hydrological data and accurate landslide inventory which are still scarce.

Recently, numerous river catchments in Rwanda have been equipped with ground-water monitoring wells, piezometers, river water level gauges as well as the automated weather stations equipped with soil moisture sensors (<https://waterportal.rwb.rw/>, last access: 2 June 2021). However, often, the recorded data are insufficient to build historical time series that overlap the time period of landslide inventories and that could be incorporated into landslide hazard assessment thresholds. The Landslide Inventory for the central section of the Western branch of the East African Rift LIWEAR has also made an effort to systematically document landslide hazards in Africa and hence shaping interests for landslide researchers in the region (Depicker et al., 2020, 2021b; Monsieurs et al., 2018c,a,b, 2019). Despite that, however, many landslide events are likely to be missed in the inventory due to the fact that for Africa mostly only newspapers, govern-

ment reports, and other media are used as a source for landslide inventory. While the reliance on these data sources is likely to result in a bias towards large and/or impactful landslides that involve casualties and economic damage, this landslide inventory can nevertheless serve as a basic starting point to define landslide thresholds in Rwanda.

While in-situ gauge based precipitation are accurate but often sparse and point based, satellite precipitation data have proven to offer valuable, spatial and temporal information for use in landslide hazard assessment (Hong et al., 2006; Kirschbaum et al., 2009, 2017; Brunetti et al., 2018; Monsieurs et al., 2018b). Similar to precipitation, hydrological processes also exhibit high spatial variability influenced by the spatial variation of other soil properties like soil texture and land cover in addition to the high dependence on spatial variability of precipitation in tropical areas (Dewitte et al., 2022; Kirschbaum et al., 2012; Sekaranom et al., 2020). This spatial variability is hardly covered by the on-site hydrological monitoring equipment due to the sparse observation networks, themselves providing point-scale observations only. Therefore, hydro-meteorological information from satellite and hydrological models could be a potential alternative for meaningful landslide hazard assessment over large regions in Rwanda.

1.2. RESEARCH CONCEPTS AND STATISTICAL APPROACHES

1.2.1. LANDSLIDE TRIGGER-BASED THRESHOLDS

The majority of landslide thresholds are mainly inferred from empirical methods which are based on statistical analysis of historical precipitation characteristics and landslide inventories to distinguish the landslide conditions from no-landslide conditions. However, some limitations, constraints and uncertainties associated with empirical precipitation thresholds have been highlighted (Peres et al., 2017; Prenner et al., 2018; Bogaard and Greco, 2018). Some limitations are due to the fact that empirical thresholds are mainly based on the rainfall events during which one or more landslides occurred, which is in reality the actual landslide trigger. Hereafter, these thresholds are therefore referred to as *landslide trigger-based thresholds* with various time scales depending on rainfall event duration. Such landslide trigger-based thresholds include the intensity-duration (I-D) (Caine, 1980; Guzzetti et al., 2007, 2008; Ma et al., 2018; Roccati et al., 2018; Hong et al., 2017); event-duration (E-D) and event-intensity (E-I) (Peruccacci et al., 2017; Robbins, 2016). These landslide trigger-based thresholds have been increasingly recognized to neglect the causal hydrological processes that predispose the slope to near failure (Peres et al., 2017; Bogaard and Greco, 2018; Mostbauer et al., 2018). Disregarding this information may thus be one of the reasons for the typically occurring rates of both, false and missed alarms associated with the empirical trigger-based precipitation thresholds and hence less suitable for a robust LEWS.

1.2.2. LANDSLIDE CAUSE-TRIGGER-BASED THRESHOLDS

The dynamic hydrological conditions regulate the disposition of a slope to near failure (Bogaard and Greco, 2018; Sidle et al., 2019) and thus the root cause of landslide occurrence in a region. To include this, a number of researchers considered the possible hydrological causes in terms of antecedent precipitation, catchment storage, soil moisture indices and or soil water status prior to the landslide triggering event or storm

(Crozier, 1999; Glade, 2000; Ciavolella et al., 2016; Mostbauer et al., 2018). These hydrological conditions are defined prior to the landslide triggering conditions and then combined with precipitation to make *landslide cause-trigger-based thresholds*. The concept of the landslide cause-trigger was proposed by Bogaard and Greco (2018) and has been adopted using either in-situ observed or modelled soil moisture and precipitation to define the landslide hydro-meteorological thresholds (Mirus et al., 2018a; Prenner et al., 2018). Similar concepts were also adopted in other studies (Crozier, 1999; Glade, 2000; Aleotti, 2004; Ciavolella et al., 2016; Mostbauer et al., 2018; Prenner et al., 2019; Monsieus et al., 2019, 2018a). Some landslide studies discussed different effects that groundwater system may have on landslide initiation (Bronnimann, 2011; Cascini et al., 2010; Corominas et al., 2005a; Duan et al., 2019; Hong and Wan, 2011; Trigo et al., 2005; Zhao et al., 2016). However, the asset that regional groundwater level information may have in predicting landslide initiation thresholds on a regional scale is still underexplored. The novelty of this work is therefore not only on the landslide thresholds definition approach in a country where they have not been defined before, but also on the use of groundwater data and soil moisture information derived from both satellite and hydrological models.

1.2.3. SINGLE VARIABLE AND BILINEAR THRESHOLDS

Traditional trigger-based threshold models commonly used the power-law function between precipitation variables like intensity-duration I-D and event-duration E-D (e.g. Caine (1980); Guzzetti et al. (2007, 2008); Ma et al. (2015); Hong et al. (2017)). A threshold model line is used as the best separator for landslide and no-landslide conditions sometimes defined based on the experts judgment.

More advanced statistical approaches that include the frequentist, probabilistic and receiver operating characteristics methods have been adopted and replaced the deterministic method. The frequentist methods (Brunetti et al., 2010; Peruccacci et al., 2017; Melillo et al., 2018; Piciullo et al., 2018) define the threshold line separating landslide from no-landslide conditions based on the targeted exceedance probabilities. The probabilistic methods (Berti et al., 2012; Robbins, 2016) fundamentally rely on Bayes' prior and marginal probabilities for landslide occurrence. The probabilistic methods are criticized for the biased prior and marginal probabilities due to the incompleteness of typical landslide inventory data (Berti et al., 2012). The frequentist methods are also constrained by their high dependency on a large and well distributed dataset to achieve significant results (Brunetti et al., 2010; Monsieus et al., 2019). The receiver operating characteristic (ROC) curve method compares the landslide and no-landslide conditions based on the area under the curve (AUC) while indicating the trade-off between true and false positive rates associated to each level of the tested predictor variable or model. In landslide studies, the ROC approach has been mostly used to evaluate the performance of landslide prediction models (Hong et al., 2017; Wicki et al., 2020) despite its capability to define the landslide initiation thresholds once associated with other statistical metrics like the true skill statistics and radial distance.

Some research that incorporate the hydrological parameters in landslide prediction models also used the exponential or power-law function (e.g. Crozier (1999); Monsieus et al. (2018a, 2019)). Monsieus et al. (2018a, 2019) used the frequentist statistical methods to define the landslide power-law threshold model line between antecedent rain-

fall and landslide susceptibility. Similarly, Crozier (1999) defined the exponential function between antecedent water status and daily rainfall in Wellington City, New Zealand. However, recent research (Mirus et al., 2018a) used the ROC curve and other statistical metrics (true skill statistics, radial distance, and threat score) to define the landslide threshold for each tested landslide predictor variable. These statistical metrics are used to identify the optimum threshold of each tested predictor variable. Then after, these optimum thresholds are plotted in 1D here referred to as *single variable threshold model line* beyond which landslide are high likely to occur. Furthermore, these optimum thresholds are combined and plotted in 2D here referred to as *bilinear threshold model lines* beyond which landslide are high likely to occur and have been firstly proposed by Mirus et al. (2018a). In this work, the bilinear relationship between hydrological and meteorological variables has been adopted based on the fact that the majority of landslide conditions were clustered in the upper right corner of the 2D plane.

1.3. RESEARCH OBJECTIVE

This research aims to define the landslide hydro-meteorological thresholds following the cause-trigger concept in a bilinear framework towards the development of landslide early warning system in Rwanda. Specifically, the following objectives were addressed:

1. To determine the key hydro-geological and meteorological characteristics of the typical hillslopes prone to landslide and possible implication in landslide initiation;
2. To identify precipitation-related variables with the highest landslide explanatory power and predictive capability;
3. To evaluate the asset that regional groundwater level information have on landslide initiation thresholds and warning capabilities;
4. To assess the potential of satellite and model derived precipitation and soil moisture information for landslide initiation thresholds

1.4. RESEARCH OUTLINE

Following the introduction chapter, the content of this thesis is structured as follow: Chapter 2 provides a description of the study area that includes the geographic location, climatic controls, topography and geomorphology, hydro-geology and tectonic movement, land use change, population pressure, and landslide hazards experience. Chapter 3 identifies the key hydro-geological and meteorological characteristics of the typical hillslopes prone to landslides hazards in northwestern Rwanda. Chapter 4 identifies precipitation-related variables with the highest explanatory power for landslide occurrence and defines the cause-trigger hydro-meteorological thresholds using antecedent precipitation index and rainfall. Chapter 5 assesses the added value of regional groundwater level information to precipitation, to improve landslide predictions with an empirical-statistical model based on the concept of cause-trigger hydro-meteorological thresholds. Chapter 6 evaluates the prospect of satellite and model derived precipitation and soil moisture information in landslide hazard assessment thresholds. Chapter 7 summarizes

the overall knowledge generated by the research, presents the capabilities of the defined hydro-meteorological thresholds, their limitations and potentialities for future research.

2

STUDY AREA DESCRIPTION AND LANDSLIDE HAZARD EXPERIENCE

Parts of this chapter are based on:

Uwihirwe, J., Hrachowitz, M., and Bogaard, T. (2020). *Landslide precipitation thresholds in Rwanda*. *Landslides* 17, 2469–2481, <https://doi.org/10.1007/s10346-020-01457-9>

Uwihirwe, J., Hrachowitz, M., and Bogaard, T. (2022). *Integration of observed and model derived groundwater levels in landslide threshold models in Rwanda*. *Nat. Hazards Earth Syst. Sci.*, 22, 1723–1742, <https://doi.org/10.5194/nhess-22-1723-2022>

Uwihirwe, J., Pavez R. A., Wanjala, H., Schellekens, J., Weiland, S.F., Markus Hrachowitz, M., and Bogaard, T. (2022). *The potential of satellite derived hydro-meteorological information for landslide initiation thresholds in Rwanda*. *Nat. Hazards Earth Syst. Sci.*, 22, 3641–3661, <https://doi.org/10.5194/nhess-22-3641-2022>

2.1. GEOGRAPHIC LOCATION

This research has been conducted in Rwanda, an evergreen landlocked country geographically located between 1° – 3° S and 28° – 31° E in African Great Lakes region of the central east Africa, with a total area of $26,338\text{km}^2$. Rwanda, south of equator, extends over the western branch of the East African Rift characterised by active continental rifting due to the persistent divergence of the Victoria and Nubia microplates (Glerum et al., 2020) and hence a potential spot for landslide hazards (Dewitte et al., 2021; Froude and Petley, 2018; Monsieurs et al., 2018c). The tectonic rifting gave rise to the two parallel North-south oriented mountainous rift shoulders enclosing Lake Tanganyika and Lake Kivu, ones of the African great Lakes. The Lake Kivu is located on the western edge of Rwanda bordering to the Democratic Republic of the Congo. Lake Kivu outflows by Ruzizi river in the southwest of Rwanda and drains into lake Tanganyika. Rwanda is bounded by Uganda on the north, Burundi in the south, Tanzania on the east and Democratic Republic of Congo on the west (Figure 2.1).

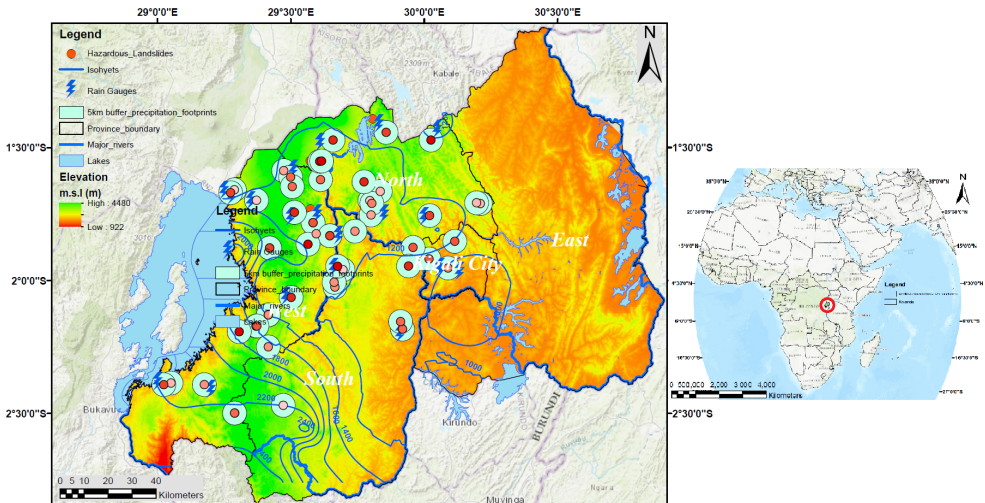


Figure 2.1: Location of Rwanda in Africa, elevation, rain gauges and isohyets (mm) indicating rainfall distribution; spatial and temporal distribution of landslides with light to dark red dots indicating old to new landslides recorded from 2006–2019 (Uwihirwe, 2021), 5km buffer for Satellite precipitation foot prints

2.2. CLIMATIC CONTROLS AND VARIABILITY

Rwanda is characterised by a subtropical highland climate with a long term mean annual rainfall greater than 1200mm in highland regions of northwest and less than 1000mm in eastern Savanah (Figure 2.1) and a mean annual temperature of about 19°C . The country has two rainy seasons, the long and heavy rainy season that extends from March through mid-May (MAM) and the shorter one from September to December (SOND) (Kimani et al., 2017; Ngarukiyimana et al., 2017; Nicholson, 2017). The MAM has more and intense rainy days and thus referred to as long rain season while the SOND has less and low intensity rainy days and hence referred to as short rainy season. A number of factors

is known to influence the seasonal rainfall regime and the high spatio-temporal variability of rainfall. These factors include the topography, lakes, and the seasonal dynamics of tropical circulation. The tropical air circulations that influence the immense spatial and temporal variability of rainfall are seasonal variation of the location of the Inter-Tropical Convergence Zone (ITCZ), subtropical anticyclones, tropical cyclones, monsoons, El Niño Southern Oscillation (ENSO) and la Niña episodes (Ngarukiyimana et al., 2017; Nicholson, 2017). During the MAM and SON, the ITCZ is boosted by the convergence of strong westerly winds from the Atlantic Ocean and southeasterly winds from the Indian Ocean. During the extreme rainy years, these winds convey moist air mass, leading to rainfall events. These extreme wet years coincided with the El Niño events. On the other hands, the easterly winds carry dry air during the dry years that coincide with the La Niña episodes (Ngarukiyimana et al., 2017). Overall, the topography, large water bodies and tropical air circulations, lead to frequent extreme and prolonged rainfall events that consequently result into flooding and landslide hazards during the MAM and SON rainy seasons in Rwanda.

2.3. TOPOGRAPHY AND GEOMORPHOLOGY

Rwanda is topographically characterised by rounded, angular hills and headlands, mountains and volcanoes (Figure 2.2) with elevation in the north western regions reaching up to about 4500m and steep slope reaching up to about 29 degrees.

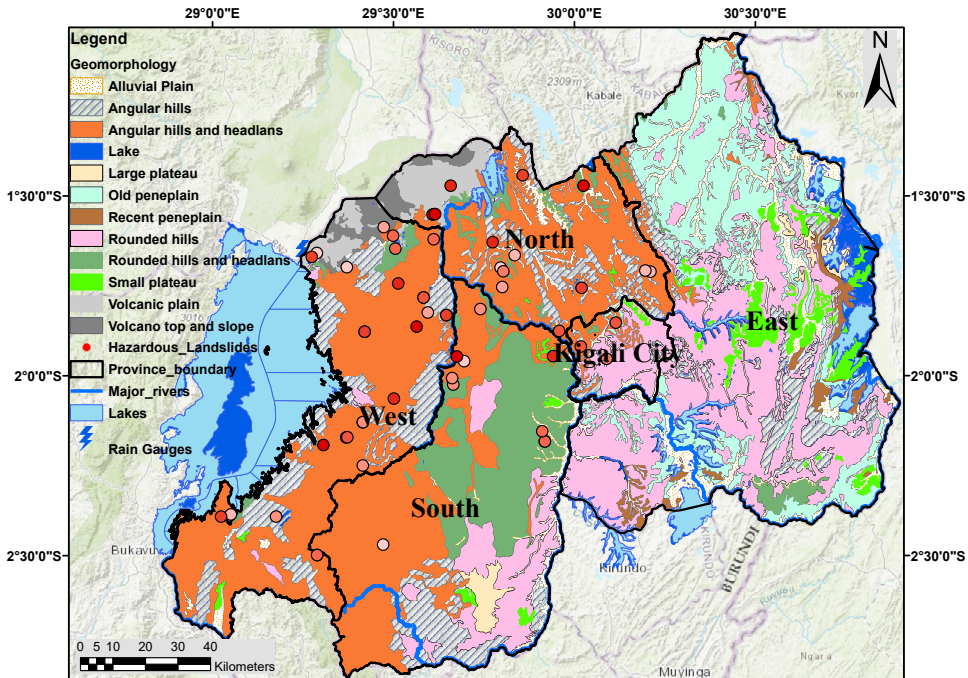


Figure 2.2: Geomorphological characteristics of Rwanda

The highest peak is on Mount Karisimbi at 4,507 m.a.s.l, located in the Volcanoes National Park while the lowest point is at 950 m.a.s.l. situated in the south-west in the Ruzizi river. Alongside the mountains and hills, the clouds often prevail in the sky and temperatures may drop to zero especially during nights. In mountainous areas also, rainfall is more frequent and can occur throughout year. The steep slope and distance to the drainage and road networks have been also identified as one of the geomorphological variables that have an impact on landslide occurrence in Rwanda (Bizimana and Sönmez, 2015; Depicker et al., 2020; Nsengiyumva et al., 2018).

2.4. HYDRO-GEOLOGY AND TECTONIC MOVEMENTS

The geology of Rwanda consists of Precambrian metasedimentary rocks mainly quartzite, sandstones and shales intruded by granites. Granitic-gneisses are dominants in north-east and south of Rwanda while Neogene and Quaternary volcanic deposits are dominants in northwest and southwest (Figure 2.3).

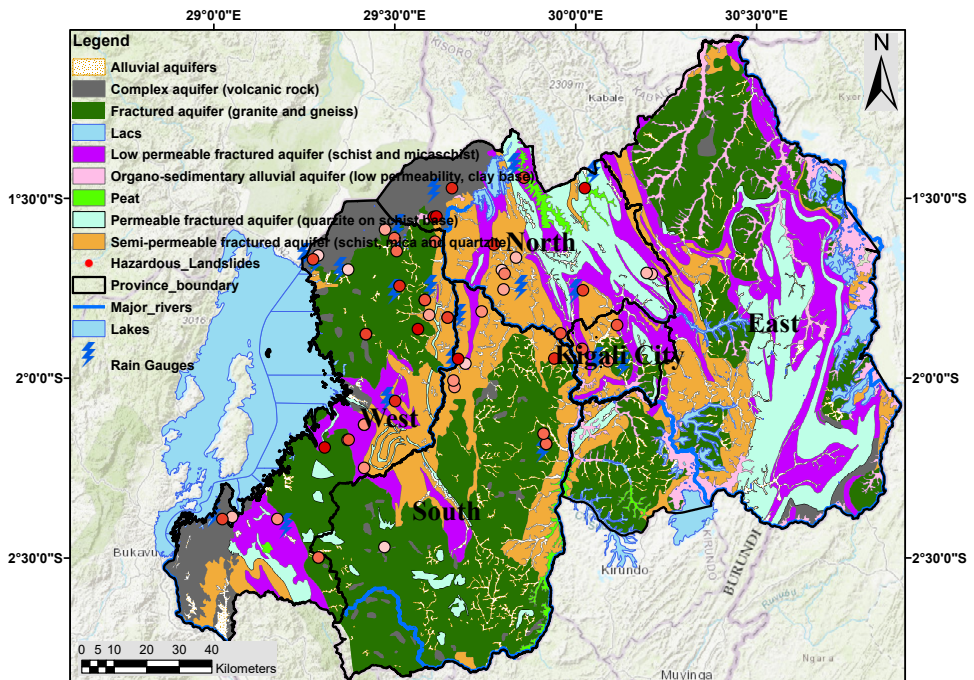


Figure 2.3: Hydro- Geology and groundwater bodies (catchments) of Rwanda and landslides (red dots) distribution

The western Rift comprises of alluvium and lake sediments of Quaternary age. The general lithostratigraphy consists of gneisses, mica schists, and granites of Paleoproterozoic age (Depicker et al., 2021a). The lithostratigraphy of Paleoproterozoic age is deeply weathered and hence susceptible to landslide hazards. The hydro-geology of Rwanda is dominated by fractured granite and gneiss aquifers, semi-permeable and permeable

fractured schist and mica schist aquifers and basaltic rock complex aquifers. Landslides are most dominant in granite and mica schist units while basaltic units are quite resistant to landslide activities.

Rwanda is located in a tectonic and seismically active region. The earthquakes, volcanoes and mountains being the results of tectonic movement exposes Rwanda, especially the western and northwest regions, susceptible to landslides (Depicker et al., 2020). In the longer term, the landslide occurrence in Rwanda is controlled by tectonic movement, and the distance to active and inactive faults. Inactive faults are found in the vicinity of the volcanoes chain while active faults are specifically found in the western parts of the country in the close proximity of Kivu Lake and thus being the most landslide susceptible region in Rwanda (Depicker et al., 2020; Nsengiyumva et al., 2018).

2.5. LAND USE CHANGE AND DEMOGRAPHIC PRESSURE

Conversion of forest land into agricultural and built up lands in Rwanda had intensively taken place over the last 2 decades (Nambajimana et al., 2020) and thus induced change in landslide intensity (Depicker et al., 2021a,b). Expansion of agricultural and construction activities coupled with deforestation have led to several environmental hazards, the most deadly ones being landslides and flooding (MIDIMAR, 2012, 2014, 2015; Nahayo and Mupenzi, 2017; Nsengiyumva et al., 2018). The large scale deforestation had been necessary to sustain life of the population that increased from 94 inhabitants per km² in 1958 to 495 inhabitants per km² by 2018 (Imasiku and Ntagwirumugara, 2020) leading to the growing demand for agricultural products, fuel wood, and natural resources and thus exacerbating landslide hazards (Depicker et al., 2021a,c).

2.6. LANDSLIDE EVENTS AND CHARACTERISTICS

The landslide inventory (with the highest temporal accuracy) in Rwanda indicated about 425 landslide victims and about 2000 injuries for the past 15 years period from January 2006 to May 2021 (Uwihirwe, 2021). The inventory counted about 68 hazardous landslides from January 2006 to May 2021. In that inventory only fatal and highly damaging landslides are mostly reported while others are likely to be missed. A field based survey conducted in the south of Mukungwa catchment located in northwestern Rwanda recorded about 560 landslides (spatially accurate but temporally not accurate). Based on Cruden and Varnes (1996), these landslides were classified as rotational slide (34%), flow (26%), translational slide (17%), fall (15%) and complex type of mass movement (7%), involving rock, debris and earth materials. The flow type of landslide include earth flow, debris flow, and debris avalanches. It has to be noted that most of the recent landslides are frequently shallow while much older landslides are deep seated ones. This is due to the fact that small shallow landslides have signatures in the landscape that last much less time than larger deep-seated landslides. Hence a temporal bias with more deep seated landslides in long timescale and shallow landslides in short timescale.



Figure 2.4: Photos of typical landslides in Rwanda taken in 2018

3

HYDRO-GEOLOGICAL AND METEOROLOGICAL BEHAVIOURS OF TYPICAL LANDSLIDE-PRONE HILLSLOPES

Abstract

Landslide hazard prevention measures that include slope stabilization or an early warning system require an understanding of the hydro-geological and meteorological behaviours of the hillslopes prone to failures. This chapter aimed to understand the hydro-geological and meteorological processes and the relationship thereof using two typical hillslopes (Karago and Rwaza) that experience slow moving rotational deformation. For each case study, geotechnical characterization and hydro-geological field and laboratory information was collected, i.e., saturated permeability measurements, soil moisture and groundwater monitoring. The surface displacements were also monitored and their linkage with hydrological processes was assessed. The geotechnical characterization indicated instability conditions ($F_s < 1$) at the Karago hillslope and marginally stable conditions ($1 < F_s < 2$) at the Rwaza hillslope. The slope deformation and landslides occurred during the wettest conditions (i.e. soil moisture close to saturation and groundwater rises up to near surface). The surface displacements control points revealed the toe and head units to move faster than the intermediate units. The highest acceleration at the toe was attributed to the external incision agents like stream erosion while cracks and steeper failure plane were responsible for acceleration at the head units. The regression analysis indicated a strong correlation ($R^2 = 79\%$) between surface displacement and depth to groundwater and thus impactful for slope deformation and landslide initiation. The role of rainfall was also significant with long lasting low intensity rainfall being more important than short and high intensity rainfall.

3.1. INTRODUCTION

In chapter 2, the landslide prone regions in Rwanda, possible causes and triggers have been broadly underlined. This chapter provides the key hydro-geological, and meteorological behaviours of the two hillslopes with one deep-seated and one shallow landslides (Karago and Rwaza) in northwestern Rwanda (Figure 3.1). The link between the key hydro-meteorological processes and surface displacement has been tested to provide an insight on the possible implication in landslide warning thresholds definition in Rwanda.

The role of water, either as groundwater in saturated zone or as soil moisture in unsaturated zone, on slope stability has been recognised for many years as highlighted in standard soil mechanics and hydrology books (Craig, 1997). Most slope failures can be induced by high intensity short lasting rainfall as well as low intensity long lasting rainfall. However, the timing of the initiation of slope displacement is controlled by the hydro-geological behaviour of the slope, the infiltration, temporarily storage and subsequent drainage in the slope. A thorough understanding of the slope failure mechanism involves therefore an understanding of the hillslope response to the dynamics of hydro-geological processes (i.e. groundwater and soil moisture).

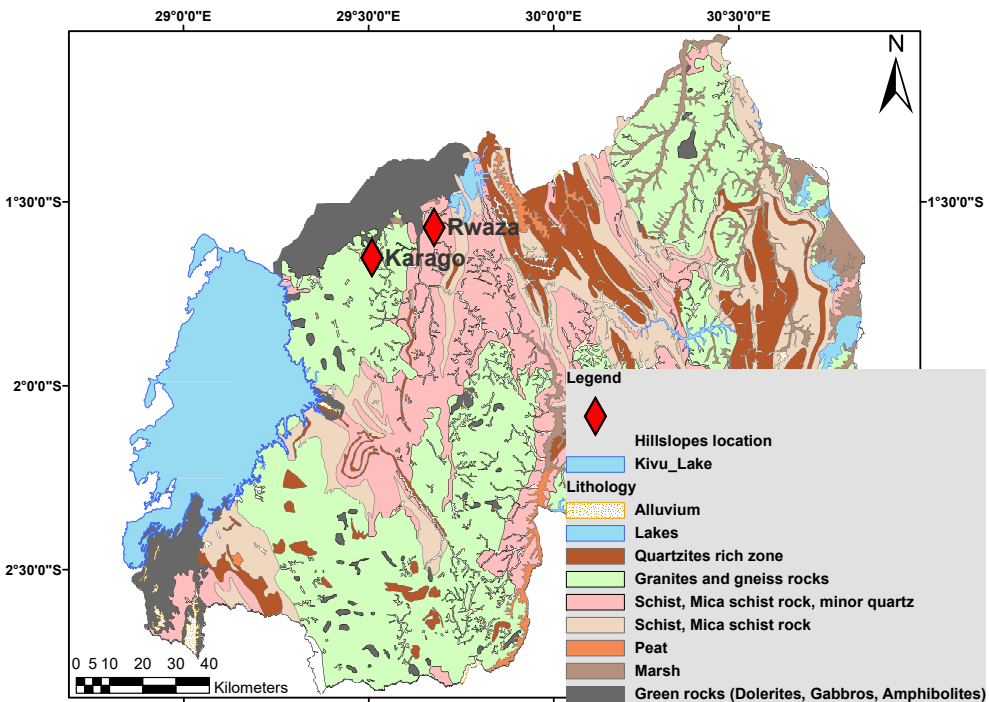


Figure 3.1: Location of the study hillslopes in the north-western region of Rwanda and lithological units

Since Rwanda hillslopes are recognised to be morphologically active landscapes (Depicker et al., 2021c) strongly affected by changes in land use that modify the hydrological

and geotechnical characteristics, this chapter aimed to make an understanding of these characteristics that could lead to the implementation of appropriate landslide prevention measures.

3.2. KARAGO HILLSLOPE

The western region of Rwanda has been identified as the most prone to landslide hazards. About 40% of its surface area is classified as high to very high susceptibility to landslide with more than 1 million of local population exposed to landslide risks (Nsengiyumva et al., 2018). The region receives abundant rainfall with a long-term mean annual rainfall of around 1500mm/yr and an estimated potential evaporation of about 900mm/yr. The Karago hillslope is geographically located at 1°39'3.3 S, 29°30'30.7 E in the western province, downslope of a paved road Mukamira-Ngororero. It is underlain by granite pegmatite geological unit and represents a landslide-prone zone with slow moving rotational landslides. The slope failure initiation occurred in April 2012 and completely failed at the end of March 2016 (Walraven, 2018). Before the slope failure, the area was under Eucalyptus trees that undergo a clear cut. Currently, there is a slow moving landslide with clear rupture, cracks/fissures at the scarp (Figure 3.2).

The scarp of the Karago landslide reveals three main layers, a sand layer, a clay layer and a rock layer, which have been further subdivided into 5 layers (Figure 3.2) based on visual observation and consistency of the soil materials. The first layer, made of light coloured sandy soil deposited from road excavation, contains no plant roots and extends from 0-4.8m. The second layer extending from 4.8-5.5m is made of the original terrain soil, some decaying roots with quite softer sand than the first layer. The third layer from 5.5-6.1m contains very hard yellowish sand with no plant roots. The fourth layer with hard light clay extends from 6.1 to 6.9m deep. The fifth layer, the failure plane of the landslide, is made of saturated soft clay at >6.9m deep. The landslide geometry is about 60m long, 40m wide, and 8m deep. The landslide body was divided into 3 separate units (Figure 3.2): head, main body and toe units for further analysis of the relationship between hydrological processes and slope displacement. On each unit, surface displacement control points were installed for weekly recording of surface displacement rates. Groundwater observation wells were installed on the landslide body as indicated by the letter M in Figure 3.2. Additionally, soil moisture monitoring tubes (T) and other groundwater observation wells (S) were installed along the hillslope for daily monitoring of groundwater and soil moisture. Downslope is a stream that undermines the landslide toe during the rainy season, causing secondary landslides.

3.3. RWAZA HILLSLOPE

The northern region has been also identified as susceptible to landslide hazards. About 23% of its total area is classified as high to very high susceptibility to landslide with more than 600,000 of local population exposed to landslide hazard risks (Nsengiyumva et al., 2018). The north region receives rainfall with a long-term mean annual rainfall of around 1200mm/yr and an estimated potential evaporation of about 800mm/yr. The Rwaza hillslope is geographically located at 29°40'39.9"E 1°34'6.7"S in northern province of Rwanda.

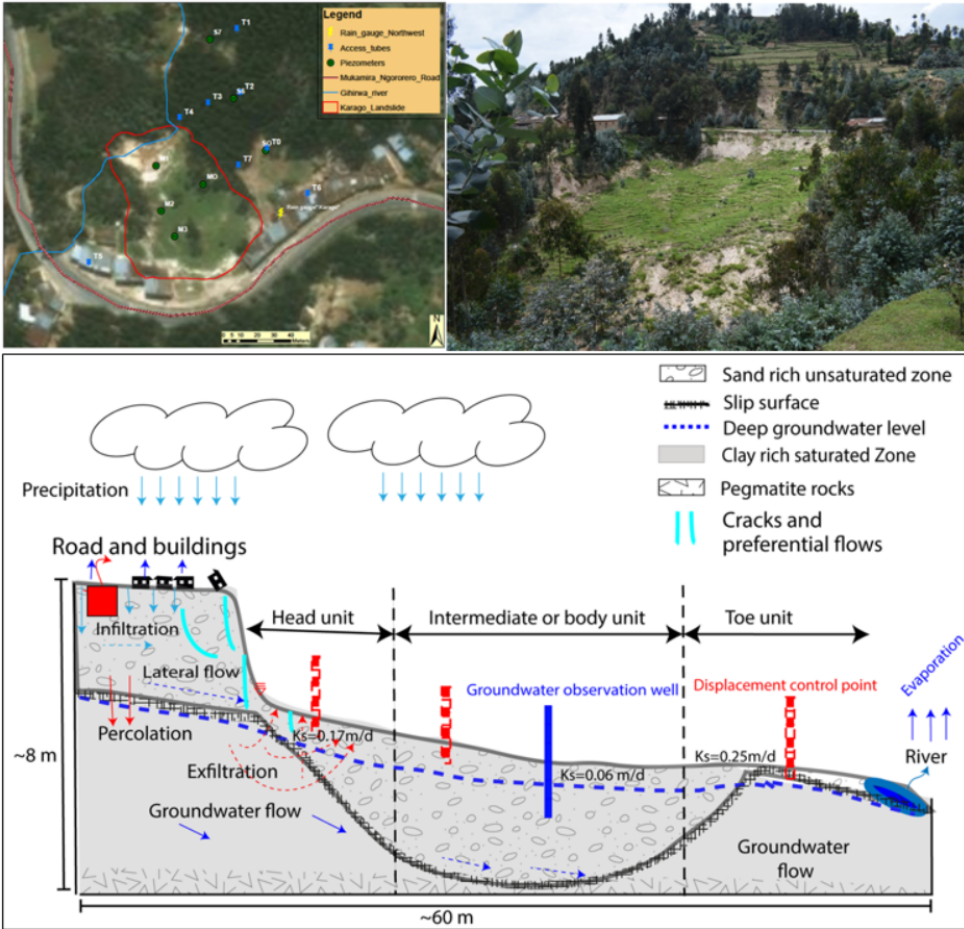


Figure 3.2: Conceptual illustration of Karago hillslope and the location of hydrological monitoring equipment along the hillslope: On the upper left image (Google imagery, 2022), T is the soil moisture access tubes; M and S are groundwater monitoring wells on the landslide body and the stable slope respectively; on the upper right is the photo of Karago hillslope taken in 2018; the conceptual illustration of Karago landslide and its different units, groundwater observation wells and surface displacement control points, K_s is the saturated hydraulic conductivity

The hillslope overlays the mica schists rock that represents a typical landslide prone zone with a slow moving reactivating rotational landslide triggered by heavy rain of April 2017. The landslide is actively advancing downslope during the rainy season and thus exposing the local people to high risks. The slope length of the landslide is about 50m long, 15m wide, and an estimated depth of about 3m. The scarp reveals four layers (Figure 3.3). The first layer ranges from 0 to 0.80m with ploughed soft clay soil layer, plant roots and no stones. The second layer made of very compact clay layer extends from 0.8m to 1.6m with no roots and no stones. The third layer, from 1.6m to 2.8m, contains a mixture of clay soil and stones of about 10-25cm diameter. The fourth layer which is

made of saturated clay layer with few stones, no roots, stands for the slope failure plane located at >2.8m.

3.4. GEOTECHNICAL ANALYSIS

For each hillslope, soil samples were collected from distinct soil layers along the landslide scarp. Geotechnical properties such as soil texture (% sand, % silt and % clay), density, Atterberg limits, and shear strength parameters were tested. The soil texture was tested using sieving and sedimentation methods and classified according to the unified soil classification system (USCS) (Casagrande, 1948). The bulk density ρ_d was tested using the core method and was used to compute the unit weight of soil γ . The cohesion C and angle of internal friction ϕ were derived from direct shear tests. In-situ and laboratory measurement of saturated hydraulic conductivity K_s was undertaken on each soil layer and at different landslide units (head, body, and toe) using the inverse auger hole and bottomless bucket methods (Mirus and Perkins, 2012). The results of these geotechnical parameters and the mean groundwater level were used for the slope stability (factor of safety F_s) analysis using the SLIP5EX model developed by Greenwood et al. (2004); Van Beek and Van Asch (2004). SLIP5EX has been developed to facilitate comparison of various stability analyses given the slope geometry and geotechnical parameterization.

3.5. HYDRO-METEOROLOGICAL PROCESSES AND SLOPE FAILURE

The monitoring of hydro-geological processes was conducted from September 2018 to June 2020 at the Karago hillslope and from April 2019 to June 2020 at the Rwaza hillslope. We installed different hydrological and meteorological monitoring equipment to have an overview of the soil moisture dynamics, groundwater fluctuation and rainfall with respect to the slope failure and landslide occurrence. For the Karago hillslope, we used meteorological data recorded from the installed rain gauge at the hillslope. Data from Ruhengeri meteorological station, located around 5km, were used for the Rwaza hillslope analysis. The soil moisture was monitored through installed soil moisture monitoring tubes using Delta-T, PR2/6 and PR1/6 soil moisture profile probes. At both hillslopes, we installed eight soil moisture monitoring tubes distributed in different land use spots to ensure for the entire hillslope representativity. Both hillslopes are covered by spots of eucalyptus trees, agricultural crops, and built-up areas.

In each land use, two soil moisture monitoring tubes were installed as indicated by the letters T in Figure 3.2 and Figure 3.3. The soil moisture was recorded daily using a disturbed soil moisture profile probe measuring at six depth: 10, 20, 30, 40, 60 and 100cm. We installed also eight groundwater monitoring wells (S and P) in the close proximity of the soil moisture monitoring tubes as shown in Figure 3.2 and Figure 3.3. Additional groundwater monitoring wells were installed on the moving landslide bodies to monitor changes in groundwater levels and their effect on surface displacement. Since the studied landslides occurred before the start of the monitoring period, we referred to another landslide that occurred during the monitoring period to have an insight on the impact of the observed hydrological processes on slope deformation.

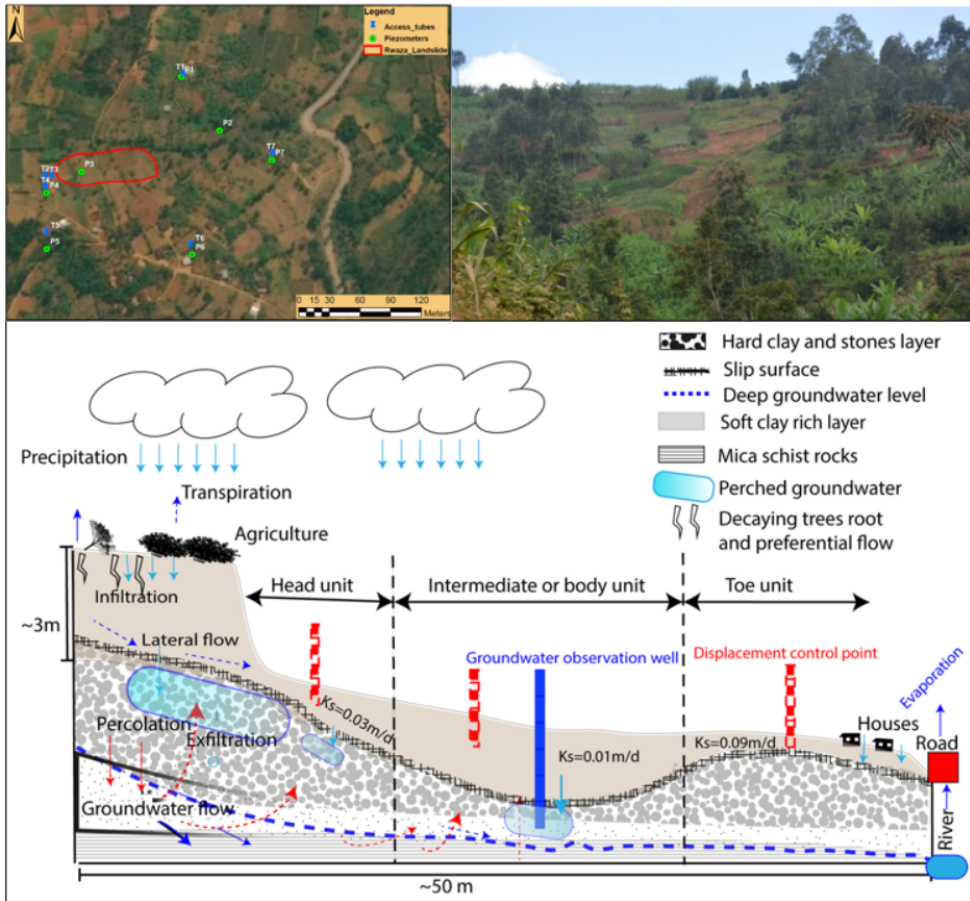


Figure 3.3: Conceptual illustration of Rwaza hillslope, hydrological and displacement monitoring equipment: On the upper left image (Google imagery, 2022), letter T represent the soil moisture access tubes; P (Piezometer) represent the groundwater monitoring wells, the upper right is the photo of Rwaza hillslope taken in 2018; the conceptual illustration of Rwaza landslide and its different units, groundwater observation wells and surface displacement control points, K_s is the saturated hydraulic conductivity

3.6. SLOPE RESPONSE TO HYDRO-METEOROLOGICAL PROCESSES

The measurements of surface displacements have been undertaken to identify the most influential hydrological and meteorological factors. On each landslide body, one line transect of seven displacement control points P1 - P7 were installed at different landslide units from the head, main body to the toe as shown in [Figure 3.2](#) and [Figure 3.3](#). A stable reference control point P0 was installed at a stable upslope and was used as a benchmark for weekly measurement of the relative distance between the control points and reference point using a measuring tape. The weekly measurement of changes in distances between the stable reference point P0 and displacement control points P1 - P7 were conducted for a period of 14 months. The GPS receiver was also used for weekly records of the location of each control points in x, y coordinates which were used for computation of the surface displacement rates with [Equation 3.1](#).

$$D = \sqrt{(X_t - X_{t-1})^2 + (Y_t - Y_{t-1})^2} \quad (3.1)$$

With D the surface displacement rate (mm week^{-1}), X_t and Y_t are the weekly measured locations of the control points (mm) while X_{t-1} and Y_{t-1} are prior measurements (mm). A simple regression analysis was used to test the relation between the hydro-meteorological parameters and surface displacement rates.

3.7. RESULTS AND DISCUSSION

3.7.1. GEOTECHNICAL CHARACTERISTICS

The results of the geotechnical parameters are summarised in [Table 3.1](#) and [Table 3.2](#) for the Karago and Rwaza hillslopes respectively. Based on the results of soil texture, Atterberg limits and according to the unified soil classification system (USCS), the soil of the Karago hillslope is classified as a well graded sand (SW) except the failure plane with poorly graded sand (SP). The soil of the Rwaza hillslope is classified as a low plastic silt (ML). However, referring to the results of texture analysis, some values of the angle of internal friction ϕ and cohesion C derived from the peak stresses at the failure envelope are likely overestimated ([Table 3.1](#)). The overestimation of C was attributed to the additional resistance required to overcome the interlocking and rearranging the soil particles especially in the upper most layer that have undergone artificial consolidation at Karago. It may also due to the size of the coarse-grained soil with some proportion of large soil particles which causes the shearing of individual grains instead of the core soil sample and thus yielding higher values of C ([Kim and Ha, 2014](#)).

Despite that however, by using the tested soil strength parameters C and ϕ , the unit weight γ from each soil layer, the measured mean depth to groundwater, and landslide geometry, the Fellenius method of stability analysis indicated unstable state of the Karago hillslope with a safety factor $F_s < 1$. Further sliding and displacement processes are therefore expected which may affect the neighbouring infrastructures and communities due to the instability of the scarp and the linked retrogressive, enlargement and advancing reactivation processes.

Based on both infinite slope and Fellenius methods, existing conditions of the perched groundwater level (1.4m), geotechnical parameters, and landslide geometry, the scarp of

Table 3.1: Geotechnical parameters and USCS classification of Karago landslide ^a

Layer No	Depth [m]	γ_{sat} [KNm^{-3}]	CU	CC	C [KPa]	ϕ [°]	USCS Class	SL [m]	SA [°]	GW [m]	Fs (ISM)	Fs (FM)
L1	0-4.8	23.6	13	2	18	28	SW					
L2	4.8-5.5	21.6	14	1	0	35	SW					
L3	5.5-6.1	20.6	12	2	0	40	SW	60	26	0.20	1.12	0.90
L4	6.1-6.9	20.7	11	2	0	50	SW					
L5	>6.9	20.7	17	1	11	40	SP					

^aMoist bulk unity weight γ ; Saturated bulk unity weight γ_{sat} ; Groundwater GW (m below surface); Coefficient of uniformity CU; Coefficient of curvature CC; Factor of safety FoS; Slope length SL; Slope angle SA; Well graded sand SW; Infinite slope method ISM; Felenius method FM

Table 3.2: Geotechnical parameters and USCS classification of Rwaza hillslope ^b

Layer No	Depth [m]	γ_{sat} [KNm^{-3}]	WP	WS	WL	IP	IC	Cu [KPa]	ϕ_u [°]	IP	IC	USCS Class	SL [m]	SA [°]	GW	Fs (ISM)	Fs (FM)
L1	0-0.8	27	0.34	0.24	0.39	0.05	1.0	10	26	LP	Hard	ML	50	26	1.4	1.6	1.8
L2	0.8-1.6	25	0.34	0.22	0.43	0.09	1.0	16	23	LP	Hard	ML					
L3	1.6-2.9	23	0.32	0.21	0.40	0.07	1.2	21	23	LP	Very hard	ML					
L4	>2.9	25	0.31	0.19	0.36	0.05	1.0	27	21	LP	Hard	ML					

^bPlastic limit WP; Shrinkage limit WS; Liquid limit WL; Plasticity index IP; Consistency index IC; Water content WP; Low plasticity LP; Low plastic silt ML; Groundwater GW (m below surface)

Rwaza shows marginally stable conditions with $1 < Fs < 2$. This indicates no current retrogression but there is a rather advancing reactivation and thus exposing the downslope local population at high risks.

3.7.2. SOIL MOISTURE DYNAMICS AND LANDSLIDE OCCURRENCE

The dynamics of soil moisture at the Karago and Rwaza hillslopes are summarized in Figure 3.4 and Figure 3.5. The highest soil moisture content at the Karago hillslope was recorded in deep layers from 40-100cm resulting from water exchange between groundwater and unsaturated zone. Contrarily, at the Rwaza hillslope, the highest soil moisture content was recorded in shallow layers, 0-40cm, indicating a very low permeable or impediment layer at around 40cm depth.

The soil moisture response time to rainfall was quite similar in all soil profile layers at the Karago hillslope while at the Rwaza hillslope, shallow layers respond faster than deep layers due to the high clay content that slows down the infiltration rate and the wetting process. Figure 3.4 and Figure 3.5 show that landslide occurred at the peak soil moisture in deep layers at Karago and shallow layers at Rwaza.

Furthermore, the effect of different land uses on soil moisture response was noticed. The soil moisture in deep layers of the built-up and fully grown eucalyptus was frequently lower ($< 0.5 m^3 m^{-3}$) than other land uses due to the low infiltration rate in built up area and high rainfall interception by trees canopy and transpiration in fully grown trees.

The high soil moisture recorded in agricultural land implies the loss of soil strength not only due to the lack of additional strength provided by trees roots but also the built up of high pore water pressure, lack of pressure dissipation processes like transpiration and thus frequent slope failures. While the influence of groundwater is obvious

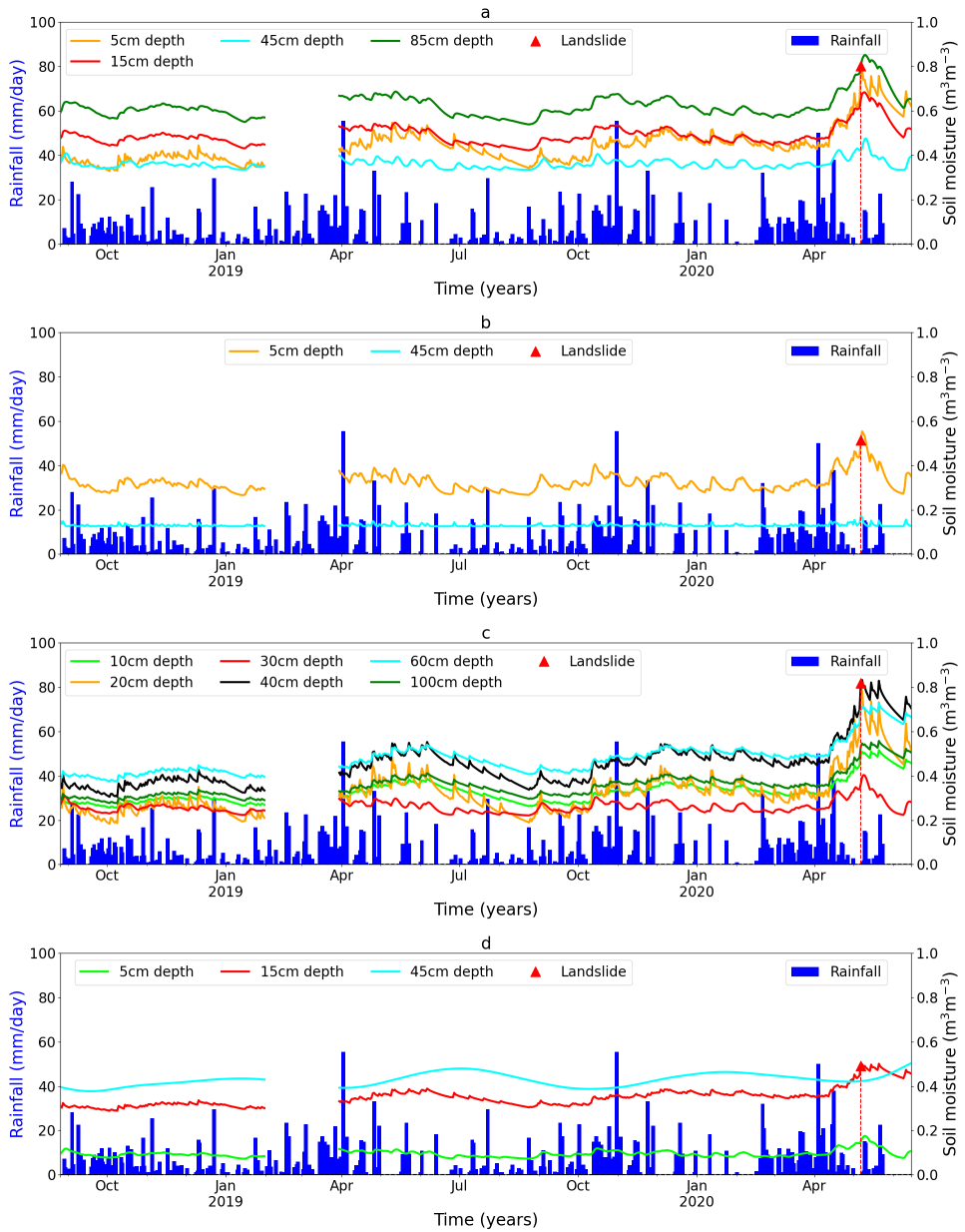


Figure 3.4: Soil moisture content, rainfall and landslide occurrence at Karago hillslope a) agricultural land, b) built up land c) Eucalyptus coppices, d) fully grown Eucalyptus

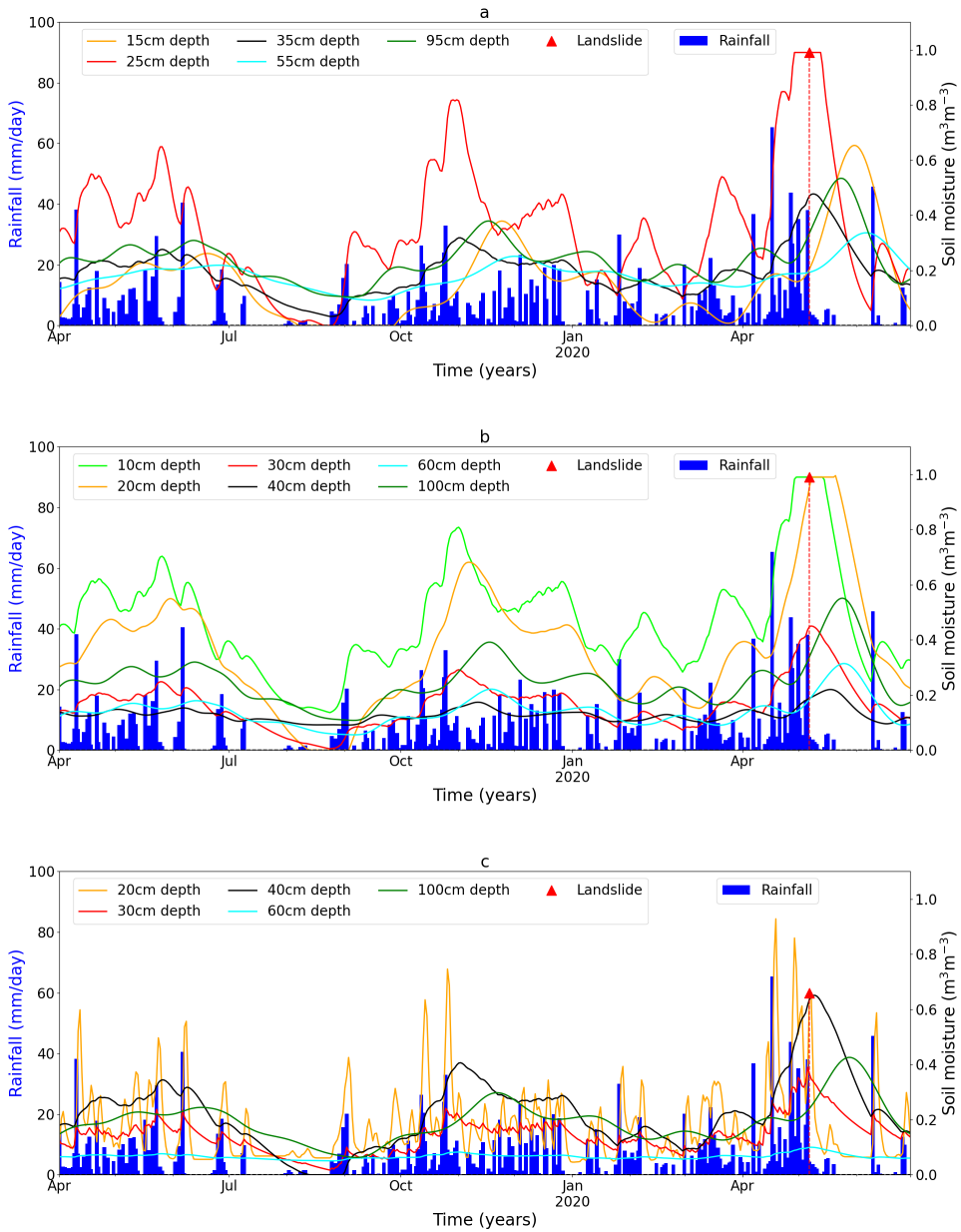


Figure 3.5: Soil moisture content, rainfall and landslide occurrence at Rwaza hillslope a) agricultural land b) built-up land c) Eucalyptus forest land

on shear strength and the factor of safety, the soil moisture content also influence the shear strength through changes in suction forces and the saturation index. This role of soil moisture on suction force and soil strength is not frequently considered probably due to the fact that the main soil strength parameters (c' , ϕ') are not directly affected. Talebi et al. (2007) studied the role of soil moisture by considering the total cohesion C_t , the moist unit weight γ_m , degree of saturation and matric suction on slope stability conditions but found no significant effect on the factor of safety F_s .

3

3.7.3. GROUNDWATER FLUCTUATIONS AND LANDSLIDE OCCURRENCE

Groundwater levels at the Karago hillslope were monitored from three groundwater observation wells located in three land use spots: agricultural land S0, eucalyptus coppices S6 and fully grown eucalyptus trees S7 as presented in Figure 3.6.

At the Rwaza hillslope, the groundwater levels were measured under three land use spots: Agriculture P1, Built-up P2 and Built-up P7 as depicted in Figure 3.7.

The groundwater observation wells installed in built-up land at Karago and in Eucalyptus trees at Rwaza were dry during the entire monitoring period and are not presented here. The results of groundwater levels in different observation wells are plotted in Figure 3.6 and Figure 3.7 for both Karago and Rwaza respectively. The groundwater information indicated shallower and slow responding groundwater levels in agricultural land as compared to other land use. The built-up and forest lands respond very fast to the drying conditions as compared to agricultural lands. This can be explained by the high level of surface evaporation and overland flow in built-up areas and high level of rainfall interception and transpiration in forest areas and thus less groundwater inputs compared to outputs. The landslide occurred at the peak groundwater level and after the long lasting rainfall. The impact of groundwater levels on shear strength (saturated soil) is caused by the increase in pore water pressure that increases shear stress, reduces the effective normal stress and thus soil strength and the factor of safety. Even though the fluctuations of groundwater levels may have been affected by land use type and the linked hydrological processes such as evaporation, transpiration, and interception, these processes are beyond the scope of this study. Furthermore, the impact of tensile strength of roots either from forest trees or crops have not been tested to confirm their effect on soil stresses and strength parameters.

3.7.4. SURFACE DISPLACEMENT

The weekly records of the locations of the displacement control points were carried out from 3rd April 2019 to 27th May 2020 at the Karago hillslope and from 6th April 2019 to 30th June 2020 at the Rwaza hillslope. Figure 3.8 indicates that both the Karago and Rwaza hillslopes undergo obvious surface displacement. The mean horizontal cumulative displacements of the landslide bodies were 340mm and 176mm with a mean weekly displacement rate of about 6.4mm week⁻¹ and 2.7mm week⁻¹, equivalent to about 330mm year⁻¹ and 140mm year⁻¹ at Karago and Rwaza, respectively.

The measurements of displacements show that the landslide body movements have never completely stopped since the start of the continuous monitoring, although the rates reduced significantly during the dry periods from July to August and from January to March as shown by the white background in Figure 3.8. Even though the landslide

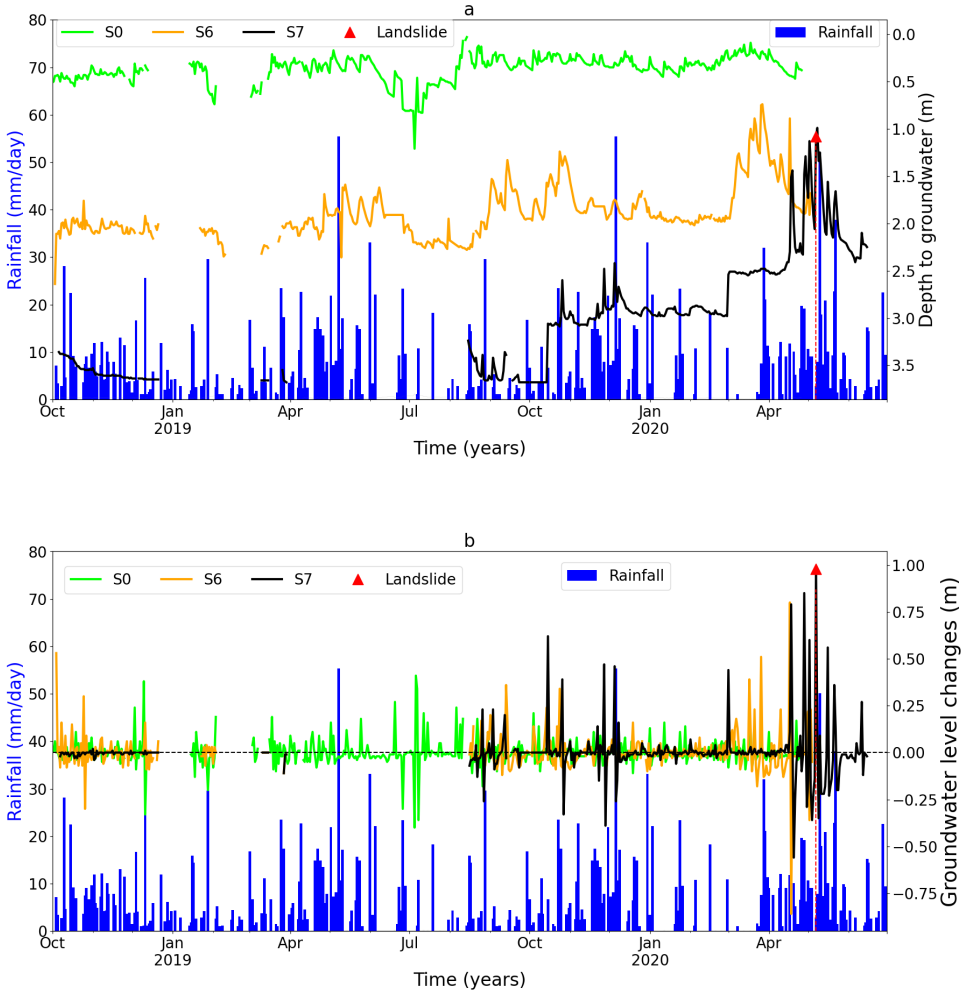


Figure 3.6: Groundwater information from different groundwater observation wells installed in agricultural land (S0), in Eucalyptus coppices (S6) and fully grown eucalyptus (S7) and landslide occurrence at the Karago hillslope: a) depth to groundwater (m below surface) and landslide b) groundwater level changes (m/day) and landslide

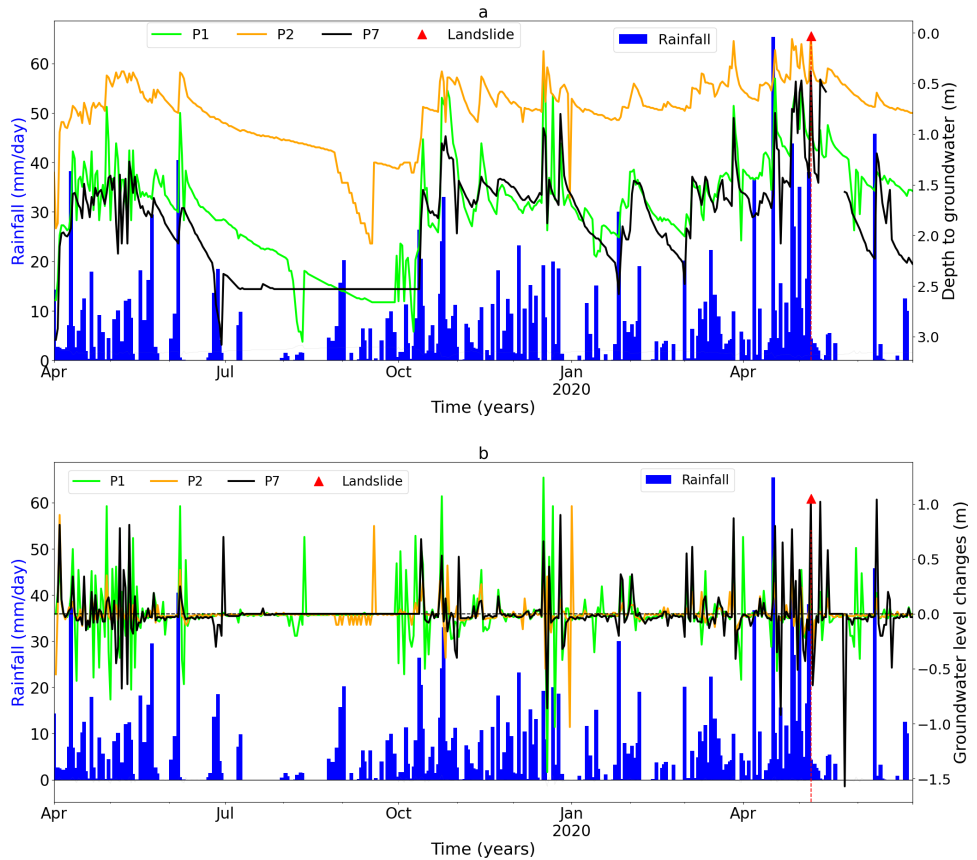


Figure 3.7: Groundwater information from different groundwater observation wells installed in agricultural land (P1), in built-up 1 (P2) and built-up 2 (P7) and landslide occurrence at the Rwaza hillslope: a) depth to groundwater (m below surface) and landslide b) groundwater level changes (m/day) and landslide occurrence

bodies move quite synchronically, the fastest displacement rates for both hillslopes were generally observed in control points P3 and P1 located at the toe unit of the landslides with cumulative displacement of about 540mm and 385mm for the Karago and Rwaza hillslopes, respectively. Note that the control point P1, located at the toe of the Karago landslide, was quickly displaced and lost at the very beginning of the monitoring period. The control points located at the head of the landslide also exhibited faster displacement as compared to the control points located in the intermediate units of the landslide body (P4, P5). This indicates that the intermediate units of landslides are less active as compared to other parts. The intermediate units are quite stable probably due to the new equilibrium created by the reverse slope at the arc shaped failure plane.

The fastest displacement rates at the toe of Karago landslides are accelerated by a stream that undercuts the landslide toe during the rainy season, causing secondary slides. When the destabilised soil materials are removed from the edge of the toe unit, the materials in the intermediate unit starts moving at a distance that depends on the velocity of the destabilised materials, the strength, the angle and the resistance along its path.

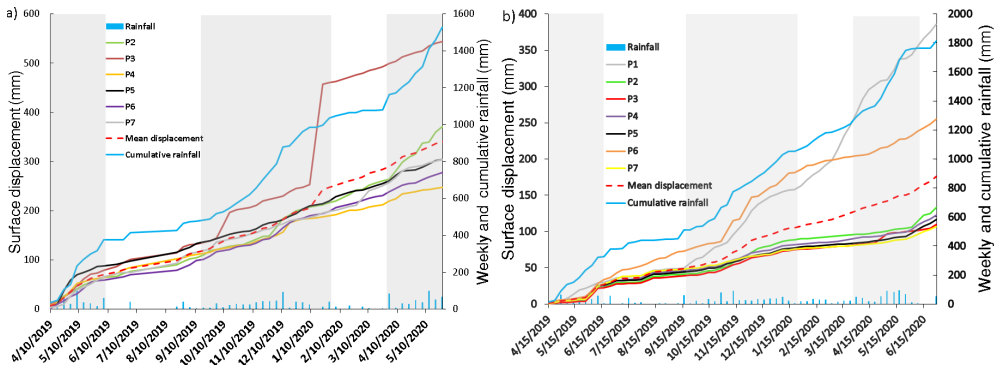


Figure 3.8: Cumulative surface displacement and rainfall at a) Karago and b) Rwaza hillslopes

3.7.5. SLOPE RESPONSE TO HYDRO-METEOROLOGICAL PROCESSES

The recorded surface displacements rates were separated into two classes to facilitate the regression analysis. The values of 10mm/week and 5mm/week were subjectively found as separating lines between the two classes. The first class with displacement rates <10mm/week and <5mm/week were hypothesised to be small and referred to as “minor displacements” while the class with >10mm/week and 5mm/week were hypothesised to be significant and referred to as “major displacements”. The relationships between the tested hydrological processes and the defined classes of surface displacement are shown in Figure 3.9 and Figure 3.10.

At the Karago hillslope, the regression analysis (Figure 3.9) indicated a strong negative correlation ($R^2=0.79$) between groundwater levels and major displacement rates.

The regression model express that 79% of the proportion of the major displacements could be explained by the depth to groundwater. The model indicates that the major displacement rates decrease with increasing depth to groundwater and that the former

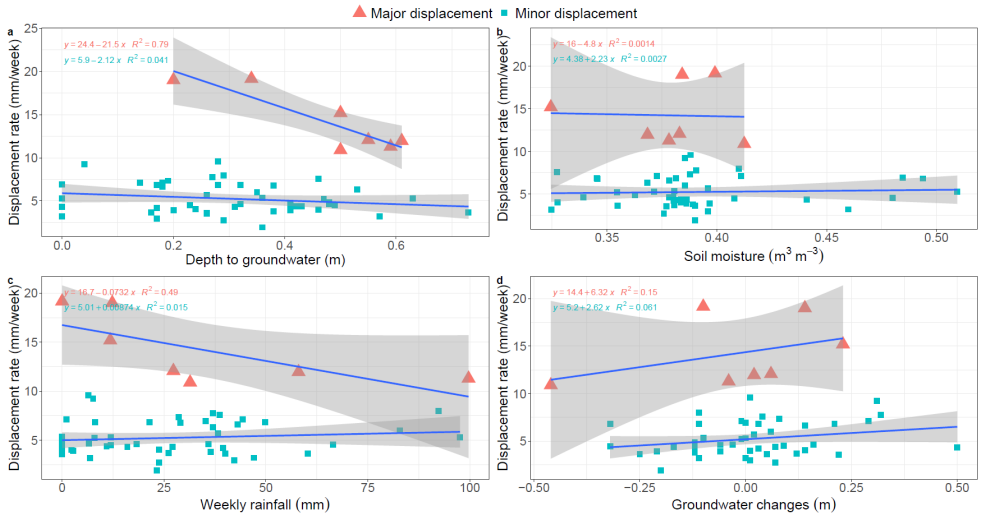


Figure 3.9: Karago hillslope: Regression analysis between hydro-meteorological processes and slope displacement

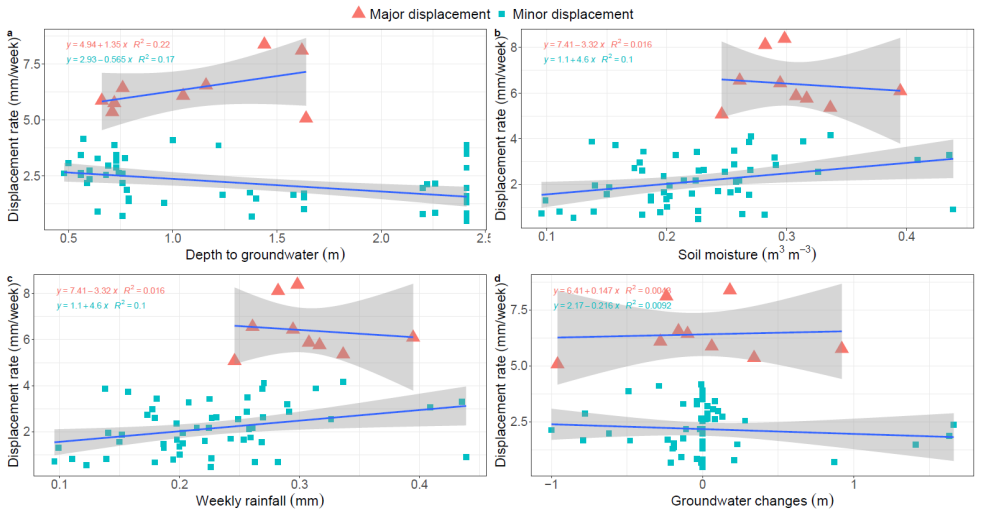


Figure 3.10: Rwaza hillslope: Regression analysis between hydro-meteorological processes and slope displacement

could be easily predicted using the latter. Contrarily, there was no correlation between minor displacements and groundwater. However, it is generally observed that the majority of the minor displacements occur when the groundwater rises to near surface while the major displacements frequently occur during the groundwater drawdown phase at Karago hillslope. A negative correlation was also found between rainfall and displacement rates. It indicated that only about 50% ($R^2 = 0.50$) of the variance in major displacement could be explained by the rainfall information.

Most of the displacement either major or minor occurred at low long-lasting rainfall intensities between 20-60mm/week. This explains that the long lasting low rainfall intensity have sufficient time to infiltrate and rise up the groundwater and pore water pressure and thus inducing more surface displacement as compared to short and high intensity rainfall with frequent overland flow than infiltration. The soil moisture information in the unsaturated zones showed no significant impact on surface displacement at the Karago hillslope. This suggests that the movement of deep seated landslides in sand rich soils like Karago (>6.9m) are more linked to groundwater rather than rainfall and soil moisture. The groundwater induced displacement frequently occurs in a considerable time after rainfall as function of the rainfall infiltration time, the distance between the surface and the ground water table, the hydraulic properties of the soil materials and the depth of the slip plane.

Contrarily, at the Rwaza hillslope whose slip plane is shallow (2.8m) with clay dominated soil texture, the major displacement occurred at higher soil moisture $> 0.25m^3/m^3$. This suggests that in clay dominated soil textures, shallow landslides are likely due to the above normal soil moisture or rainfall. Similar findings were noted by [Bordoni et al. \(2015\)](#), who indicated that shallow landslides with $< 2m$ thickness are easily induced by rainfall due to the progressive infiltration of the rainwater up to the hard layer while deep seated landslide are frequently induced by groundwater fluctuations.

Despite the role of hydro-meteorological processes as accelerators, it has to be noted that the minor surface displacements frequently occur due to gravity force in sloppy areas.

3.8. CONCLUSION

This chapter aimed to understand the hydro-geological and meteorological processes and the relationship thereof using two typical hillslopes (Karago and Rwaza prone to landslides in northwestern Rwanda. The geotechnical characterization indicated instability conditions at the Karago hillslope and marginally stable conditions at the Rwaza hillslope. It was observed that landslides occur during the wettest period (i.e. soil moisture close to saturation and groundwater rises to near surface). Even though, the landslide body masses moved quite synchronically, the surface displacements control points revealed the toe and head units to move faster than the intermediate units. The highest acceleration at the toe was attributed to the external incision agents like stream erosion while cracks and steeper failure plane are responsible for acceleration at the head unit. The regression analysis indicated a strong correlation between surface displacements and depth to groundwater at Karago and thus important for landslide initiation thresholds definition. The role of rainfall was also significant with long lasting low intensity rainfall being more impactful than short and high intensity rainfall.

4

LANDSLIDE PRECIPITATION THRESHOLDS IN RWANDA

This chapter is based on: Uwihirwe, J., Hrachowitz, M. and Bogaard, T. A.: Landslide precipitation thresholds in Rwanda, *Landslides*, (December 2019), doi:10.1007/s10346-020-01457-9, 2020.

Abstract

This chapter aims to use landslide and precipitation data in an empirical-statistical approach to (1) identify precipitation-related variables with the highest explanatory power for landslide occurrence and (2) define both trigger and trigger-cause hydro-meteorological thresholds for landslides in Rwanda. Receiver operating characteristics (ROC) and area under the curve (AUC) metrics were used to test the suitability of a suite of precipitation-related explanatory variables. A Bayesian probabilistic approach, maximum true skill statistics and the minimum radial distance were used to determine the most informative threshold levels above which landslides are highly likely to occur. The results indicated that the event precipitation volumes E , cumulative one day rainfall (RD_1) that coincide with the day of landslide occurrence and 10 days antecedent precipitation (API_{10}) are variables with the highest discriminatory power to distinguish landslide from no landslide conditions. The highest landslide prediction capability in terms of true positive alarms was obtained from single rainfall variables based on trigger-based thresholds. However, that predictive capability was constrained by the high rate of false positive alarms and thus the elevated probability to neglect the contribution of additional causal factors that lead to the occurrence of landslides and which can partly be accounted for by the antecedent precipitation indices. Further combination of different variables into trigger-cause pairs and the use of suitable hydro-meteorological thresholds in bilinear format improved the prediction capacity of the real trigger-based thresholds.

4.1. INTRODUCTION

In chapter 3, precipitation was identified as the most important trigger and the main source of other hydrological processes that induce the slope displacement and landslides in Rwanda. It is worthwhile to test its value in landslide hazard assessment and its predictive capability using empirical-statistical approaches. Empirical-statistical models defined from precipitation data have been widely adopted to define the landslide early warning thresholds at local (Crozier, 1999; Prenner et al., 2018; Mirus et al., 2018b,a); regional (Martelloni et al., 2012; Roccati et al., 2018; Ciavolella et al., 2016); national (Robbins, 2016; Peruccacci et al., 2017; Rosi et al., 2016; Brunetti et al., 2010; Hong et al., 2017); and global scales (Caine, 1980; Guzzetti et al., 2008). These empirical-statistical models typically relate precipitation characteristics, such as cumulative event precipitation, precipitation intensity and precipitation duration or combination thereof to the occurrence of landslides. However, some limitations are associated with these widely used precipitation thresholds due to the fact that empirical thresholds are mainly based on the precipitation event during which a landslide occurred, which is in reality the actual landslide trigger. Such landslide trigger-based thresholds include the intensity-duration (I-D) (Caine, 1980; Guzzetti et al., 2007, 2008; Ma et al., 2018; Hong et al., 2017; Roccati et al., 2018) event-duration (E-D) and event-intensity (E-I) (Peruccacci et al., 2017; Robbins, 2016).

Landslide trigger-based thresholds have been increasingly recognized to neglect the causal hydrological processes that predispose the slope to failure (Peres et al., 2017; Bogaard and Greco, 2018; Mostbauer et al., 2018). To include this, a number of researchers considered the possible hydrological causes in terms of antecedent precipitation, catchment storage, soil moisture indices and or soil water status prior to the landslide triggering event or storm (Crozier, 1999; Glade, 2000; Aleotti, 2004; Ciavolella et al., 2016; Mostbauer et al., 2018). These temporally variable hydrological conditions, define the hydrological predisposition of a region to landslide occurrence and are thus, besides its geomorphological predisposition the root cause of landslide occurrence in a region. The hydrological conditions are defined prior to the landslide triggering conditions and then combined to make landslide trigger-cause based thresholds referred to as hydro-meteorological thresholds. As a first step towards the integration of landslide hydrological processes in landslide empirical statistical thresholds in Rwanda, this chapter explores the usefulness of antecedent precipitation index to account for the soil wetness state prior to the triggering precipitation conditions. Specifically, we aimed to:

1. identify precipitation-related variables with the highest explanatory power for landslide occurrence in Rwanda
2. quantify both, landslide trigger-based and cause-trigger-based hydro-meteorological thresholds as a first step towards robust landslide early warning systems in Rwanda

4.2. LANDSLIDE DATA

4.2.1. LANDSLIDE INVENTORY

Part of the landslide inventory for Rwanda was accessed from the NASA global landslide catalogue (<https://data.nasa.gov/Earth-Science/Global-Landslide-Catalog/>)

h9d8-neg4, last access: 26 June 2019) uploaded mainly by the LIWEAR project. The catalogue was extended through compilation of other rainfall-induced landslides as reported from local newspapers, blogs, technical reports and field observations. For the catalogue extension, we followed the global landslide inventory methods using standard indices adopted by Kirschbaum et al. (2012) and Monsieurs et al. (2018c). Seven elements were recorded for each landslide: i) landslide location (e.g. village, cell, sector, district or town); ii) time of occurrence (date); iii) triggering event (e.g. rainfall); iv) landslide type based on Hungr et al. (2014) classification depending on the availability of background information; v) latitude and longitude with relative locational accuracy; vi) information about the impact (number of fatalities, injuries and damages); vii) the accessible source of information was also mentioned with links to online source of information. Only hazardous (fatal and highly damaging) landslides are mostly reported while nonhazardous ones are likely to be missed. Based on the inventory, about 99% of landslides occurred from 2006 while the remaining occurred far before 2006. Therefore, 2006 was taken as the threshold year and landslides that occurred between 2006 and 2018 were used in this Chapter.

4.2.2. RAINFALL AND REPRESENTATIVE RAIN GAUGES

We used daily rainfall time series recorded from 35 rain gauges in Rwanda over a period of 13 years from 2006 to 2018. The rainfall dataset was accessed from Rwanda Meteorology Agency. Among the 35 rain gauges, representative rain gauges (Figure 2.1) were selected to identify the rainfall conditions for each or multiple landslide. The representative rain gauges were selected based on their weights (W) estimated based on the rainfall event volume E (mm) until the landslide day, the distance between rain gauge and landslide d (mm), and duration D (days) firstly proposed by Melillo et al. (2018) using Equation 4.1.

$$W = \frac{E^2}{d^2 D} \quad (4.1)$$

The number of rain gauges to be weighted for each landslide were chosen based on their location inside the buffer radius around the landslide location. The higher the weight, the higher the chance for the rain gauge to represent the rainfall conditions responsible for the landslide. Based on the highest weights (W), 22 rain gauges out of 35 were found to be representative for the rainfall conditions responsible for the landslide occurrence. A single dataset of rainfall conditions from 22 rain gauges was made to pinpoint the landslide triggering conditions from non-triggering conditions.

4.3. METHODOLOGY

4.3.1. DEFINITION OF LANDSLIDE RAINFALL CONDITIONS

The landslide conditions were divided into 4 categories based on their time scale. The first category considers the entire rainfall event during which, one or more landslides occurred and is referred to as the maximum probable rainfall event (MPRE). The second, third and fourth categories respectively consider the accumulation of very recent rainfall over the last 3 days (RD_3), 2 days (RD_2), and 1 day (RD_1) with the last day coinciding with

the day of landslide occurrence. The RD_3 , RD_2 and RD_1 for each day during the 2006-2018 study period were calculated, irrespective of a landslide occurring or not. MPRE was here defined as individual periods of days with recorded rain $\geq 1 \text{ mmd}^{-1}$ interrupted by dry periods of at least two dry days. The rainfall event E (mm/E) was then computed as the accumulated rainfall during each MPRE which is equivalent to the event duration D (d). The event intensity (mmd^{-1}) was then computed as a ratio of E and D . Landslide causal conditions were represented by the Antecedent Precipitation Index (API) considered as a proxy for soil moisture accumulation. The API was calculated as a cumulative rainfall occurring over a predefined time periods prior to the landslide triggering conditions. For this study, time periods of $T=30, 10$ and 5 days were considered to define the API_{30} ; API_{10} and API_5 , respectively. A decay coefficient $k=0.95$ was used to estimate $API_T(t)$ for each day t over the study period according to the Equation 4.2.

$$API_T(t) = R(t) + kR(t-1) + k^2R(t-2) + k^3R(t-3) \dots R(t-T) \quad (4.2)$$

Where R is the daily rainfall (mmd^{-1}), k is the decay coefficient (-), t is the individual day and T is the antecedent accumulation period (d) (30, 10 and 5d) prior to the starting day of the rainfall triggering conditions (MPRE, RD_3 , RD_2 , and RD_1).

4.3.2. QUANTIFICATION OF LANDSLIDE EXPLANATORY PRECIPITATION VARIABLES

The landslide explanatory precipitation variables which include the landslide causal (pre-disposing) and triggering conditions were explored using receiver operating characteristic (ROC) curves (Hong et al., 2017; Postance and Hillier, 2017; Mirus et al., 2018a; Prencher et al., 2018). The ROC is a graphical representation created by plotting the false positive rate (FPR) of wrongly predicted landslides against the true positive rate (TPR) of correctly predicted landslides. The ROC curves are made of a suite of possible threshold levels at which a balance between each threshold's true positive rate and the corresponding false positive rate is evaluated. The area under the ROC curve (AUC) is used as an indicator of the variable performance, where a perfect test variable would result in an $AUC = 1$. The AUC indicates the capacity of the considered test variable to correctly distinguish landslide from no-landslide conditions. Thus, the AUC was used on the one hand as a statistical metric to compare the tested precipitation variables against random guessing i.e $AUC = 0.5$. On the other hand, it was used to find precipitation-related variable with the highest explanatory power for landslide. The true positive rate (TPR) associated with each threshold level on ROC curves is calculated with Equation 4.3.

$$TPR = \frac{TP}{TP + FN} \quad (4.3)$$

The false positive rate (FPR) is calculated by Equation 4.4.

$$FPR = \frac{FP}{FP + TN} \quad (4.4)$$

Where TP are true positives i.e. the number of landslides correctly predicted by the threshold; FN are false negatives, and thus the number of landslides that occurred in

reality but that were not predicted, i.e. the number of landslide triggered by rainfall conditions below the defined threshold. FP are false positives i.e. incorrect predictions of landslide occurrence by the threshold model while in reality there was no landslide reported. TN are true negatives, i.e. are correct predictions of no landslide occurring.

4.3.3. THRESHOLD DEFINITION TECHNIQUES

Since the AUC only indicate which precipitation variable or combination of variables that can significantly distinguish landslide from no landslide and the ROC curves indicating all possible thresholds and their respective balance of TPR and FPR, it is also necessary to define the optimum threshold levels above which landslide are high likely to occur. We used 3 different techniques to do that: Bayesian probabilistic approach (Prob), maximum true skill statistic (TSS) and minimum radial distance (Rad). The Bayes' theorem defines the conditional probability of an event A (here: landslide occurrence) given an event B, here represented by different precipitation variables. To reduce the high rainfall data scattering, specific magnitude-frequency distributions for each rainfall variable were defined using bins. Based on the extent of the dataset, bins of 5 mm were used for E, RD, and API while 2mm d^{-1} and 2d were used for event intensity and event duration respectively. The specific magnitude-frequency pairs were then converted into probabilities based on Bayes terminologies. The Bayes prior probability of an event A, $P(A)$ stands for the global probability of landslide to occur regardless of the event B. If N_{AT} denotes the total number of landslide conditions (total number of landslides) and N_{BT} the total number of rainfall events (landslide + no landslide conditions) recorded over the predefined period (here 2006-2018), $P(A)$ is calculated with Equation 4.5.

$$P(A) = \frac{N_{AT}}{N_{BT}} \quad (4.5)$$

If we define also N_{BS} as the number of events B with specific magnitude (e.g: 20 mm < E < 25 mm), the prior probability for an event B denoted as $P(B)$ is thus expressed with Equation 4.6 and indicate the probability to have an event B regardless of whether landslide occurs or not.

$$P(B) = \frac{N_{BS}}{N_{BT}} \quad (4.6)$$

The conditional probability $P(A|B)$ expressed in Equation 4.7 indicates the probability for landslide occurrence given the specific magnitude of rainfall variable.

$$P(A|B) = \frac{P(B|A) \cdot P(A)}{P(B)} \quad (4.7)$$

$$P(B|A) = \frac{P(A|B) \cdot P(B)}{P(A)} \quad (4.8)$$

or

$$P(B|A) = \frac{N_{AS}}{N_{AT}} \quad (4.9)$$

With N_{AS} denoting the number of landslides that occur within a specific rainfall magnitude BS (e.g number of landslide that occurs when rainfall intensity was between 8 and

10 $mm d^{-1}$ ($8 < I < 10$). The probabilistic threshold values are defined by comparing the prior $P(A)$ to the posterior probability $P(A|B)$ (Berti et al., 2012; Robbins, 2016; Peres et al., 2017). If the posterior landslide probabilities $P(A|B)$ differ from the prior landslide probability $P(A)$, the rainfall variable (B) has a significant effect on landslide occurrence (A). Contrary, when $P(A|B)$ is objectively smaller or equal to $P(A)$, there is no significant effect of variable B. The probabilistic threshold value for a variable B to initiate landslide (A) is objectively taken as the specific magnitude or level at which the posterior probability distribution curve $P(A|B)$ goes beyond the prior probability distribution curve of $P(A)$ as shown in Figure 4.1. The cumulative probability curve $cumP(B|A)$ indicates the probability to have landslides below and above the threshold level of B, respectively. This is equivalent to the false negative (FNR) and true positive rates (TPR) on the ROC curve as expressed by equations Equation 4.10 to Equation 4.12.

$$FNR = cumP(B|A) \quad (4.10)$$

or

$$FNR = \frac{FN}{FN + TP} \quad (4.11)$$

$$TPR = 1 - cumP(B|A) \quad (4.12)$$

The thresholds definition based on the maximum true skill statistics TSS (Ciavolella et al., 2016; Peres et al., 2017) and the minimum radial distance Rad (Postance and Hillier, 2017; Mirus et al., 2018a) have been particularly used in landslide studies. The true skill statistics is expressed as a balance between the true positive rate and false positive rate as indicated on Equation 4.13 and its maximum value indicate the optimum threshold. For a perfect threshold, the TSS would be a unity, i.e. with zero false positive rate. On the ROC curve, the radial distance (Equation 4.14) indicates the relative distance from the defined threshold to the optimum point whose TPR is a unit and FPR is zero. Thus, the minimum radial distance would be zero for a perfect threshold (Postance and Hillier, 2017).

$$TSS = TPR - FPR \quad (4.13)$$

$$RAD = \sqrt{FPR^2 + (TPR - 1)^2} \quad (4.14)$$

4.3.4. HYDRO-METEOROLOGICAL/CAUSE-TRIGGER-BASED THRESHOLDS DEFINITION

The cause-trigger-based thresholds were defined by combining the best performing thresholds selected from one of the techniques described in section 4.3.3. According to Postance and Hillier (2017), the ideal landslide warning threshold is the one leading to the maximum positive alarms (TP), minimum missed alarms (FN) and also with minimum number of false alarms (FP). Based on these criteria, the most realistic threshold was selected among the ones defined either by Bayesian probabilistic approach, maximum true skill statistics or minimum radial distance. These thresholds were plotted on both axis of landslide triggering and causal variables in Y, X pairs as I-API₃₀, I-API₁₀, I-API₅,

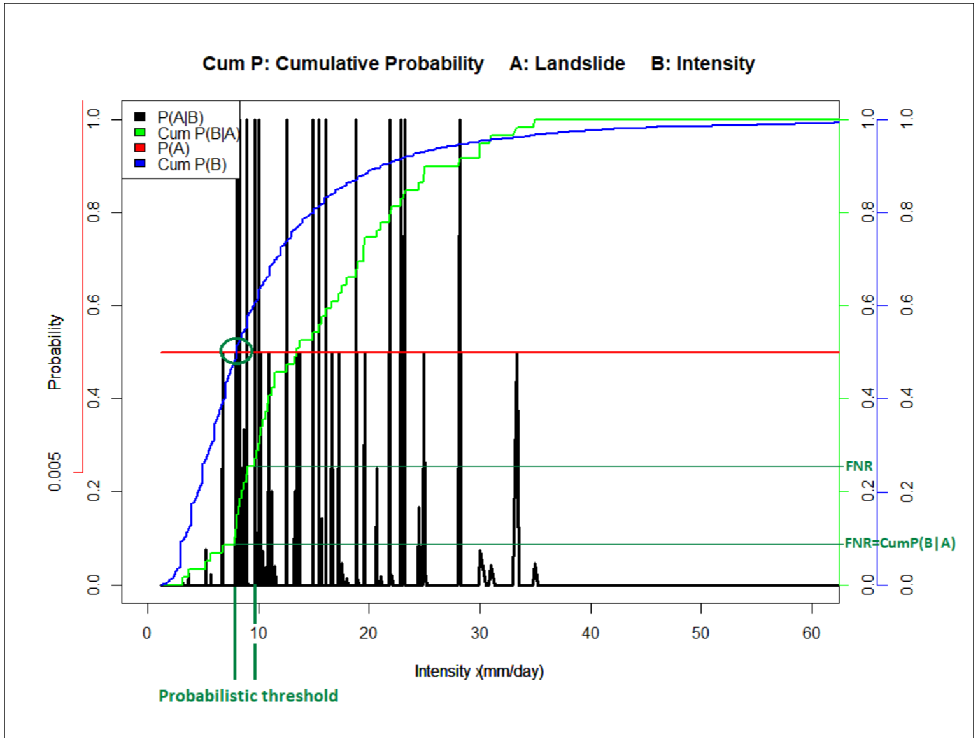


Figure 4.1: Probabilistic threshold definition: on X axis is the magnitude of event intensity I ; on Y primary axis: the red constant curve is the prior landslide probability $P(A)$; the black axis represent the conditional probability to have landslide given a specific magnitude of I ($P(A|B)$). On secondary Y axis: the light green axis is the cumulative probability to have an event intensity I of specific magnitude given that landslide occurs $Cum P(B|A)$; the blue axis represent the cumulative probability of I regardless of landslide occurrence or not ($Cum P(B)$). The dark green sphere and 2 vertical lines indicate the specific magnitude or level at which $P(A|B)$ goes beyond $P(A)$ and this represent the probabilistic threshold intensity which is between 8 and 10 mm/day. The dark green horizontal lines indicate the resulting false negative rate equivalent to the $Cum P(B|A)$ represented by the light green curve.

E-API₃₀, E-API₁₀, E-API₅, RD₁-API₃₀, RD₁-API₁₀, RD₁-API₅, RD₂-API₃₀, RD₂-API₁₀, RD₂-API₅, RD₃-API₃₀, RD₃-API₁₀, RD₃-API₅. To evaluate the performance of the newly adopted method, a confusion matrix for each pair was performed and the resulting rate of positive alarms, false alarms, missed alarms and true negatives were quantified.

4.4. RESULTS AND DISCUSSION

4.4.1. LANDSLIDE EXPLANATORY RAINFALL VARIABLES AND THRESHOLDS

A total number of 9353 MPRE from 34438 rainy days (RD) that include landslide and no landslide conditions were recorded in Rwanda from 2006 to 2018. From this MPRE and RD catalogue, 59 MPRE and 60 RD (total number of landslides) were highlighted as conditions responsible for the occurrence of one or more landslides recorded in the inventory. The area under the curve (AUC) of each variable of the MPRE and RD in Fig-

Figure 4.2 indicated the probability of all test variables to correctly distinguish landslide from no-landslide conditions. The AUC was highest for entire rainfall event volume E and the cumulative 1day rainfall RD_1 as compared to other landslide triggering precipitation variables. This suggests that in the study region the cumulative rainfall received on the day of a landslide has more impact to trigger landslides than previously recorded rainfall. It also indicates that shorter timescale triggering conditions are more relevant for landslide occurrence than longer timescales. Even though, rainfall event volumes E have also scored higher at distinguishing landslide from no-landslide conditions, it is critical to note that E has variable timescales that should be normalised by the event duration D and thus ending up with event intensity I as the most informative test variable.

The overall performance of antecedent precipitation indices (API), here considered as landslide cause, indicate that the cumulative rainfall over 10 days (API_{10}) prior to the landslide triggering conditions has the most influential effect on landslide occurrence as compared to longer (30days) and shorter (5days) antecedent periods. On one hand, this can be attributed to the hydro-geotechnical properties of soil like hydraulic conductivity, permeability and soil texture that contribute to subsequent interplay between infiltration, evaporation and drainage and thus the drawdown of the longer antecedent precipitation (API_{30}) period. On other hand, this may indicate the lags in water flow to reach the critical layer of the regolith for shorter periods like API_5 . The ROC curves in Figure 4.2 indicates the possible threshold levels for each tested variable and the respective balance of TPR and FPR. The optimum threshold levels above which landslide are high likely to occur are presented with different symbols on the curve depending on the technique used. The detailed information of the defined optimum thresholds is summarized in Table 4.1.

The maximum true skill statistics (TSS) indicated that landslide are high likely to occur when the cumulative rainfall event volume E goes beyond 29.9 mm/E and this threshold level resulted to about 93% of correct predictions of landslide i.e. true positive alarms and about 41% of false alarms. A similar threshold was obtained based on Prob, indicating the highest probability for landslides to occur beyond 30-35 mm/E with a mean value of 32.5 mm/E. However, the minimum radial distance (Rad) approach revealed a higher threshold level of about 45.9 mm/E associated with quite lower positive alarms (76.3%) in favour of a lower rate of false alarms (26.2%). From TSS, Prob and Rad, the critical event duration was inferred to be around 4 days which would lead to the normalized event E_n thresholds of about 7.5 mmd^{-1} , 8.1 mmd^{-1} and 11.5 mmd^{-1} respectively. These thresholds are similar to the defined event intensity thresholds of 7.9 mmd^{-1} , between $8-10 \text{ mmd}^{-1}$ and 10.1 mmd^{-1} respectively from TSS, Prob and Rad. Based on daily rainfall (RD) variables in Table 4.2, the optimum threshold levels above which landslide are high likely to occur were 12.5 mmd^{-1} (Prob), 20.9 mmd^{-2} (Rad) and 27.0 mmd^{-3} (TSS and Rad) for RD_1 , RD_2 and RD_3 respectively.

The optimum API threshold levels were also defined as indicated on Figure 4.2 and Table 4.1 and Table 4.2. The most informative thresholds were 45.5 mm (Prob), 23.6mm (Rad) and 7.7mm (Rad) for API_{30} , API_{10} and API_5 respectively prior to the landslide triggering event (MPRE). The API thresholds for RD variables are also presented in Table 4.2. It has to be understood that the API thresholds indicate the levels below which no influence of antecedent precipitation would be expected to contribute to the landslide trig-

Table 4.1: MPRE landslide explanatory precipitation variables and their thresholds defined using probabilistic approach (Prob), maximum true skill statistics (TSS) and minimum radial distance (Rad)

Variables	Bayesian probabilistic thresholdp					Maximum True skill statistics (TSS)					Minimum radial distance (Rad)				
	Threshold	1-P(B/A)/TPR	FPR	TSS	Rad	Threshold	TPR	FPR	TSS	Rad	Threshold	TPR	FPR	TSS	Rad
1. Trigger-based thresholds															
Event E (mm E ⁻¹)	32.5	0.847	0.376	0.472	0.406	29.95	0.932	0.409	0.523	0.415	45.90	0.763	0.262	0.501	0.353
Intensity (mmd ⁻¹)	9.00	0.746	0.419	0.327	0.490	7.87	0.915	0.517	0.399	0.524	10.05	0.712	0.362	0.350	0.463
Duration (days)	4.00	0.695	0.279	0.415	0.414	4.50	0.695	0.279	0.415	0.414	4.50	0.695	0.279	0.415	0.414
2. Cause based thresholds															
API ₃₀ (mm)	47.50	0.712	0.485	0.227	0.564	66.81	0.559	0.286	0.273	0.526	66.81	0.559	0.286	0.273	0.526
API ₁₀ (mm)	37.50	0.475	0.201	0.273	0.563	37.73	0.475	0.199	0.276	0.562	23.57	0.627	0.399	0.228	0.546
API ₅ (mm)	12.50	0.542	0.283	0.260	0.538	12.49	0.542	0.283	0.260	0.538	7.65	0.644	0.398	0.247	0.534

gering conditions. However, it has to be noted that API thresholds are very sensitive to the timescale of the triggering conditions. Shorter time scale triggering conditions like RD_1 require higher threshold levels of API as compared to RD_2 or MPRE. This shows that relying on trigger-based thresholds for landslide early warning could lead to biased results rather than relying more on API's thresholds. Thus, shorter timescale triggering conditions should be preferred as confirmed based on AUC.

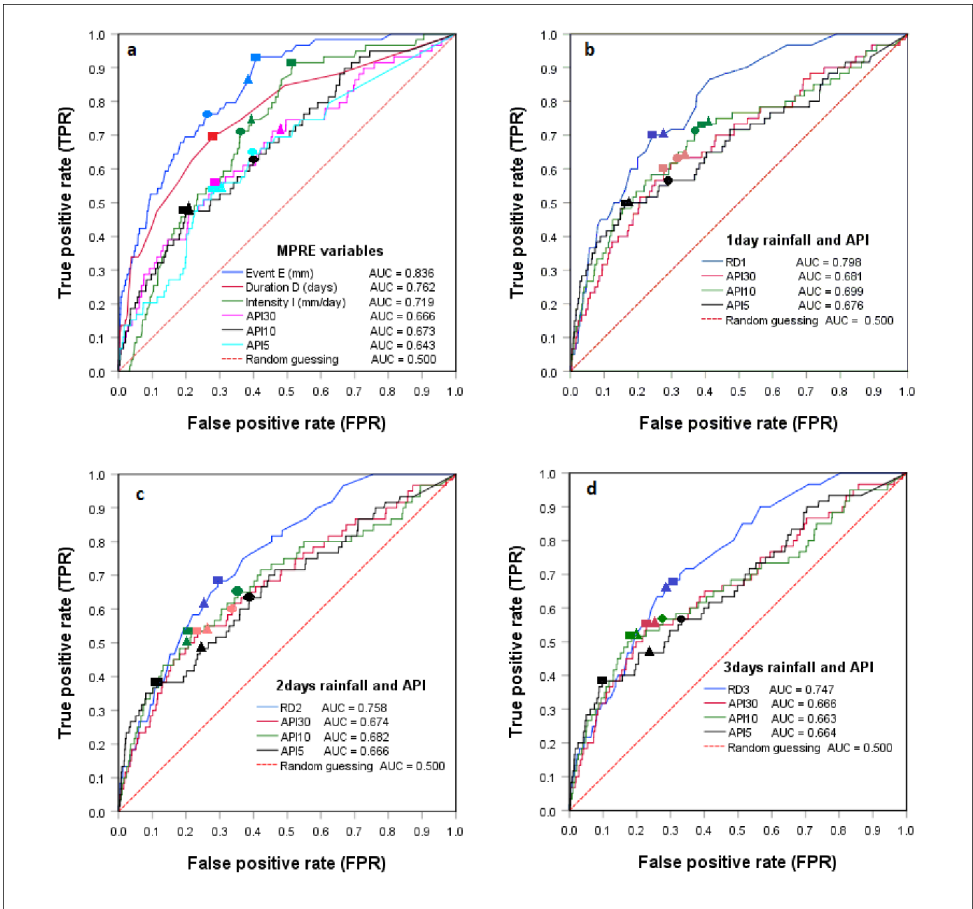


Figure 4.2: Receiver operating characteristic (ROC) curves for: a) MPRE variables, b) RD_1 variables, c) RD_2 variables and d) RD_3 variables; variable significance based on the area under the curve (AUC) and the optimum thresholds defined using Bayesian probabilistic approach (triangle shaped marker); maximum true skill statistics (rectangle shaped marker) and the minimum radial distance (sphere shaped marker). Once two or more techniques revealed similar threshold with similar TPR and FPR only one symbol is used. The figure also indicates corresponding true positive rate (TPR) and false positive rate (FPR) for each threshold level

4.4.2. LANDSLIDE TRIGGER AND TRIGGER-CAUSE BASED HYDRO-METEOROLOGICAL THRESHOLDS AND IMPLICATION FOR LANDSLIDE PREDICTION

The results of bilinear combinations of explanatory variables show that in some cases a single variable threshold can be sufficient to predict landslides (Figure 4.3 and Figure 4.4, horizontal blue lines). Based on the maximum TSS threshold (Figure 4.2, Table 4.1 and Table 4.2) 91.5% of the landslides are correctly predicted once an event intensity threshold level of 7.9 mmd^{-1} is exceeded. Similarly, 93.5% of the landslides are highly likely to occur when the rainfall event E exceeds 30.0 mm while 71.7% of the landslides are highly likely to occur when daily rainfall (RD_1) exceed 12.5 mmd^{-1} . These threshold levels are all trigger-based as they only refer to the recent rainfall/event during which one or more landslides occur. However, these trigger-based thresholds should be constrained by relatively high rates of false alarm (FPR) of about 52%, 41% and 30% for I, E and RD_1 respectively. Moreover, it should be noted that many landslides occur not only due to the trigger itself but rather due to a combination of trigger and cause, the latter represented by API. For example in Figure 4.3a, it can be seen that only 23.7% of the observed landslides which is equivalent to about 26% of the correctly predicted landslides using event intensity (I) threshold, was due to the triggering event while the remaining 74% of the predicted landslides were due to the combined effect of both I and API. As pointed out, the API thresholds indicate the critical level below which the impact of antecedent precipitation is considered unimportant for landslide predictions.

On the contrary, once the API threshold is exceeded, its contribution should be counted as one of the landslide causal factor and thus resulting into trigger-cause-based thresholds. The top left and right panels of Figure 4.3 and Figure 4.4 indicate the improved prediction capacity of the trigger-based threshold once combined with a cause-based threshold. For example Figure 4.3 indicates that the prediction capacity (TPR) of the event intensity threshold increased by about 44%, 27% and 30% once combined with API as trigger-cause based thresholds in a bilinear format as I-API₃₀, I-API₁₀ and I-API₅ respectively. Figure 4.4 indicates also an improved prediction rate of RD_1 trigger-based threshold by about 15%, 35% and 12% once combined as RD_1 -API₃₀, RD_1 -API₁₀ and RD_1 -API₅ respectively. Therefore, the concept of bilinear thresholds (Mirus et al., 2018a) or trigger-cause-based thresholds does not only minimize the false alarm rates but can also be utilised to quantify the impact of each and both landslide triggering and causal condition to the landslide occurrence. Figure 4.3d and Figure 4.4d show the resulting rate of true alarms (TPR), false alarms (FPR), failed alarms (FNR) and true negative rate (TNR) from different trigger-cause based thresholds. This approach should further be explored to be utilized for API based landslide early warning system development.

Table 4.2: Cumulative recent rainfall variables (RD_1 , RD_2 , RD_3), antecedent precipitation index (API) and landslide initiation thresholds defined using probabilistic (Prob), maximum true skill statistics (TSS) and the minimum radial distance (Rad) techniques

Variable	Bayesian probabilistic threshold (Prob) ^p			Maximum True skill statistics (TSS)			Minimum radial distance (Rad)								
	Threshold	1 - P(B A)/TPR	FPR	TSS	Rad	Threshold	FPR	TPR	TSS	Rad	Threshold	FPR	TPR	TSS	Rad
1. Trigger-based thresholds															
RD_1 (mmd ⁻¹)	12.50	0.717	0.298	0.418	0.411	14.45	0.245	0.700	0.455	0.387	14.45	0.700	0.245	0.455	0.387
RD_2 (mmd ⁻²)	22.50	0.617	0.257	0.360	0.461	22.05	0.258	0.617	0.359	0.462	20.85	0.683	0.295	0.389	0.432
RD_3 (mmd ⁻³)	27.50	0.667	0.291	0.376	0.442	26.95	0.307	0.683	0.376	0.441	26.95	0.683	0.307	0.376	0.441
2. Cause-based thresholds															
API ₃₀ (mm) ^a	92.50	0.633	0.320	0.487	0.313	99.08	0.277	0.600	0.323	0.487	92.97	0.633	0.317	0.317	0.484
API ₁₀ (mm) ^a	42.50	0.733	0.408	0.326	0.487	44.37	0.385	0.733	0.349	0.468	45.58	0.717	0.371	0.346	0.466
API ₅ (mm) ^a	42.50	0.500	0.173	0.327	0.529	44.04	0.160	0.500	0.340	0.525	31.79	0.567	0.290	0.277	0.521
API ₃₀ (mm) ^b	102.50	0.533	0.250	0.283	0.529	105.34	0.235	0.533	0.299	0.522	88.02	0.617	0.344	0.273	0.515
API ₁₀ (mm) ^b	62.50	0.517	0.202	0.315	0.524	61.05	0.215	0.533	0.318	0.514	45.87	0.650	0.354	0.296	0.498
API ₅ (mm) ^b	32.50	0.483	0.263	0.220	0.580	49.51	0.113	0.383	0.270	0.627	24.57	0.633	0.387	0.247	0.533
API ₃₀ (mm) ^c	102.50	0.550	0.248	0.302	0.514	105.79	0.229	0.550	0.321	0.505	105.79	0.550	0.229	0.321	0.505
API ₁₀ (mm) ^c	62.50	0.517	0.202	0.315	0.524	65.01	0.184	0.517	0.333	0.517	53.22	0.567	0.278	0.289	0.515
API ₅ (mm) ^c	32.50	0.467	0.258	0.209	0.592	52.16	0.097	0.383	0.286	0.624	27.31	0.567	0.332	0.234	0.546

^pThe probabilistic threshold is a mean value from different probabilistic range for example a threshold value of 32.5 is a mean value ranging between 30-35 and a threshold value of 27.5 is ^a mean value between 25-30

^a 30,10 and 5 days antecedent precipitation index prior to 1 day triggering rainfall coinciding with landslide day

^b 30,10 and 5 days antecedent precipitation index prior to 2 days triggering rainfall whose last day coincides with landslide day

^c 30,10 and 5 days antecedent precipitation index prior to 3 days triggering rainfall whose last day coincides with landslide day

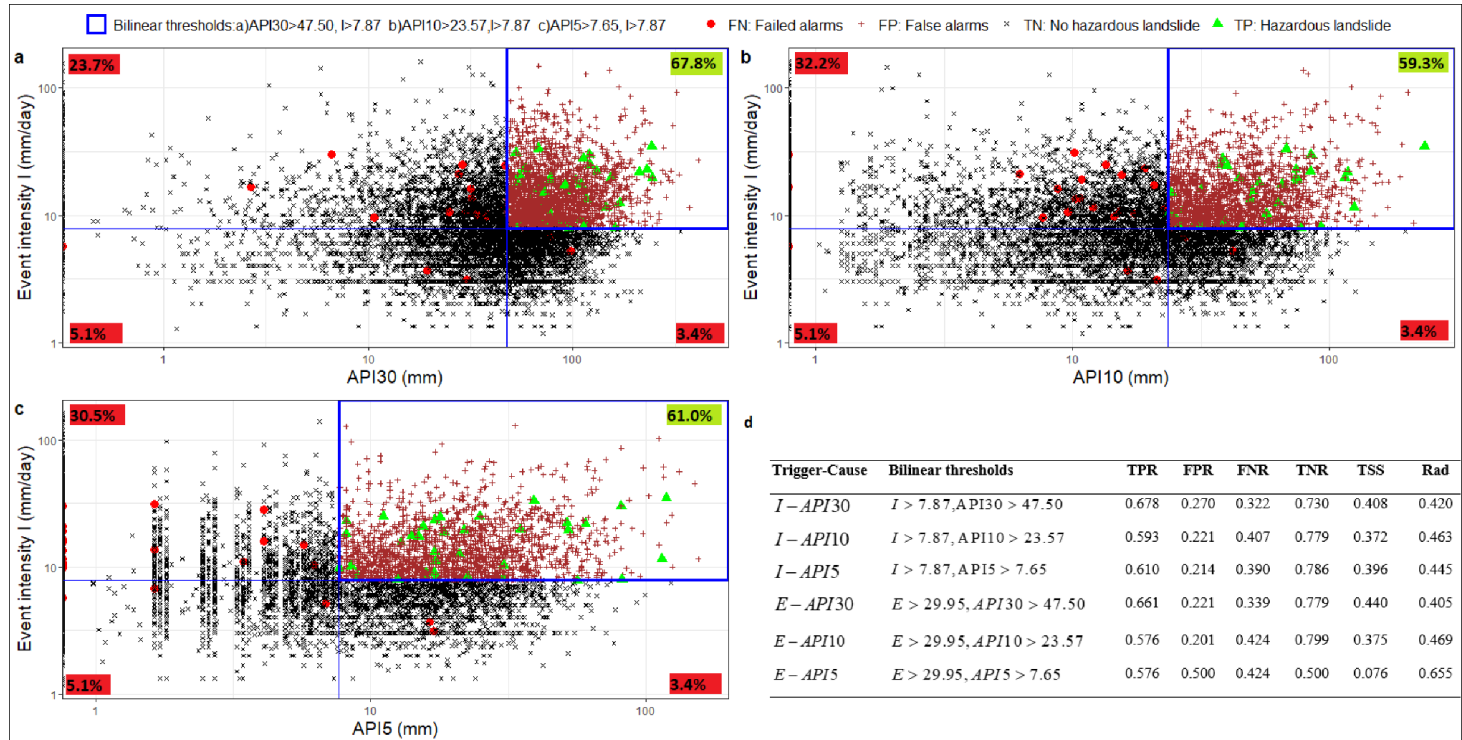


Figure 4.3: Bilinear relation between landslide trigger represented by event intensity I and cause represented by antecedent precipitation indices of different timescale: a) 30 days prior to the triggering event intensity; b) 10 days prior to the triggering event intensity; c) 5 days prior to the triggering event intensity; d) Implication for warning based on the rate of true warnings (TPR) represented by green triangles on a b and c; rate of false alarms (FPR) represented by red cross on a b and c; rate of failed alarms (FNR) represented by red dots on a b and c; true negative rate (TNR) or no landslide represented by black cross on a b and c

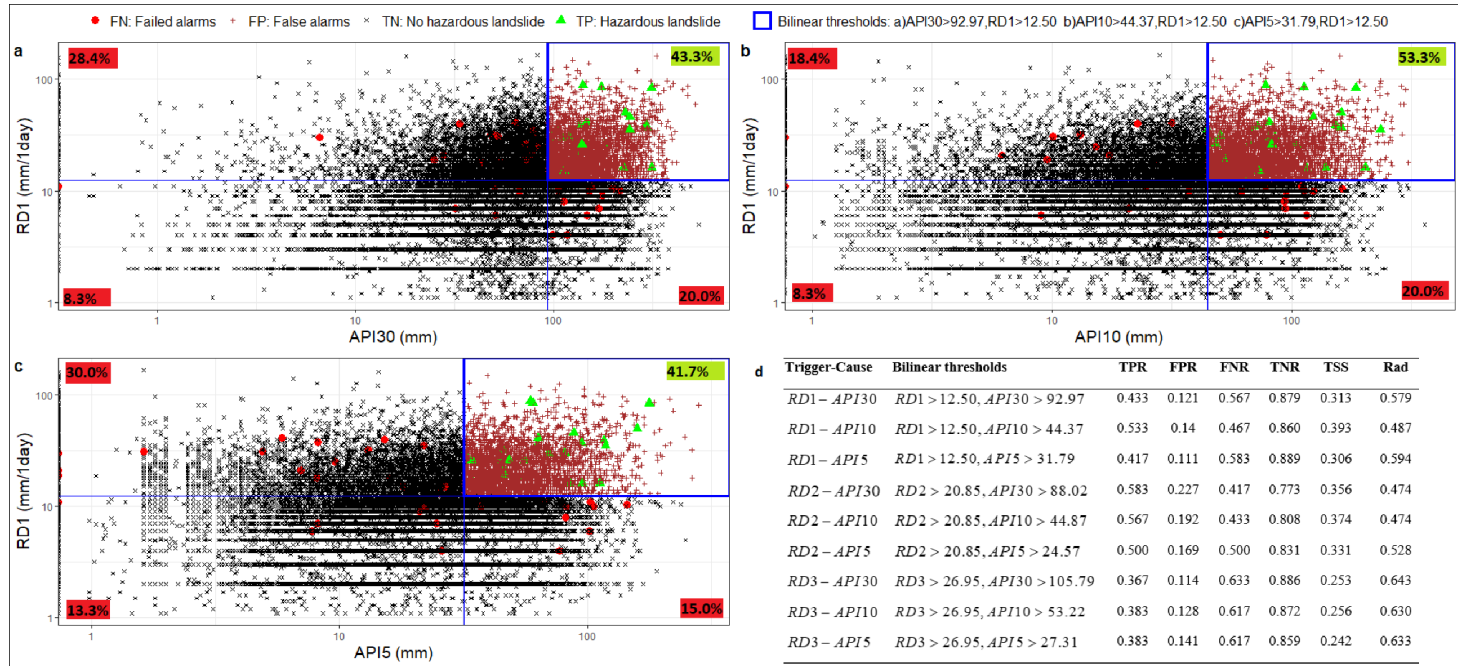


Figure 4.4: Bilinear relation between landslide trigger represented by 1day rainfall (RD_1) and cause represented by antecedent precipitation indices (API) of different timescale: a) 30days prior to the triggering rainfall; b) 10 days prior to the triggering rainfall; c) 5 days prior to the triggering rainfall; d) Implication for warning based on the rate of true warnings (TPR) represented by green triangles on a b and c; rate of false alarms (FPR) represented by red cross on a b and c; rate of failed alarms (FNR) represented by red dots on a b and c; true negative rate (TNR) or no landslide represented by black cross on a b and c

Lastly, the landslide inventory used for this research relied largely on the information from newspapers, government reports, and other media where many landslide events are likely to be missed. While the reliance on these data sources is likely to result in a bias towards large and/or impactful landslides that may involve casualties and economic damage, this landslide inventory is the most comprehensive currently available in Rwanda.

4.5. CONCLUSION

This chapter aimed to use landslide and precipitation data in an empirical-statistical approach to define both trigger and trigger-cause based thresholds for landslides initiation in Rwanda and to quantify their predictive performance. The findings indicated that the normalized event E and the cumulative one day rainfall (RD_1) that coincide with the landslide day are the most informative explanatory variables to distinguish landslide from no landslide conditions. Among the antecedent precipitation indices, API_{10} i.e 10 days precipitation prior to the landslide triggering conditions was the most informative to distinguish between landslide and no-landslide conditions based on its AUC. API_5 was too short while API_{30} was too long. This underlines the critical role of hydrology (infiltration, storage, evaporation/drainage) and particularly the timing of pore pressure changes in the subsurface profile. It was also generally observed that all used threshold definition techniques, Bayesian probabilistic approach, maximum true skill statistic and minimum radial distance, resulted in quite similar thresholds values. The highest landslide prediction capability (rate of positive alarms) was obtained using a single rainfall variable, so a trigger-based threshold. However, that predictive capability simultaneously resulted in a high rate of false alarms. Constraining the trigger-based threshold with a causal variable in a bilinear framework as proposed by [Mirus et al. \(2018a\)](#), improved the overall prediction capacity by reducing the number of false alarms. The findings indicated also that the concept of trigger-cause-based thresholds in bilinear format could not only be useful to minimize the false alarms but also to explore the impact of each or combined triggering and causal conditions on landslide occurrence.

5

INTEGRATION OF OBSERVED AND MODEL-DERIVED GROUNDWATER LEVELS IN LANDSLIDE THRESHOLD MODELS IN NORTHWESTERN RWANDA

This chapter is based on:

Uwihirwe, J., Hrachowitz, M. and Bogaard, T.: Integration of observed and model derived groundwater levels in landslide threshold models in Rwanda, *Nat. Hazards Earth Syst. Sci.* (August), 1–24, 2021, doi.org/10.5194/nhess-2021-222.

Abstract

Incorporation of specific regional hydrological characteristics in empirical statistical landslide threshold models has considerable potential to improve the quality of landslide predictions towards reliable early warning systems. The objective of this Chapter is to test the value of regional groundwater level information, as a proxy for water storage fluctuations, to improve regional landslide predictions with empirical models based on the concept of threshold levels. Specifically, we investigated: i) the use of a data driven time series approach to model the regional groundwater levels based on short duration monitoring observations; ii) the predictive power of single variable and bilinear hydro-meteorological threshold models derived from groundwater levels and precipitation. Based on statistical measures of the model fit (R^2 and RMSE), the groundwater level dynamics estimated by the transfer function noise time series model are broadly consistent with the observed groundwater levels. The single variable threshold models derived from groundwater levels exhibited the highest landslide prediction power with 82–93% of true positive alarms despite the quite high rate of false alarms with about 26–38%. Further combination as bilinear threshold models reduced the rate of false alarms by about 18–28% at the expense of reduced true alarms by about 9–29% and thus, being less advantageous than single variable threshold models. In contrast to precipitation based thresholds, relying on threshold models exclusively defined using hydrological variables such as groundwater can lead to improved landslide predictions due to their implicit consideration of long term antecedent conditions until the day of landslide occurrence.

5.1. INTRODUCTION

In chapter 4, we defined the first empirical landslide precipitation threshold, which is an important step forward in landslide early warning in Rwanda. The defined precipitation based landslide thresholds considered the antecedent precipitation index as an indirect proxy for hydrological conditions. However, the resulting rates of true and false alarms are not satisfactory and require further improvement for a robust early warning system development. The exclusive reliance on meteorological data and the lack of considering the real pre-event hydrological processes and specific characteristics of the study region that predispose the slope to near failure could be the reasons for the poor performance.

Hydrology, being an important aspect in landslide hazard assessment, is still not sufficiently explored although many landslides are hydrologically caused and meteorologically triggered. The need for landslide hydro-meteorological based thresholds was highlighted and further postulated that both false and missed alarms could be significantly reduced if the wetness state is incorporated in landslide prediction models. However, research that incorporates hydrological parameters into landslide prediction models using in situ data is scarce due to absence of long-term hydrological monitoring of sufficient spatial and temporal coverage in most regions worldwide. Once available, frequently, the recorded data is insufficient to build historical time series that match the time period of landslide inventories and that could be incorporated into landslide hydro-meteorological threshold models.

Some landslide studies discussed different effects that groundwater system may have on landslide initiation (Bronnimann, 2011; Cascini et al., 2010; Corominas et al., 2005a; Duan et al., 2019; Hong and Wan, 2011; Trigo et al., 2005; Zhao et al., 2016). However, the asset that regional groundwater level information may have in predicting landslide initiation on a regional scale is still underexplored. It is hypothesized that the more water stored in the catchment, the higher the probability a certain rain event will trigger landslides in a catchment. Therefore, estimates of catchment water storage could be used as a pre-event hydrological process that predispose a slope to near failure and thus be among the hydrological landslide predictor variables. However, as this information is scarce in Rwanda, we presuppose regional groundwater level to be a potential proxy of the relative regional catchment storage and used as a hydrological landslide predictor variable that could be useful once incorporated in landslide threshold model definition. This chapter aims to improve the landslide forecast quality by incorporating the catchment specific groundwater levels as a proxy for regional water storage. More specifically, we here tested the hypotheses that the incorporation of model derived groundwater levels in empirical landslide hazard assessment thresholds could improve the landslide warning capability in Rwanda.

5.2. STUDY AREA

This study was conducted using data from three catchments; Lake Kivu, upper Nyabarongo and Mukungwa (Nieuwenhuis et al., 2019); located in north western region of Rwanda (Figure 5.1). The north western region is geomorphologically characterised by rounded, angular hills and headlands, mountains and volcanoes with elevation up to about 4500m and steep slope up to 55%.

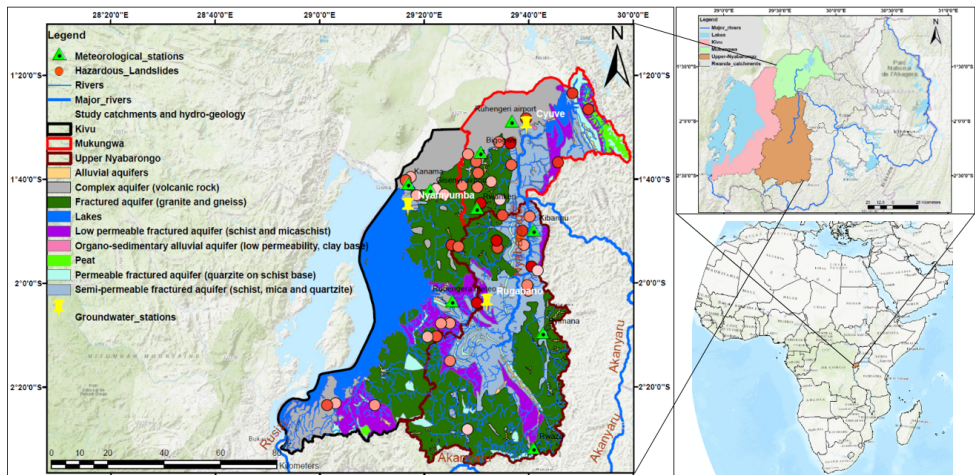


Figure 5.1: Location of the study catchments: Lake Kivu, upper Nyabarongo and Mukungwa in Rwanda and Africa; hydro–geology of the study catchments; spatial and temporal distribution of landslides with light to dark red dots indicating old to new landslides recorded from 2006–2018 (Uwihirwe et al., 2020) ; groundwater stations in yellow symbols and meteorological stations in light green symbols

5

The total area of Lake Kivu catchment is about 7,323 km², 2,425 km² of which is located in Rwanda. The mean annual rainfall is around 1500 mm/yr while potential evaporation is estimated at about 860 mm/yr (Figure 5.2). The Lake Kivu catchment is dominated by basaltic aquifers (volcanic rock) in the north and south west, fractured granite and gneiss aquifers in central and south east, schists and mica schists in the centre and south while pegmatite are found in intermediate areas.

The upper Nyabarongo catchment is located entirely within Rwanda with an area of about 3,348 km². The mean annual rainfall is around 1200 mm/yr and potential evaporation is estimated at around 870 mm/yr (Figure 5.2). Granite and gneiss aquifers are dominant in southern and to a lesser amount in north west part while quartz rich schists and mica schists dominate in central parts of the catchment (Figure 5.1).

The Mukungwa catchment covers a total area of 1,949 km² and is topographically dominated by the volcanic highlands region that receive abundant rainfall with a long-term mean annual rainfall of around 1200 mm/yr with an estimated actual evaporation of about 800 mm/yr (Figure 5.2). The hydro–geology of the catchment (Figure 5.1) is characterized by volcanic deposits with basalt in the north. Granite and pegmatite basement aquifers are found in the south western areas while quartzite and mica schist are in the south east and eastern part of the catchment.

Landslides are most dominant in granite and mica schist units while basaltic units seem to be quite resistant to landslide activities. This can be explained by the weathering products of volcanic rocks that produce a relatively permeable top layer but tend to form a brecciated or intruded sills of low permeability layer at shallow depth and thus hampering deep groundwater recharge and thus less prone to groundwater induced landslides. Contrarily, the weathering products of granites are generally coarse-grained that tend to develop and preserve open joint systems that increase permeability and thus fast

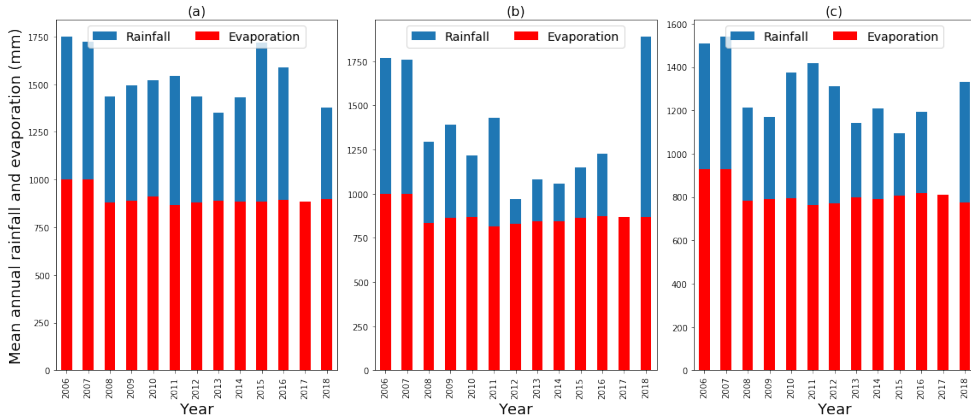


Figure 5.2: Mean catchment annual rainfall and potential evaporation in a) Kivu, b) Upper Nyabarongo and c) Mukungwa catchments

groundwater response that leads to landslide hazards. The weathering product of mica schists include clay minerals that tend to fill up the fractures and thus slowing the permeability. However, mica schists are prone to landslides due to rapid weathering, easy splitting along the joints and bedding planes and loss of strength induced by the high content of mica.

5.3. GROUNDWATER MODELLING: DATA AND METHODOLOGY

5.3.1. METEOROLOGICAL DATA AND SELECTION OF LANDSLIDE REPRESENTATIVE METEOROLOGICAL STATIONS

The rainfall dataset was accessed from Rwanda meteorology agency while potential evaporation E_p time series were calculated with Thornthwaite method (Thornthwaite, 1948) using the mean daily temperature and monthly heat index. We used time series of daily rainfall and potential evaporation from nine meteorological stations located within the studied catchments for a period of 13 years from 2006 to 2018. The meteorological stations (see Figure 5.1) spatially distributed in the three studied catchments were selected based on their relative proximity to the observed locations of the landslides and include Rubengera, Kanama and Gisenyi meteorological stations in the Kivu catchment; Byimana, Kibangu and Rwaza stations in the upper Nyabarongo catchment; and Ruhengeri, Bigogwe and Rwankeri meteorological stations in the Mukungwa catchment as presented in Figure 5.1.

5.3.2. GROUNDWATER DATA AND SELECTION OF LANDSLIDE REPRESENTATIVE GROUNDWATER STATIONS

The time series of groundwater levels were accessed from the Rwanda water portal (<https://waterportal.rwb.rw/data/groundwater>, last access: 2 June 2021). We selected three groundwater observation stations (Figure 5.1) with a temporal resolution of one

day and a minimum continuous duration of one year. The three groundwater observation stations, Nyamyumba, Rugabano and Cyuve, located within the Kivu, upper Nyabarongo and Mukungwa catchments respectively, recorded data from December 2016 till December 2018. However, the intrinsic limitation of this database is linked to the coarse spatial resolution of the data recording equipment and the recorded data are insufficient to build historical time series that match the time period of landslide inventories (2006–2018). Nevertheless, this database has been previously used for computation of water balance and catchment storage and proved to be useful in Rwanda (Nieuwenhuis et al., 2019).

5.3.3. TRANSFER FUNCTION NOISE (TFN) TIME SERIES MODEL

A transfer function noise (TFN) time series model describes the dynamic relationship between a single output series and one or more input series. The TFN model was used in this research to simulate groundwater levels (model output) using both rainfall and potential evaporation as model inputs (Bakker and Schaars, 2019; Collenteur et al., 2019). With Transfer function noise modelling, the groundwater response to both rainfall and evaporation is simulated with a scaled Gamma response function. The structure of a TFN model to simulate groundwater levels is expressed with Equation 5.1.

$$h_t = \sum_{s=1}^S h_s(t) + d + r(t) \quad (5.1)$$

Where h_t is the groundwater levels (m) at time t , $h_s(t)$ is the contribution of stresses s at time t ($m d^{-1}$), S is the total number of stresses (-) that contribute to the groundwater level change here represented by rainfall and evaporation, d is the base elevation of the model (-), and $r(t)$ are the residuals (m). Each model can have an arbitrary number of stresses S that contribute to the head. Hydrological stresses may include rainfall, evaporation, river levels, and groundwater extractions. The contribution of stress s to the groundwater level at time t is computed through convolution with Equation 5.2.

$$h_s(t) = \int_{-\infty}^t S_s(\tau) \theta_s(t - \tau) d\tau \quad (5.2)$$

With s_s denoting the time series of stress s , and θ_s expressing the impulse response function for stress s . The groundwater response is estimated using the scaled Gamma response function that indicates the relationship between the variation in the inputs time series (rainfall and evaporation) and the variation in the groundwater levels as in Equation 5.3.

$$\theta(t) = A \frac{t^{n-1}}{a^n \Gamma(n)} e^{-t/a} \quad (5.3)$$

With A denoting the scaling factor (-); a and n are shape parameters (-) while Γ expresses the Gamma function

5.3.4. GROUNDWATER MODELLING APPROACH: PASTAS

We used the Transfer Function Noise TFN time series Model implemented in Pastas, a new open source Python package for analysis of groundwater time series. The TFN

modelling explains an observed time series (here the observed groundwater levels) by one or more other time series (here rainfall and potential evaporation time series). The TFN model inputs time series, rainfall and potential evaporation, were available for the entire study period 2006–2018, whereas the observed groundwater level were available for December 2016 to December 2018. We have therefore used the two years available groundwater observation time series and these short term data were only used for model calibration and no validation was carried out due to the data limitations.

By using the TFN modelling approach, we aimed for hindcasting and thus the reconstruction of past groundwater levels to overlap with the time period of the recorded landslide inventory in Rwanda (2006–2018). We used the fully available time series of rainfall and evaporation as model inputs or model stresses. Each model can have an arbitrary number of hydrological stresses that contribute to the groundwater level changes. These hydrological stresses include rainfall, evaporation, river levels, and groundwater extractions. For this study however, we used rainfall and potential evaporation and assumed runoff and groundwater pumping to be negligible though not accessed in our study area. The impulse groundwater response function to the stresses was fitted with the scaled Gamma distribution function and the calibrated parameters were A , n , a , d as previously described. The output of the TFN model was then daily groundwater levels h_t (m) over the entire 13 years study period from 2006 to 2018.

Apart from hindcasting, the TFN model spatially extrapolated the groundwater information accounted by different precipitation and potential evaporation inputs from the nine spatially distributed meteorological stations, Rubengera, Kanama, Gisenyi, Byimana, Kibangu, Rwaza, Ruhengeri, Bigogwe and Rwankeri, shown in [Figure 5.1](#). The extrapolation was undertaken by changing the model inputs and model parameters at the location of each of the meteorological stations and by implicitly relying on the main assumption here that other hydro–geomorphological parameters do not exhibit spatial variability within the individual catchment. This is an assumption made, given the data scarcity and some intrinsic limitation of the database in the east Africa rift region in general ([Monsieurs et al., 2018a](#)) and Rwanda in particular. The modelled groundwater levels were standardised and used in the regional hydro–meteorological hazard assessment thresholds definition. The standardisation was computed with [Equation 5.4](#).

$$y_s = \frac{(x_i - \bar{x})}{\sigma} \quad (5.4)$$

Where y_s is the standardised value of groundwater time series (-); x_i is the value of time series (m) at time step i ; \bar{x} is the average value of time series (m); σ is the standard deviation of time series (m); i is the subsequent time step in a time series.

5.4. REGIONAL LANDSLIDE ASSESSMENT: DATA AND METHODOLOGY

5.4.1. LANDSLIDE INVENTORY

The available landslide inventory for Rwanda contains landslides recorded from 2006 to 2018. It was accessed from the NASA global landslide catalogue (<https://data.nasa.gov/Earth-Science/Global-Landslide-Catalog/h9d8-neg4>, last access: 26 June

2019) uploaded by the Landslide Inventory for the central section of the Western branch of the East African Rift (LIWEAR) project. The catalogue was further extended through compilation of additional rainfall induced landslides as reported from local newspapers, blogs, technical reports and field observations. Between 2006 and 2018, the catalogue counts for 42 accurately dated landslides located within the studied region (Figure 5.1). However, the detailed characteristics of these landslides such as the accurate size, types, cause and triggers are frequently not recorded by the landslide hazard reporters.

5.4.2. DEFINITION OF LANDSLIDE HYDROLOGICAL AND METEOROLOGICAL CONDITIONS

The outputs from the TFN model, groundwater levels, were used to define the landslide hydrological conditions in each of the studied catchments. The landslide hydrological conditions consist of standardized groundwater levels modelled on landslide day h_t and prior to the landslide triggering event h_{t-1} and were here considered as landslide cause/predisposing conditions. The meteorological conditions used here include event rainfall volumes E (mm E^{-1}), event rainfall intensity I (mm d^{-1}) as well as event duration D (d) and were considered as landslide triggers. The event duration D was defined as individual periods of days with recorded rain interrupted by dry periods of at least two days. The event rainfall volume E was computed as the accumulated rainfall during each individual event periods of duration D . The event rainfall intensity was then computed as a ratio of E and D . Both hydrological and meteorological conditions were binary classified into landslides and no landslide conditions depending on whether they have resulted into landslide or not.

5.4.3. QUANTIFICATION OF LANDSLIDE PREDICTOR VARIABLES

The landslide predictor variables which include the predisposing conditions h_t and h_{t-1} as well as the triggering conditions E , I and D were tested for their relevance using a receiver operating characteristic (ROC) curves and the area under the curve (AUC) metrics. ROC is used as a statistical tool indicating the trade-off between false positive rate (FPR) and true positive rate (TPR) associated to each threshold level on the curve (Hong et al., 2017; Postance and Hillier, 2017; Mirus et al., 2018a; Prenner et al., 2018). In landslide studies, the AUC is an indicator of the capacity of the test variable to correctly distinguish landslide from no landslide conditions. It is therefore used as statistical metric that compares the test variables to random guessing $\text{AUC}=0.5$ and thereby indicating their significance where the perfect test variable has an AUC equal to unity. The TPR and FPR corresponding to each threshold level on ROC curves are calculated with Equation 4.3 and Equation 4.4.

5.4.4. LANDSLIDE THRESHOLD DEFINITION TECHNIQUES

The optimum or the most informative threshold level above which landslide are high likely to occur have been defined using two statistical techniques i.e. the maximum true skill statistic (TSS) and minimum radial distance (Rad). The true skill statistics (TSS) is expressed as a balance between the true positive rate and false positive rate as indicated in Equation 4.13. The radial distance (Rad) shows the relative distance from the defined threshold level to the perfect model or optimum point whose true positive rate (TPR) is

a unit and null FPR and is computed in Equation 4.14.

5.4.5. SINGLE VARIABLE AND BILINEAR THRESHOLD MODELS AND LANDSLIDE PREDICTIVE CAPABILITIES

According to Postance and Hillier (2017), the optimum landslide threshold model is the one that maximizes the true positive alarms (TP) while minimizing failed (FN) and false alarms (FP). Based on this criteria, the optimum threshold was here selected among the ones defined either by maximum true skill statistics or minimum radial distance. These optimum thresholds were firstly plotted in 1D here referred to as single variable threshold model line beyond which landslide are high likely to occur. Furthermore, these optimum thresholds were combined and plotted in 2D here referred to as bilinear threshold model line beyond which landslide are high likely to occur. The bilinear threshold models made of hydrological and meteorological predictors were formulated using x,y pairs such as h_t-E , h_t-I , $h_{t-1}-E$ and $h_{t-1}-I$ and referred to as hydro-meteorological threshold models. Furthermore, the thresholds from classical landslide prediction models that exclusively rely on precipitation, such as event-duration E-D and intensity-duration I-D were also defined in a bilinear framework and used as benchmarks for comparative performance evaluation. The predictive performance of these threshold models was evaluated using a confusion matrix and the resulting rate of positive alarms (TP), false alarms (FP), missed alarms (FN) and true negatives (TN).

5.5. RESULTS AND DISCUSSION

5.5.1. REGIONAL GROUNDWATER MODELLING

The outputs of the Transfer Function Noise TFN time series model were daily groundwater levels (m) simulated over 13 years from 2006 to 2018 as presented in Figure 5.3. The results demonstrate that the TFN time series model can broadly reproduce the main features of observed groundwater level fluctuations based on the metrics of goodness of the model fit i.e. R^2 and RMSE between observed and simulated groundwater levels. Overall, the model explains between 60–87% of the variance in the observed groundwater data from the three studied catchments. The values of RMSE 0.09–1.84m similarly suggested a reasonable model fit across the catchments. More specifically, while the TFN model captures groundwater fluctuations rather well in the Kivu and Mukungwa catchments (RMSE<0.5m), the model is somewhat less robust for the upper Nyabarongo (RMSE>0.5m). The weaker model fits observed in upper Nyabarongo catchment are mostly the consequence of the relatively large distance between the groundwater well and the meteorological stations as also highlighted as potential source for poor TFN model fits by Bakker and Schaars (2019). They further postulated that TFN time series models are relatively simple, as they include only a handful number of parameters and has the higher skill to simulate groundwater levels than more detailed models.

5.5.2. CATCHMENT STANDARDISED GROUNDWATER LEVELS AND LANDSLIDE ACTIVITIES

The standardised daily groundwater levels and the linked landslide hazards are presented in Figure 5.4 for the Kivu, upper Nyabarongo and Mukungwa catchments respec-

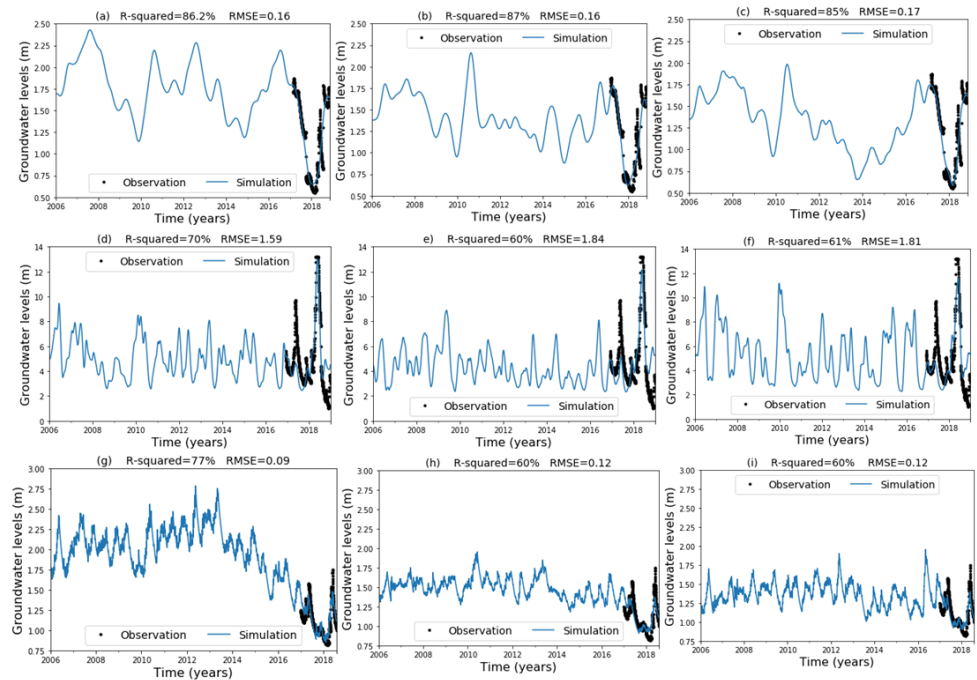


Figure 5.3: Groundwater simulation with TFN model: (a-c) TFN model calibrated with groundwater observations from Nyamyumba groundwater well; rainfall and potential evaporation E_p time series as model inputs from three meteorological stations (a) Rubengera (b) Kanama (c) Gisenyi located in Kivu catchment; (d-f) TFN model calibrated with groundwater observations from Rugabano groundwater well; rainfall and potential evaporation E_p time series as model inputs from three meteorological stations (d) Byimana (e) Kibangu, (f) Rwaza located in upper Nyabarongo catchment; (g-i) TFN model calibrated with groundwater observations from Cyuve groundwater well; rainfall and potential evaporation E_p time series as model inputs from three meteorological stations (g) Ruhengeri (h) Bigogwe (i) Rwankeri located in Mukungwa catchment

tively. The simulated groundwater levels were standardised based on the assumption that landslides occur when the groundwater levels positively deviate from the long-term mean up to a critical level for landslide initiation. The comparisons of mean daily rainfall and standardised groundwater levels across the three studied catchments, calculated by averaging of data within each catchment, indicates general similarities in terms of landslide triggering and predisposing but also reveal systematic differences between the groundwater responses. For example, Mukungwa catchment is slowly responding and also quite drier from 2014 to 2018 than the other catchments despite its elevated landslide hazard during that period.

The results indicated that landslides are likely to occur at a certain level above the long-term mean groundwater level and thus justifying the importance of groundwater and catchment wetness in terms of slope failure predisposition. They also indicate that landslides occur when the catchment groundwater reaches a certain peak level above the long-term mean which is a function of the rainfall received in the past depending on the time memory of each catchment. Even though, the most hazardous landslides in the studied catchments are shallow seated landslides which are mostly rainfall induced, the conducted field based inventory indicated that the most frequently recorded landslides in north western Rwanda are deep seated which are high likely linked to the combined effects of groundwater and other hydro–geological factors. The critical positive deviation of groundwater levels up to 3m from the mean was noticed to be the range where most of landslide activities happen in the studied region. However, [Van Asch et al. \(1999\)](#) highlighted that deep seated landslide at about 5–20m deep are induced by rising groundwater level with about 4m below the ground surface being the critical threshold for landslide reactivation. [Hong and Wan \(2011\)](#); [Duan et al. \(2019\)](#) forecasted the groundwater fluctuation and indicated that landslides are likely to occur when groundwater level increases by about 8m from the datum. Even so, these absolute threshold values were not statistically approved using appropriate landslide threshold definition techniques.

5.5.3. LANDSLIDE PREDICTOR VARIABLES AND DISCRIMINATORY POWER

The discriminatory power of each landslide predictor variable was evaluated using a receiver operating characteristic (ROC) curves and area under the curve metrics as presented in [Figure 5.5](#). Based on the results, the standardized groundwater levels h_t modelled on a landslide day with AUC between 0.76–0.80 and the event rainfall volume E whose AUC ranges from 0.74–0.93 were identified as the hydrological and meteorological variables with the highest discriminatory power to distinguish landslide from no-landslide conditions and thus, the most dominant control on landslide occurrence in the studied region.

The standardised groundwater levels h_{t-1} recorded prior to the landslide triggering event, with AUC ranging from 0.63–0.74, were not as significant as h_t . This is likely a consequence of the hydro–geological properties of soil such as soil texture, presence of fissures, porosity and permeability that contribute to aquifer leakage, drainage and seepage of longer cumulated groundwater levels. Although the AUC metric was used to identify the variable with the highest skill to distinguish landslide from no-landslide conditions, it does not indicate the optimum threshold levels above which landslide are

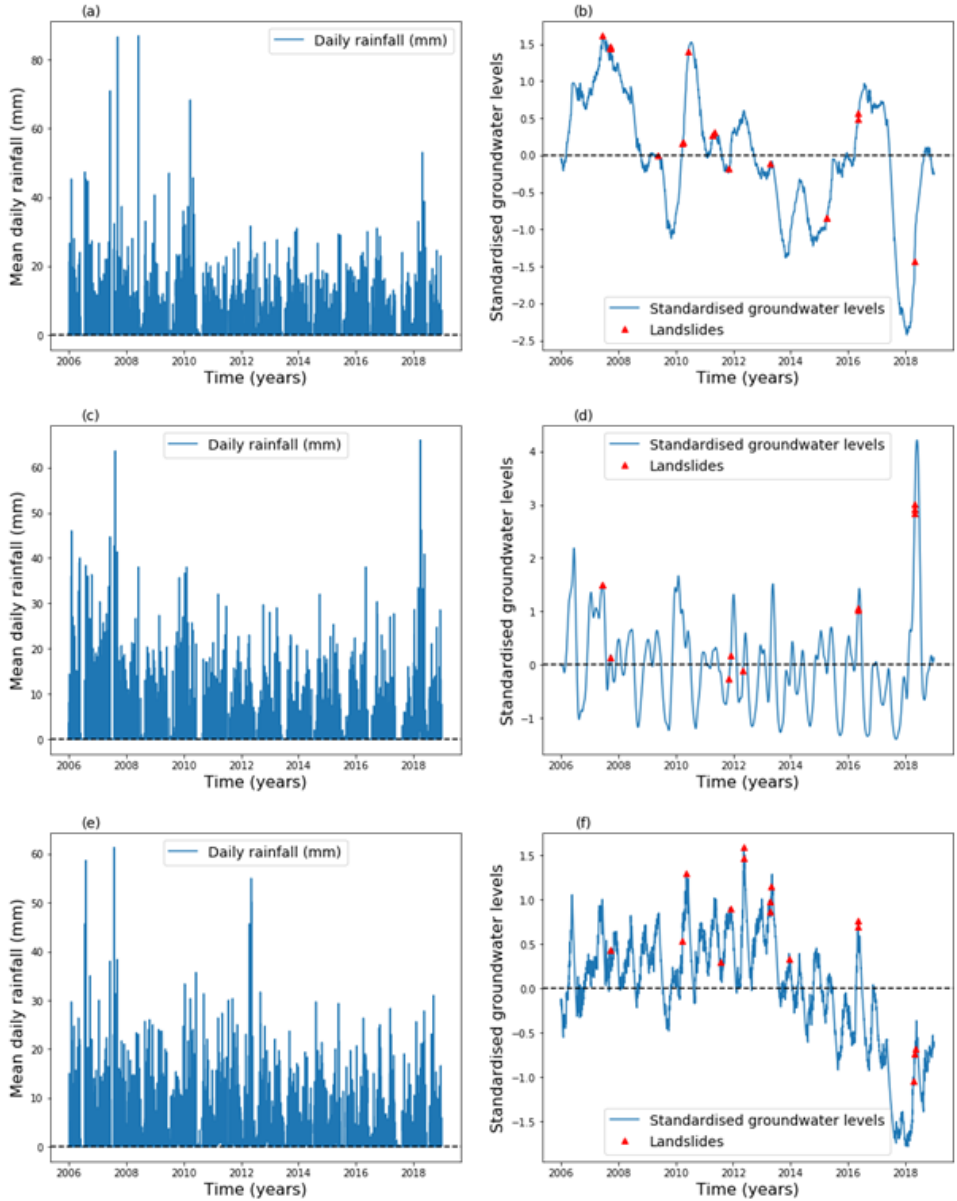


Figure 5.4: (a) Mean daily catchment rainfall and (b) catchment mean standardised groundwater simulated with TFN model using meteorological data from Kivu catchment as model inputs (c) mean daily catchment rainfall and (d) catchment mean standardised groundwater simulated with TFN model using meteorological data from upper Nyabarongo catchment as model inputs (e) mean daily catchment rainfall and (f) catchment mean standardised groundwater simulated with TFN model using meteorological data from Mukungwa catchment as model inputs; landslides represented with red dots

high likely to occur. Therefore the maximum true skill statistics (TSS) and minimum radial distance (Rad) statistical metrics were used to identify the optimum thresholds represented by the dots on the ROC curves and the corresponding balance of true positive (TPR) and false positive rate (FPR) are presented in Figure 5.5 and detailed in Table 5.1. The maximum TSS and minimum Rad indicated for example that landslides are high likely to occur when standardised groundwater levels h_t positively deviate by about 0.21 to 0.48 from the long-term mean and these threshold levels resulted to about 82–93% of correct predictions of landslides i.e. true positive rate and about 26–38% of false positive rate. Similarly, both TSS and Rad indicated 66.8mm as the optimum threshold rainfall volume E with 64% of true positive rate and 15% of false positive rate in Kivu catchment. However, the optimum thresholds E between 44.7–63.5 mm were defined by Rad in upper Nyabarongo and Mukungwa catchment and correctly predict about 73–92% of landslides with 18–24% of false positive rate. These findings indicated that the used statistical metrics TSS and Rad lead to quite similar results expressing their identical capabilities in landslide thresholds definition.

5.5.4. COMPARATIVE PREDICTION POWER OF SINGLE VARIABLE AND BILINEAR THRESHOLD MODELS

5

The defined landslide thresholds for each predictor variables include the hydrological h_t , h_{t-1} and meteorological E, I, D variables. The landslide predictive capability was evaluated for each variable in 1D here considered as single variable threshold model presented in Table 5.1 and by each of the blue line in Figure 5.6- Figure 5.8. The landslide predictive capability was also evaluated through combination of variables in 2D as X-Y pairs here considered as bilinear threshold models summarised in Table 5.2 and by the intersection of both blue lines in Figure 5.6 - Figure 5.8. A recall from Postance and Hillier (2017) indicates that the basic strategy for selection of accurate landslide threshold model is to choose the one that offers the greatest level of true positive alarms (TPR) and that provide the lowest rate of failed (FNR) and false alarms (FPR). Therefore, the findings indicated that single variable threshold models either hydrological or meteorological have the greatest landslide predictive capability in terms of elevated true positive rate and low level of failed alarms as compared to the bilinear threshold models. For example with groundwater level modelled on landslide day h_t with threshold values between 0.2–0.48 above the mean, 82–93% of landslides were correctly predicted (TPR) with 25–38% of wrongly predicted landslides (FPR).

Similarly, the event rainfall intensity I between 7.5–12.5mm d^{-1} as single variable thresholds were able to correctly predict 64–92% of landslides with 25–37% of false alarms. Contrarily, the resulting bilinear threshold models h_t -I were able to correctly predict 64–85% with 8–15% of FPR. The greatest landslide prediction capability of single variables threshold models in terms of TPR was also noticed in Chapter 4. However, it was noticed that relying on single variable threshold models that are exclusively defined using precipitation variables like event rainfall volume E, and event intensity I considered as landslide triggers could lead to biased results due to the fact that many landslides occur not only due to the trigger itself but a rather combination of both trigger and prevent hydrological conditions.

Contrarily, relying on single variable threshold models exclusively defined using hy-

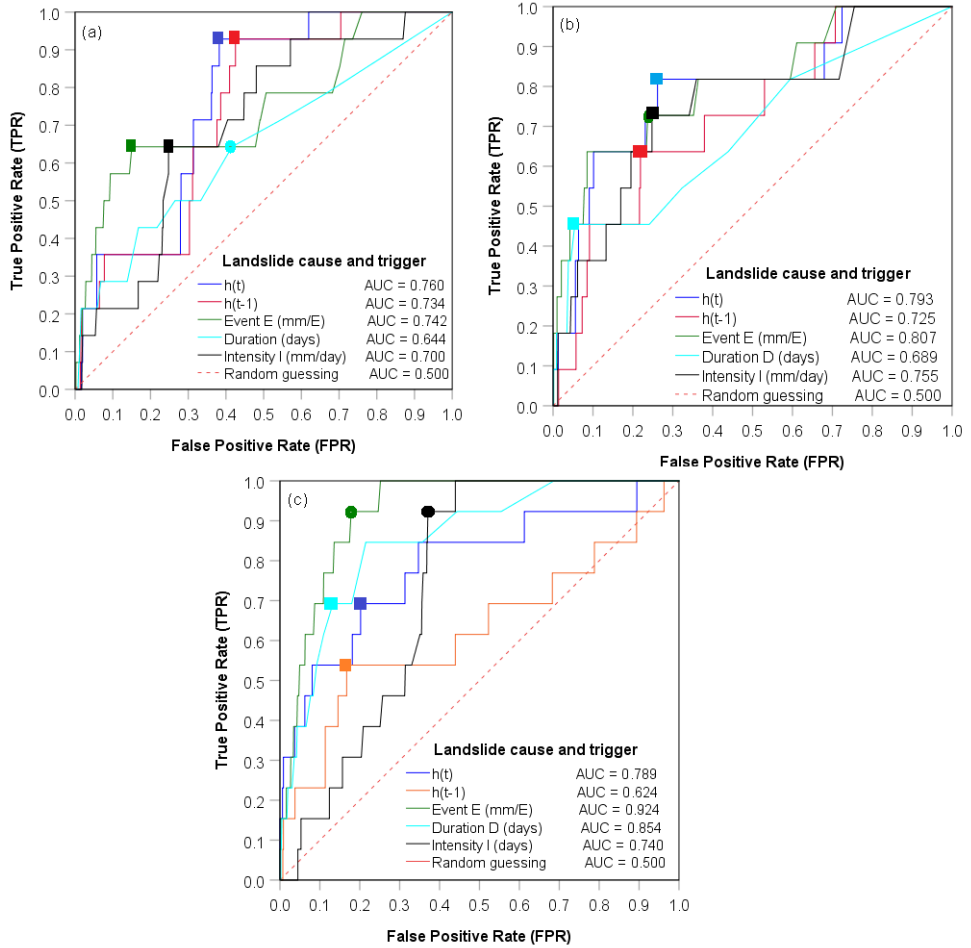


Figure 5.5: Receiver operating characteristic (ROC) curves and area under the curve (AUC) for each landslide predictor variable in the studied catchments: (a) Kivu, (b) upper Nyabarongo and (c) Mukungwa; the optimum thresholds defined using the maximum true skill statistics (TSS) are presented with square shaped markers while circle shaped markers are thresholds defined with the minimum radial distance (Rad); once TSS and Rad reveals different threshold values the optimum (with maximum TPR and minimum FPR) is kept; once TSS and Rad reveals similar threshold values only the square shaped marker (TSS) is kept; the corresponding balance of true and false positive rate are also presented

Table 5.1: Single variable landslide thresholds definition with the maximum true skill statistics (TSS) and minimum radial distance (Rad) and their predictive power

Variables	Threshold TSS	TPR	FPR	FNR	TNR	TSS	Rad	Threshold Rad	TPR	FPR	FNR	TNR	TSS	Rad
Kivu catchment														
h_t ^a	0.21	0.93	0.38	0.07	0.62	0.55	0.39	0.21	0.93	0.38	0.07	0.62	0.55	0.39
h_{t-1} ^b	0.05	0.93	0.43	0.07	0.58	0.50	0.43	0.05	0.93	0.43	0.07	0.58	0.50	0.43
E (mm) ^c	66.75	0.64	0.15	0.36	0.85	0.49	0.39	66.75	0.64	0.15	0.36	0.85	0.49	0.39
D (d) ^d	7.50	0.43	0.17	0.57	0.83	0.26	0.60	3.50	0.64	0.42	0.36	0.58	0.23	0.55
I (mm/d) ^e	10.84	0.64	0.25	0.36	0.75	0.40	0.44	10.84	0.64	0.25	0.36	0.75	0.40	0.44
Upper Nyabarongo catchment														
h_t	0.46	0.82	0.26	0.18	0.74	0.56	0.32	0.46	0.82	0.26	0.18	0.74	0.56	0.32
h_{t-1}	0.64	0.64	0.22	0.36	0.78	0.42	0.42	0.64	0.64	0.22	0.36	0.78	0.42	0.42
E (mm)	90.50	0.64	0.09	0.36	0.92	0.55	0.37	44.70	0.73	0.24	0.27	0.76	0.49	0.36
D (d)	12.50	0.46	0.06	0.55	0.95	0.40	0.55	12.50	0.46	0.06	0.55	0.95	0.40	0.55
I (mm/d)	12.48	0.73	0.25	0.27	0.75	0.48	0.37	12.48	0.73	0.25	0.27	0.75	0.48	0.37
Mukungwa catchment														
h_t	0.48	0.85	0.35	0.15	0.65	0.50	0.38	0.82	0.69	0.20	0.31	0.80	0.49	0.37
h_{t-1}	0.92	0.54	0.17	0.46	0.83	0.37	0.49	0.92	0.54	0.17	0.46	0.83	0.37	0.49
E (mm)	46.75	1.00	0.25	0.00	0.75	0.75	0.25	63.50	0.92	0.18	0.08	0.82	0.75	0.19
D (d)	7.50	0.85	0.22	0.15	0.79	0.63	0.26	7.50	0.85	0.22	0.15	0.79	0.63	0.26
I (mm/d)	6.78	1.00	0.44	0.00	0.56	0.56	0.44	7.55	0.92	0.37	0.08	0.63	0.55	0.38

^aGroundwater levels recorded on the day of landslide ^bGroundwater levels recorded prior to landslide triggering event ^cEvent rainfall volume ^dEvent duration ^eEvent rainfall intensity

drological variables like groundwater levels h_t , could lead to unbiased landslide predictions due to their high consideration of long-term antecedent conditions until the day of landslide occurrence. The bilinear threshold models lead to a minimized level of false positive rate (FPR) which is the main focus behind the cause-trigger and bilinear thresholds concepts proposed by [Bogaard and Greco \(2018\)](#); [Mirus et al. \(2018a\)](#) with a rather reduced rate of true positives (TPR).

5.5.5. COMPARATIVE ANALYSIS OF THE WARNING CAPABILITIES OF LANDSLIDE HYDRO–METEOROLOGICAL THRESHOLDS AND PRECIPITATION BASED THRESHOLDS

The landslide hydro–meteorological threshold models defined as X–Y pairs in a 2D bilinear framework and their warning capabilities in Kivu catchment are presented in [Figure 5.6](#). The combined groundwater level–event rainfall intensity h_t –I [$h_t > 0.205$, $I > 10.84 \text{ mm d}^{-1}$] threshold model outperforms other combinations in terms of true positive alarms with about 64%. Comparing the predictive capabilities of h_t –I, a hydro–meteorological threshold model, to I–D, a precipitation threshold model, significant improvement of about 28% in terms of the rate of true alarms was achieved. This confirms the high landslide prediction and warning capability of hydro–meteorological thresholds over precipitation based thresholds. However, there was no significant improvement from E–D to h_t –E and h_{t-1} –E in terms of true alarms. This suggests that the combinations involving event rainfall volume E have lower landslide warning skill than the ones that consider the event rainfall intensity I. This may be explained by the fact that rainfall event volume E is estimated over various time scale D making E an unstandardized variable which could be normalized by the respective time duration and thus, favouring the event rainfall intensity I. Unexpectedly, there was no significant improvement in terms of reduced false alarms FPR by the tested landslide hydro–meteorological threshold models as compared

Table 5.2: Landslide bilinear threshold model and warning capabilities

Cause-Trigger	Bilinear threshold models	TPR	FPR	FNR	TNR	TSS	Rad
Kivu catchment							
h_t -E	$h_t > 0.205, E > 66.75$	0.57	0.07	0.43	0.93	0.50	0.43
h_t -I	$h_t > 0.205, I > 10.84$	0.64	0.10	0.36	0.90	0.55	0.37
h_{t-1} -E	$h_{t-1} > 0.052, E > 66.75$	0.57	0.08	0.43	0.93	0.50	0.44
h_{t-1} -I	$h_{t-1} > 0.052, I > 10.84$	0.64	0.11	0.36	0.89	0.54	0.37
E-D	$D > 3.5, E > 66.75$	0.57	0.14	0.43	0.86	0.43	0.45
I-D	$D > 3.5, I > 10.84$	0.36	0.06	0.64	0.94	0.29	0.65
Nyabarongo catchment							
h_t -E	$h_t > 0.457, E > 44.7$	0.73	0.08	0.27	0.92	0.64	0.29
h_t -I	$h_t > 0.457, I > 12.48$	0.73	0.08	0.27	0.92	0.65	0.28
h_{t-1} -E	$h_{t-1} > 0.636, E > 44.7$	0.55	0.07	0.45	0.93	0.48	0.46
h_{t-1} -I	$h_{t-1} > 0.635, I > 12.48$	0.64	0.07	0.36	0.93	0.56	0.37
E-D	$D > 12.5, E > 44.7$	0.45	0.05	0.55	0.95	0.40	0.55
I-D	$D > 12.5, I > 12.48$	0.36	0.01	0.64	0.99	0.36	0.64
Mukungwa catchment							
h_t -E	$h_t > 0.483, E > 63.5$	0.77	0.11	0.23	0.90	0.66	0.25
h_t -I	$h_t > 0.483, I > 7.55$	0.85	0.15	0.15	0.85	0.70	0.21
h_{t-1} -E	$h_{t-1} > 0.921, E > 63.5$	0.46	0.03	0.54	0.97	0.43	0.54
h_{t-1} -I	$h_{t-1} > 0.921, I > 7.55$	0.54	0.06	0.46	0.94	0.48	0.47
E-D	$D > 7.5, E > 63.5$	0.85	0.14	0.15	0.86	0.71	0.21
I-D	$D > 7.5, I > 7.55$	0.77	0.06	0.23	0.94	0.71	0.24

to the precipitation based threshold models in Kivu catchment.

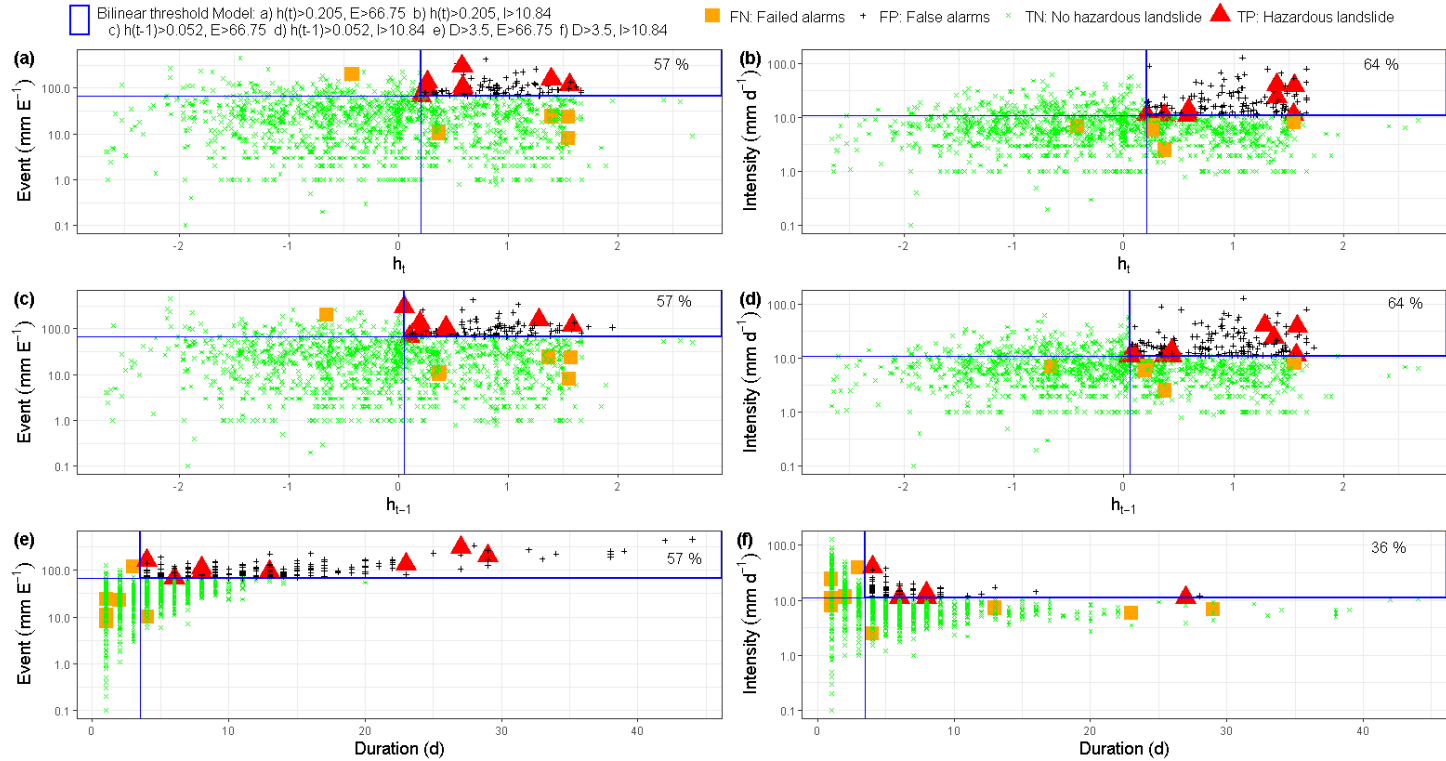


Figure 5.6: Landslide warning capabilities of the hydro-meteorological and precipitation threshold models: (a) h_t -E; (b) h_t -I; (c) h_{t-1} -E; (d) h_{t-1} -I; (e) E-D; (f) I-D in Kivu catchment

The defined landslide hydro–meteorological threshold models in upper Nyabarongo catchments are presented in [Figure 5.7](#). Similar to Kivu catchment, the landslide hydro-meteorological threshold models h_t -E, h_t -I, h_{t-1} -E and h_{t-1} -I performs much higher with 55–73% of correctly predicted landslides (TP) than precipitation threshold models E-D and I-D with around 36–45% of true alarms. A significant reduction of the rate of failed /missed alarms (FN) with about 37% from I-D to h_t -I and about 28% from E-D to h_t -E was also observed. Unexpectedly, there was no significant improvement in terms of reduced false alarms by the landslide hydro–meteorological thresholds as compared to the landslide precipitation thresholds.

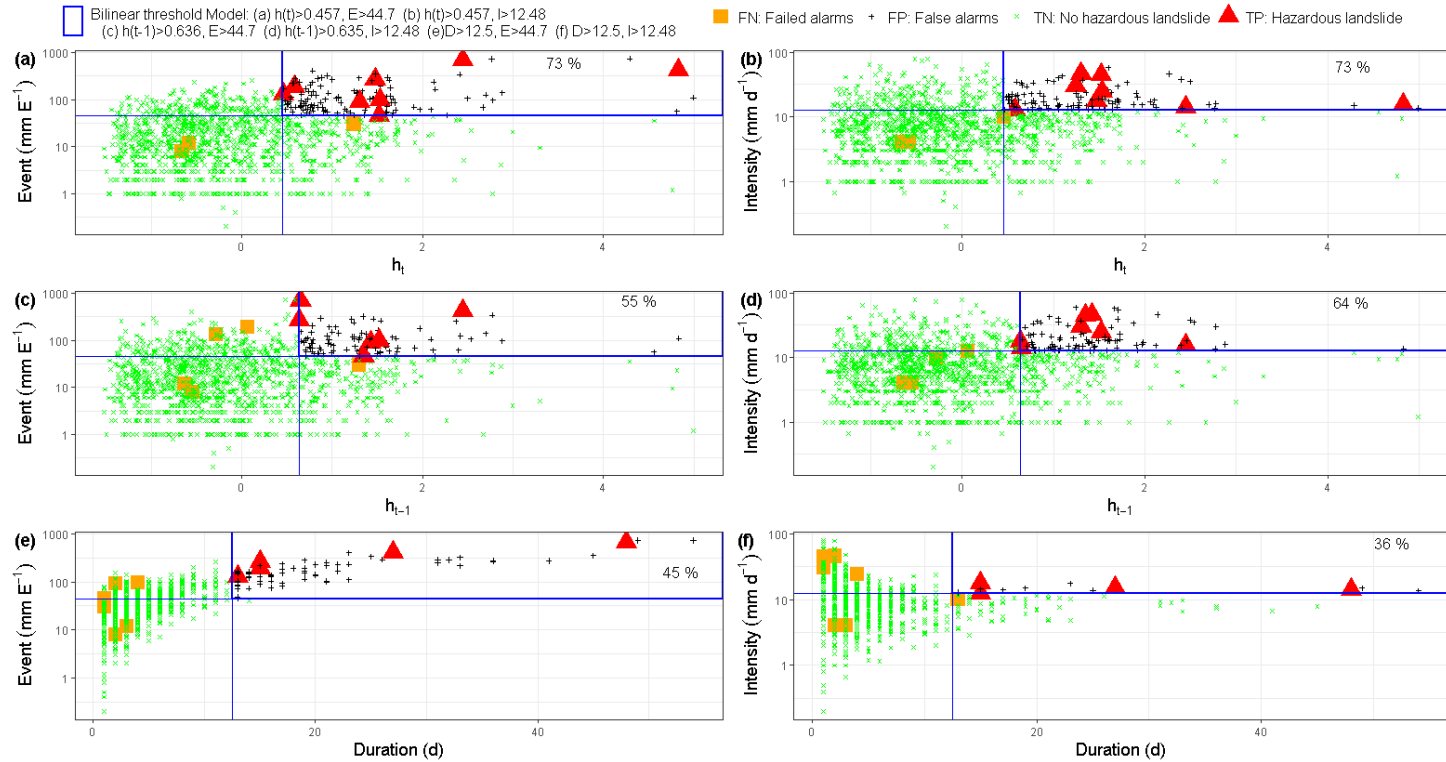


Figure 5.7: Landslide warning capabilities of the hydro-meteorological and precipitation threshold models: (a) h_t - E ; (b) h_t - I ; (c) h_{t-1} - E ; (d) h_{t-1} - I ; (e) E - D ; (f) I - D in upper Nyabarongo catchment

The defined landslide hydro–meteorological threshold models in Mukungwa catchment are shown in [Figure 5.8](#). Although, there was no significant improvement in terms of false positive alarms (FP) reduction as expected, the best landslide hydro–metrological thresholds models h_t -I outperforms the precipitation based threshold I-D models in terms of elevated rate of true positive alarms TP with about 85% as compared to 77% and low rate of failed alarms FN with 15% compared to 23%. The highest prediction level in terms of true alarms with 85% was observed from both h_t -I and E-D hydro–meteorological and precipitation based threshold models. Contrary to Kivu and upper Nyabarongo catchments, precipitation based threshold models E-D and I-D performed quite similar to h_t -I and even better than other tested hydro–meteorological threshold models in Mukungwa catchments. This could be explained by the catchment specific hydro–geological characteristics that probably makes the catchment to be a very slow groundwater responding system and thus, a rather more precipitation induced landslide than groundwater levels.

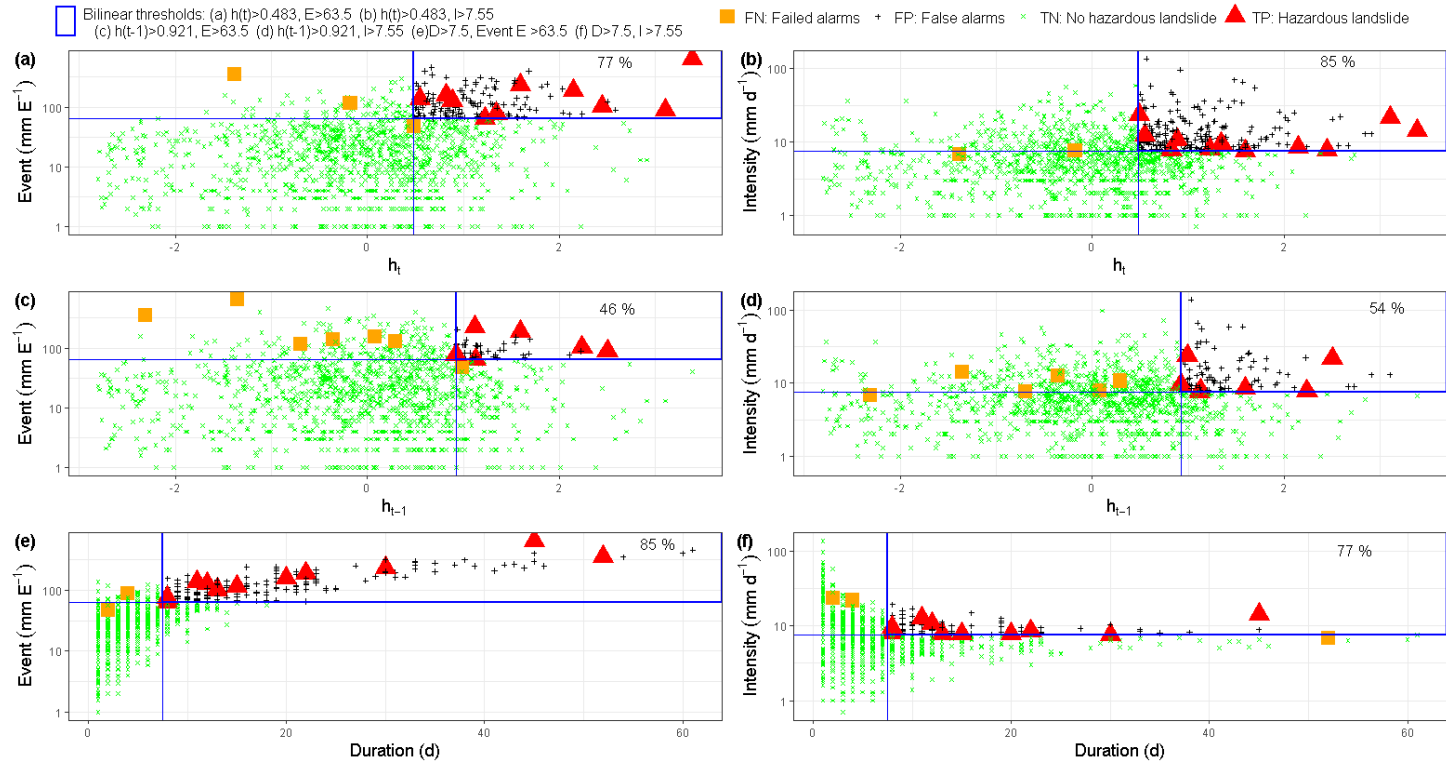


Figure 5.8: Landslide warning capabilities of the hydro-meteorological and precipitation threshold: (a) h_t -E; (b) h_t -I; (c) h_{t-1} -E; (d) h_{t-1} -I; (e) E-D; (f) I-D in Mukungwa catchment

5.5.6. ADAPTABILITY AND LIMITATION OF THE DEFINED LANDSLIDE THRESHOLD MODELS

Within the framework of this Chapter, we defined the landslide hydro–meteorological thresholds using continuous historical precipitations time series and groundwater level time series as a proxy for the catchment water storage. We mainly analysed the difference in landslide thresholds and warning capabilities as a result of the differences in catchment water storage, estimated from the groundwater responses to precipitation. It was observed that the catchment with complex or slow groundwater responding system such as Mukungwa, the warning capability of the groundwater based thresholds have less performance as compared to the fast and clear groundwater responding systems like Nyabarongo and Kivu catchments. This is truly owed by the catchment specific hydrogeological and geomorphological characteristics.

Nevertheless, the in deep analysis of the hydrogeological and geomorphological differences between the three catchments and how they could be among the explanatory factors of the observed difference in landslide thresholds and the warning capabilities was not fully conducted. However, with reference to [Figure 5.1](#), Mukungwa catchment is hydrogeologically characterized by complex aquifer in volcanic rocks and thus being a complex or slow groundwater responding system. This is probably due to the weathering products of volcanic rocks that produce a relatively permeable top layer but tend to form a brecciated or intruded sills of low permeability layer at shallow depth and thus hampering deep groundwater recharge.

Contrarily, Nyabarongo and Kivu catchments are dominated by fractured granites with overall high transmissivity and recharge and hence fast and clear groundwater responding systems. The weathering products of granites are generally coarse grained that tend to develop and preserve open joint systems that increase permeability and thus fast groundwater response. In Nyabarongo and Kivu catchments therefore, the landslide warning capability of groundwater based thresholds performed higher than precipitation thresholds as opposed to Mukungwa catchment. This is to say that in regions with very slow groundwater responding system where rainfall induced shallow landslides prevail, precipitation based thresholds can still practically be useful for landslide prediction and warning. However, the need for hydrological thresholds is true for both shallow and deep seated landslides ([Cascini et al., 2010](#); [Corominas et al., 2005b](#); [Duan et al., 2019](#); [Hong and Wan, 2011](#)) and thus, being more powerful than precipitation based thresholds. More studies also confirm the high warning capability of hydro–meteorological thresholds over precipitation-based thresholds after incorporation of either soil moisture or catchment storage ([Ciavolella et al., 2016](#); [Mirus et al., 2018a](#); [Prenner et al., 2018](#); [Thomas et al., 2019](#); [Wicki et al., 2020](#)).

From the previous chapter, the highest predictive capability of precipitation-based threshold in a bilinear framework that used the antecedent precipitation API and event rainfall intensity I as API_{30-I} , was about 68% of true alarms associated with 27% of false alarms. However, this prediction level was further improved through this research by considering the catchment specific groundwater levels where the best predictor h_t-I was able to correctly predict 85% of landslides (TP) with 15% of false alarms. Although, the catchment water storage would have been a better landslide predictor, this type of information is scarce. Therefore, the groundwater level was considered as a proxy and used

as a hydrological landslide predictor variable.

The component of groundwater has been on one hand considered as landslide triggering factor and on the other hand as landslide predisposing factor (Cascini et al., 2010; Corominas et al., 2005a; Duan et al., 2019; Hong and Wan, 2011). Being a hydrological parameter, it was subjectively considered as landslide predisposing factor and plotted on x axis of a 2D plot as a cause in a cause–trigger framework. However, the neutral use of groundwater levels (neither trigger nor cause) in a single variable threshold model h_t provided excellent prediction results up to 93% of true alarms and only 7% of missed alarms with a rather high rate of false alarms up to 38%.

The adopted approach for hydro–meteorological threshold model definition aimed to reduce the rate of false alarms associated with single variable thresholds and follows the cause–trigger concept (Bogaard and Greco, 2018) in which the groundwater levels as cause were combined with precipitation variables as trigger in a bilinear framework (Mirus et al., 2018a). We have tested different combinations of the optimum hydrological and meteorological threshold variables such as h_t –E, h_t –I, h_{t-1} –E, and h_{t-1} –I and the combination of groundwater levels on the day of landslide and event rainfall intensity h_t –I proved to have higher skill for landslide prediction and warning with high rate of true alarms 64–85% and reduced rate of false alarms 8–15% as compared to other combinations.

We remain convinced that the combination of appropriate threshold variables into cause–trigger framework should consider the timescale of each variable to avoid overlapping time scales between hydrological and meteorological variables. However, the combinations of h_t –E, and h_t –I may led to overlapping time scale between groundwater levels and rainfall event. This would be very true for longer time scale triggers and very fast groundwater responding system with very short time memory which was not the case in our studied catchments. To account on this constraints, we have also considered the groundwater level recorded prior to landslide triggering events h_{t-1} –E and h_{t-1} –I combinations but the result was not as significant as h_t –E and h_t –I.

The single variable and bilinear threshold models were adopted rather than the power law models commonly used in landslide precipitation threshold like intensity–duration and event–duration. These single variable and bilinear threshold models were selected based on our dataset that displays most of the landslide conditions in the upper right corner of the plots as shown in Figure 5.6, Figure 5.8, Figure 5.7 and the achieved landslide predictive capabilities summarized in Table 5.1 and Table 5.2. Although one is free to choose any other model that fit the dataset, the single variable and bilinear threshold models proved to be more efficient for hydro–meteorological threshold model definition (Mirus et al., 2018a).

Furthermore, the transfer function noise TFN time series model was used for groundwater modelling because of its simplicity, less data requirement and above all its higher skill in groundwater simulation (Bakker and Schaars, 2019; Collenteur et al., 2019). However, like other models, 100% of the observed data cannot fit the model. Therefore, the modelled groundwater data used to define the hydro–meteorological threshold may be prone to minor errors. Additionally, the spatial extrapolation of groundwater information relied on the main assumption that other hydro–geomorphological parameters do not exhibit spatial variability within the individual catchment. This is an assumption

made, given the data scarcity in the east Africa rift region in general (Monsieurs et al., 2018a) and Rwanda in particular.

Lastly, the landslide inventory used for this study relied largely on the information from government reports, newspapers, and other media where many landslide events are likely to be missed. Although, the reliance on these data sources is likely to lead to a bias towards larger landslide events and those with impact to society, this landslide inventory is the most comprehensive currently available in the study area.

5.6. CONCLUSION

This chapter aimed to improve the landslide forecast quality by incorporating the catchment specific groundwater levels as a proxy for regional water storage. A parsimonious transfer function noise (TFN) time series model was used to simulate the groundwater levels that temporally match with the available landslide inventory. Based on the statistical measures of goodness of fit, the root mean square error (RMSE < 0.5 m) and the explained variance ($R^2 > 60\%$), the TFN time series model demonstrates sufficient skill to simulate groundwater levels.

The standardized groundwater levels modelled on a landslide day h_t with AUC between 0.76–0.80 and the event rainfall volume E whose AUC ranges from 0.74–0.93 were identified as the hydrological and meteorological variables with the highest discriminatory power to distinguish landslide from no landslide conditions and thus, the most dominant control on landslide occurrence in the studied region. The single variable threshold model derived from groundwater levels h_t indicated the highest landslide prediction and/or warning capability with about 85–93% of true positive alarms despite the resulting rate of false alarms between 26–38%. Similarly, the single variable threshold models derived from precipitation intensity I and volume E reveal also high landslide predictive skill in terms of true positive alarms with about 64–100% associated with 15–44% of false alarms.

However, it was noticed that relying on single variable threshold models exclusively derived from precipitation variables like E and I considered as landslide triggers could lead to biased results due to the fact that many landslides occur not only due to the trigger itself but a rather combination of both trigger and pre-event hydrological conditions. Contrarily, relying on single variable threshold models exclusively defined using hydrological variables like groundwater h_t , lead to unbiased landslide predictions due to their high consideration of long-term antecedent conditions until the day of landslide occurrence.

Further combination of the optimum groundwater and precipitation thresholds as bilinear threshold models reduced the rate of false alarms by about 18–28% at the expense of reduced rate of true positive alarms by about 9–29% and thus being less advantageous than single variable threshold models. However, the hydro-meteorological threshold models defined in bilinear framework as h_t – I indicated higher landslide predictive skill in terms of true positive alarms (64–85%) than traditional threshold model I – D (36–77%) that exclusively rely on precipitation. Furthermore, the integration of catchment specific groundwater levels in landslide hazard assessment in Rwanda improved the landslide prediction and warning capabilities of the existed precipitation based threshold that used the antecedent precipitation API as a proxy for hydrological condition and

event intensity I as a meteorological condition. Overall, the incorporation of observed and model derived groundwater variables in an empirical statistical approach and the use of regional specific hydrological characteristics improve the landslide prediction capacity as compared to the exclusive use of global precipitation based threshold models.

6

POTENTIAL OF SATELLITE DERIVED HYDRO-METEOROLOGICAL INFORMATION FOR LANDSLIDE INITIATION THRESHOLDS IN RWANDA

This chapter is based on:

Uwihirwe, J., Riveros A., Wanjala H., Schellekens J., Weiland S.F., Hrachowitz, M. and Bogaard, T.: The potential of satellite and model derived hydro-meteorological information for landslide initiation thresholds in Rwanda. Nat. Hazards Earth Syst. Sci, <https://doi.org/10.5194/egusphere-2022-596>.

Abstract

A combination of extreme hydro-meteorological conditions such as high soil moisture content and heavy or prolonged precipitation contribute to landslide hazard initiation in mountainous areas worldwide. On-site soil moisture monitoring equipment and rain gauges have been widely used to record these variables but they have a sparse spatial coverage and only point scale data records. Satellite-based technologies provide estimates of rainfall and soil moisture over larger spatial scales and now cover multiple decades, sufficient to explore their value for the development of landslide early warning system in data scarce regions. In this Chapter, we used statistical metrics to compare gauge-based to satellite-based precipitation products and assess their performance in landslide hazard assessment and warning in Rwanda. Similarly, the value of high-resolution satellite and hydrological model derived soil moisture was compared to in-situ soil moisture observations at Rwanda weather station sites. Based on statistical indicators, the NASA GPM-based IMERG rainfall product showed the highest skill to reproduce the main spatiotemporal precipitation patterns at the studies sites in Rwanda. Similarly, the satellite- and model- derived soil moisture time series broadly reproduce the most important trends of in-situ soil moisture observations. We evaluated two categories of landslide meteorological triggering conditions from IMERG satellite precipitation. First, the maximum rainfall amount during a multiple day rainfall event. Second, the cumulative rainfall over the past few day(s). For each category, the antecedent soil moisture recorded at three levels of soil depth, top 5cm by satellite-based technologies as well as top 50cm and 2m through modelling approaches, was included in the statistical models to assess its potential for landslide hazard assessment and warning capabilities. The results reveal the cumulative 3 day rainfall R_{D3} as the most effective landslide trigger. This was indicated not only by its highest discriminatory power to distinguish landslide from no landslide conditions with an area under the curve $AUC=0.72$ but also the resulting true positive alarms $TPR=80\%$. The modelled antecedent soil moisture in the root zone $Se_{root(t-3)}$ i.e. top 50cm was the most informative hydrological variable for landslide hazard assessment with an AUC of 0.74 and TPR of 84%. The hydro-meteorological threshold models that incorporate the $Se_{root(t-3)}$ and R_{D3} following the cause-trigger concept in a bilinear framework reveal promising results with improved landslide warning capabilities in terms of reduced rate of false alarms by about 20% at the expense of a minor reduction of true alarms by about 8%.

6.1. INTRODUCTION

In Chapter 4, a statistical approach was used to define gauge-based precipitation thresholds along with estimates of antecedent precipitation indices. In Chapter 5, we incorporated regional groundwater level measurements extended with a transfer function noise model to define the landslide hydro-meteorological thresholds for regional landslide hazard assessment. So far, both chapters relied exclusively on in-situ observed precipitation and hydrological data constrained by the sparsely distributed recording equipment with point scale resolution and gaps in the data record. There is a concern about the omission and/or overgeneralisation of information on the pre-wetting hydrological conditions at the locations of the landslide due to the sparsely distributed hydrological recording equipment. These pre-wetting conditions regulate the disposition of a slope to near failure (Bogaard and Greco, 2018; Sidle et al., 2019). Including this information in a LEWS may thus be a promising opportunity to decrease the rate of both false and missed alarms (Bogaard and Greco, 2018; Peres et al., 2017).

Similar to precipitation and other hydrological variables, soil moisture exhibits high spatial variability particularly in tropical areas (Dewitte et al., 2022; Kirschbaum et al., 2012; Sekaranom et al., 2020). This spatial variability is hardly covered by on-site monitoring equipment due to the sparse observation networks, themselves providing point-scale observations only. Alternative ways of incorporating such hydrological state information into landslide hydro-meteorological thresholds have been attempted and include the use of soil moisture estimates from satellite products (Marino et al., 2020; Thomas et al., 2019; Zhuo et al., 2019) as well as from distributed hydrological models (Mostbauer et al., 2018; Prenner et al., 2018, 2019; Wang et al., 2019; Zhao et al., 2020).

In this Chapter, we aimed to explore the usefulness of adding soil moisture from satellite-products and from a distributed hydrological model to satellite-based precipitation for the estimation of landslide hazard assessment thresholds in Rwanda. We specifically i) investigated the suitability of various satellite precipitation products as substitute for rainfall data from a sparsely distributed gauge network in Rwanda, ii) evaluated the added value of satellite and model derived soil moisture information recorded at various soil depth, and iii) assessed the potential of incorporating such information in empirical landslide initiation threshold models and the warning capabilities in Rwanda.

6.2. METHODS AND DATA

6.2.1. LANDSLIDE INVENTORY

The inventory for this study, contains landslides recorded from 2007 to 2019. It was accessed from previous chapters and was further extended and updated through compilation of additional rainfall-induced landslides as reported from local newspapers, blogs and government technical reports. This landslide inventory was compiled with respect to the methodology adopted by Kirschbaum et al. (2015); Monsieurs et al. (2018c). Between 2007 and 2019, the inventory includes 55 accurately dated landslides, 32 of which are located in the modelled catchments (Kivu, Nyabarongo upper and Mukungwa) shown in Figure 6.3. However, it is important to note that this inventory is likely to miss the non-hazardous landslides which are less reported upon than hazardous landslides that led to fatalities/injuries and considerable damages. The inventory provides the location

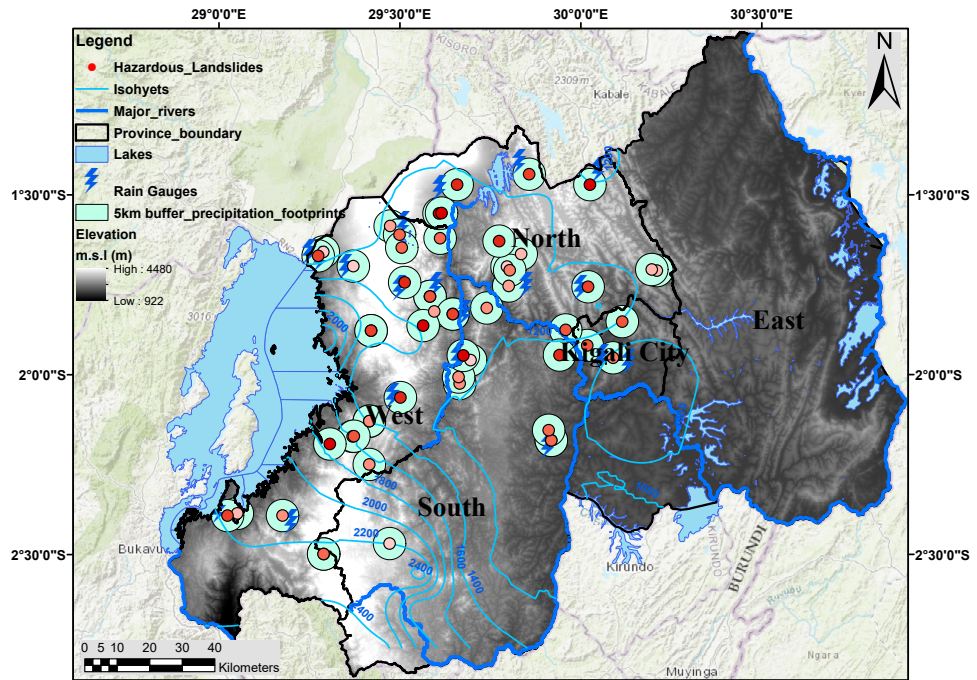


Figure 6.1: Spatial and temporal distribution of hazardous landslides with light to dark red dots indicating old to new landslides recorded from 2007–2019, representative rain gauges and rainfall distributions indicated by isohyets (sky blue lines), precipitation footprint of 5km buffer around each landslide

of each recorded landslide but with a varying spatial accuracy of 5 to 25 km depending on the smallest administrative unit recorded by the landslide event reporters. Therefore, a buffer zone of 5km, equivalent to the frequently recorded accuracy, was used around each landslide (Figure 6.2) to support the choice of the landslide representative rain gauge. The same areal buffer was used as a footprint to avail the areal satellite precipitation and soil moisture as detailed in Sections 6.2.2 and 6.2.3.

6.2.2. PRECIPITATION PRODUCTS AND PERFORMANCE EVALUATION

GAUGE BASED PRECIPITATION AND SELECTION OF LANDSLIDE REPRESENTATIVE DATA

We accessed daily precipitation data from 19 rain gauges operated by the Rwanda Meteorology Agency. These rain gauges were selected based on their location within the defined buffer of 5km around each landslide location (Figure 6.1). Once two or more rain gauges fall within the same buffer zone, the gauges are weighted using Equation 4.1 from Melillo et al. (2018) to select the most representative rain gauge. A similar procedure was used to select the representative rain gauge for landslides located far (>5km) from any rain gauge. The selected gauge-based precipitation were used as benchmarks to assess the suitability of satellite precipitation products.

Table 6.1: Pre-selected precipitation products and short description

Satellite products	Resolution Spatial	Temporal	Period	Data source description	References
TRMM 3B42 v7	0.25°	Daily	1998-2019	Passive microwave (PMW) from a variety of low Earth orbit satellites, infrared (IR) data and precipitation gauge supplied by the Global Precipitation Climatology Centre (GPCC)	(Huffman et al., 2010)
CHIRPS	0.05°	Daily	1981-present	Geostationary thermal infrared (IR); microwave satellite estimates and the in-situ precipitation observations	(Funk et al., 2015)
PERSIANN CDR	0.25°	Daily	1983-present	GridSat-B1 infrared data and bias-adjusted using the Global Precipitation Climatology Project (GPCP) monthly product and accumulated to the daily scale	(Ashouri et al., 2015)
GLDAS 2.1	0.25°	3 hourly	2000-present	Geostationary satellite infrared (IR) cloud-top temperature measurements and microwave observation techniques	(Rodell et al., 2004)
CFSv2	0.2°	6 hourly	1979-present	Satellite observations in the infrared and microwave channels and gauge observations	(Saha et al., 2014)
IMERG_GPM	0.1°	30 min	2014-present	Passive Microwave from various low Earth orbit satellites, Infrared from geosynchronous Earth orbit satellites and gauges precipitation (successor of TRMM)	(Huffman et al., 2015)
ERA5	0.25°	Hourly	1979-present	This is a non-satellite but re-analysis product. precipitation is generated employing a convection scheme along with the large-scale cloud scheme that have been upgraded with an improved representation of mixed-phase clouds and prognostic variables for precipitating rain and snow	(Hersbach et al., 2020)

SATELLITE PRECIPITATION PRODUCTS AND SELECTION OF THE BEST PERFORMING PRODUCT

With the gauge-based precipitation data as reference, we assessed the performance of seven satellite precipitation products summarized in Table 6.1. These satellite precipitation products were preliminary selected for analysis based on the criteria that their dataset i) at least partially overlap with the landslide inventory period (2007-2019), ii) has at least daily temporal resolution, and iii) is available on Google Earth Engine (GEE). Among the pre-selected satellite products, we have chosen the most suitable product for landslide hazard assessment in Rwanda based on the relative comparison with gauge-based precipitation. This was achieved using a number of statistical approaches that include: i) the use of statistical metrics of goodness of fit, ii) rainfall frequency indicators, and iii) intensity comparisons. The statistical metrics of goodness of fit include the root mean square error RMSE, Pearson correlation CC, and the long-term relative bias RB computed with Equation 6.1, Equation 6.2, and Equation 6.3.

$$RMSE = \sqrt{\frac{\sum_{i=1}^n (Y_i - X_i)^2}{n}} \quad (6.1)$$

$$CC = \frac{\sum_{i=1}^n (X_i - X_{mean})(Y_i - Y_{mean})}{\sqrt{\sum_{i=1}^n (X_i - X_{mean})^2} \sqrt{\sum_{i=1}^n (Y_i - Y_{mean})^2}} \quad (6.2)$$

$$RB = \frac{Y_{mean} - X_{mean}}{Y_{mean} + X_{mean}} \quad (6.3)$$

Where Y_i is the rain gauge observation at date i , X_i is the satellite estimate at the same date i , n is the total number of data pairs for each precipitation product considered, Y_{mean} and X_{mean} are the mean rainfall from rain gauge and satellite products respectively. The rainfall frequency indicators specify the frequency of rainy days based on the predefined threshold indices (Joshi et al., 2014; Tank et al., 2009). We used five rainfall threshold indices that reflect the number of rainy days with $>X$ mm of rain (R_{Dx}). The predefined indices are R_{D0} , R_{D10} , R_{D20} , R_{D30} , and R_{D50} indicating the number of rainy days with >0 mm as rainy days, >10 mm as heavy rainy days, >20 mm as very heavy rainy days, >30 mm as even heavier rainy days, and >50 mm as extremely heavy rainy days respectively. With intensity comparison, we compared the cumulative 30day rainfall from the satellite precipitation products to the cumulative 30day precipitation from rain gauges using scatter plots.

6

6.2.3. SOIL MOISTURE PRODUCTS AND DATA ACQUISITION

IN-SITU SOIL MOISTURE DATA FROM AUTOMATIC WEATHER STATIONS

In-situ soil moisture data, collected from the automatic weather stations (AWSs) equipped with soil moisture sensors, were accessed from the Rwanda Meteorological Agency for six AWSs as shown in Figure 6.2. The AWSs recorded the soil moisture at 20cm depth with a temporal resolution of 5-10 minutes from July 2018 to December 2019. Because the analysis focuses on a daily time-scale, we computed and used the daily average soil moisture time series recorded from July 2018 to December 2019. The in-situ AWSs soil moisture data were used as a benchmark to comparatively get an insight on the quality of other sources of soil moisture products that include satellite and model derived soil moisture estimates described in following Sections.

SATELLITE SOIL MOISTURE AND VARIABLE OF INTEREST

We used a satellite-derived near surface soil moisture product provided by Planet, formerly VanderSat (VdS) (<https://vandersat.com/data/soil-moisture/>, last access: 29 March 2022). The product relies on the Land Parameter Retrieval Model (LPRM) (Owe et al., 2008, 2001; De Jeu et al., 2014) to estimate the near surface soil moisture by combining raw data from the Advanced Microwave Scanning Radiometer 2 (AMSR-2), and Soil Moisture Active Passive (SMAP) (Bouaziz et al., 2020). The satellite product estimates volumetric soil water content or soil moisture (m^3m^{-3}) of the upper 5cm of soil down-scaled from a spatial resolution of 25×25 km to $100m \times 100m$. From VdS, we accessed daily soil water content estimates from the top 5cm of soil (θ_{top}) for the 2007-2019 period for each of the defined regions of interest (ROIs) equivalent to the 5km buffers shown in Figure 6.2.

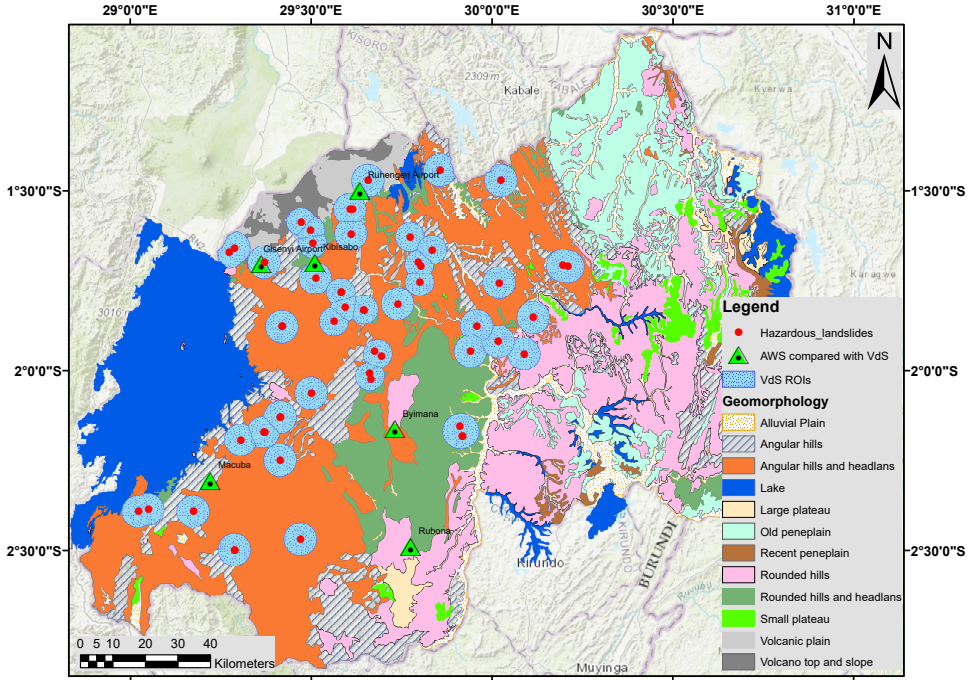


Figure 6.2: Geomorphology of Rwanda, landslide representative AWSs (Automated weather stations) with soil moisture sensors; landslides in red dots and 5km buffer zones indicating the Research Area of Interest (ROIs) for areal soil moisture acquisition

HYDROLOGICAL MODEL DERIVED SOIL MOISTURE AND VARIABLES OF INTEREST

We also used the soil moisture derived from the Wflow-sbm, a distributed hydrological model that uses the conceptual bucket model approach to estimate soil water content (Imhoff et al., 2020). With Wflow-sbm, the soil is considered as a bucket with a depth (Z) divided into 2 zones: the unsaturated store U and the saturated store S . The interface between U and S is a pseudo water table located at depth Z_w . The values of unsaturated storage U and saturated storage S are computed as in Equation 6.4 and Equation 6.5.

$$U = (\theta_s - \theta_r) Z_w - U_d \quad (6.4)$$

$$S = (\theta_s - \theta_r) Z - Z_w \quad (6.5)$$

Where θ_s , θ_r are saturated and residual water content respectively and U_d is the soil water deficit

The unsaturated store U was the variable of interest and was subdivided into 2 variables: the water content in the root zone θ_{root} [-] representing the unsaturated soil water storage of the top 50cm and the part of the soil water capacity occupied θ_{uz} [-] representing the unsaturated soil water storage of the upper 2 m. For this chapter, the model area consisted of three catchments (Kivu, Upper Nyabarongo and Mukungwa) as highlighted

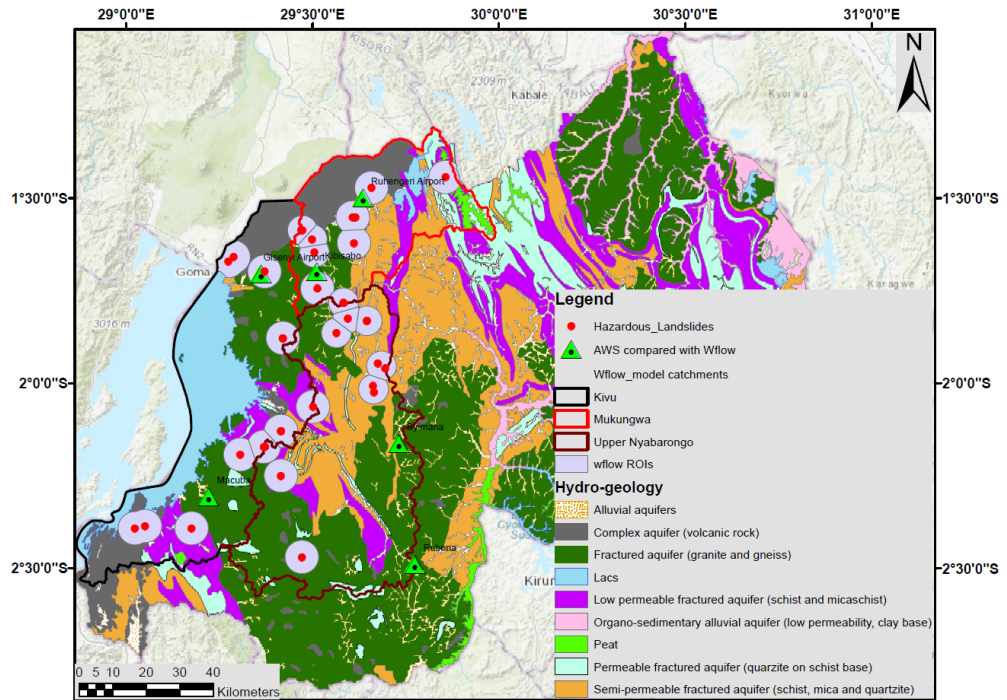


Figure 6.3: Wflow model catchments (Kivu, upper Nyabarongo and Mukungwa) and hydrogeology; landslides in red dots and 5km buffers indicating the Research Area of Interest (ROIs) for areal soil moisture acquisition from the Wflow model, Automated weather stations (AWSs) with soil moisture sensors for comparative performance evaluation of the Wflow modelled soil moisture

in Figure 6.3. We obtained time series of $\theta_{root}[-]$ and $\theta_{uz}[-]$ from 2007-2019 overlapping with the landslide inventory period from a wflow-sbm simulation based on ERA5 re-analysis meteorological data. To increase the comparability with the satellite based soil moisture (VdS), the same ROIs represented by the buffers of 5km around each landslide location were used to interpolate the unsaturated water storage time series for each ROI located in the model catchment. Similarly, only the AWSs located in the model catchment (Figure 6.3) were used for the comparative performance evaluation of the model derived soil moisture products.

6.2.4. LANDSLIDE HAZARD ASSESSMENT AND THRESHOLDS DEFINITION

LANDSLIDE METEOROLOGICAL AND HYDROLOGICAL CONDITIONS AND TEST VARIABLES

The daily rainfall data from the best performing satellite product were used to define the landslide meteorological triggering conditions. We used two categories of landslide triggering conditions. The first category defined a landslide trigger as the maximum probable rainfall event (MPRE) during which or slightly after its end, one or more landslides occurred. The MPREs were defined as individual periods of rainy days interrupted by dry periods of at least two days. Given the constraint of overestimation of the number of

rainy days with 0-10mm by satellites (Pavez, 2021), a rainy day was objectively referred to as the day with 10 mm/d while a dry day was referred to as the day with <10 mm/d. This threshold was objectively selected using the rainfall frequency indicator metric. The landslide predictor variables in this category were therefore the rainfall event volume (E), event duration (D) and event intensity (E/D). The rainfall event volume E (mm) was computed as the cumulative rainfall during each MPRE of duration D (days). The duration D equivalent to MPRE is the individual periods of days with recorded rain interrupted by inter event time (IET) of at least two dry days. The event intensity E/D is the ratio of event rainfall volume E and event duration D.

The second category defined a landslide trigger as the recent cumulative rainfall R_{Dx} at the end of which one or more landslides occurred. This category considers the total cumulative rainfall over the last three days (R_{D3}), two days (R_{D2}), and one day (R_{D1}) at the end of which, one or more landslides occurred. While MPREs time series are interrupted by the IETs, the R_{D3} , R_{D2} and R_{D1} for each day during the 2007-2019 study period were computed regardless of a rainy or dry day and thus resulting into longer time series and more data points compared to the MPREs time series. The time series of the defined meteorological triggering conditions from each category and for all precipitation foot prints were compiled in a single dataset for further statistical analysis. To provide a normalized comparison of the soil wetness, we transformed the satellite- and model-derived water content θ to effective soil moisture Se with Equation 6.6 to define the landslide predisposing hydrological conditions.

$$Se = \frac{\theta - \theta_{min}}{\theta_{max} - \theta_{min}} \quad (6.6)$$

Where Se stands for the effective soil moisture [-], θ_{max} and θ_{min} are the maximum and minimum values of the recorded or modelled soil water content θ . The normalization of soil water content θ was made for easy comparison of the observed, model-derived and satellite-based soil moisture products. However, for all compared soil moisture products, the θ_{max} and θ_{min} were 1 and 0 respectively which lead to almost similar values of Se and θ

The tested hydrological conditions include therefore, the near surface soil moisture Se_{top} , representing the soil moisture of the upper 5cm of soil, provided by the satellite techniques (VdS), the Se_{root} representing the root zone soil moisture of the upper 50cm, acquired through modelling approach (Wflow), and Se_{uz} representing the soil moisture estimates from the upper 2m of soil, obtained through modelling approach (Wflow). To assess the contribution of the pre-wetting state of the soil prior to the landslide triggering conditions, we have considered the antecedent soil moisture i.e. recorded or modelled prior to the start of the triggering meteorological conditions. The antecedent soil moisture referred to the time interval before the start of each of the defined categories of the meteorological triggering conditions. We have therefore used the $Se_{top(t-x)}$, $Se_{root(t-x)}$, $Se_{uz(t-x)}$ with t (date) and x (days) expressing the end time and the duration of the triggering conditions respectively. However, due to the transient duration of the MPREs, x was hypothetically represented by a value of 1 standing for one entire MPRE while values of 1, 2, 3 represent the duration (days) of the triggering R_{Dx} conditions. A binary classification of the defined hydrological and meteorological conditions was undertaken to

classify the landslide and no-landslide conditions. The meteorological or hydrological conditions are referred to as landslide conditions i.e. positive class, when at least one landslide occurs during its course or slightly after its end while they are referred to as no-landslide conditions i.e. negative class when no landslide occurred during its course or slightly after its end.

DISCRIMINATORY POWER OF THE LANDSLIDE TEST VARIABLES AND OPTIMUM THRESHOLDS FOR LANDSLIDE INITIATION

The landslide test variables which include the predisposing hydrological conditions $Se_{top(t-1)}$, $Se_{top(t-2)}$, $Se_{top(t-3)}$, $Se_{root(t-1)}$, $Se_{root(t-2)}$, $Se_{root(t-3)}$, and $Se_{uz(t-1)}$, $Se_{uz(t-2)}$, and $Se_{uz(t-3)}$ as well as the triggering meteorological conditions E , D , E/D , R_{D1} , R_{D2} , and R_{D3} were tested for their relevance on landslide occurrence. We used a receiver operating characteristic (ROC) and the area under the curve (AUC) metrics to evaluate the discriminatory power of each of the landslide test variables. The ROC curve is defined as a graphical plot indicating the performance of the test variable at all threshold levels by providing the trade-off between the true positive rate (TPR) and false positive rate (FPR) at each level. The AUC is a statistical metric that indicate the discriminatory power of the test variable i.e. the capacity of the test variable to correctly distinguish positive from negative classes i.e. landslide from no landslide conditions. It compares also the test variable to a random guess (AUC=0.5) and thereby indicates the statistical significance where the perfect test variable would have an AUC equal to unity. The rate of correctly (TPR, true positive rate) and incorrectly predicted landslides (FPR, false positive rate) corresponding to each cut off on the ROC curves are computed using Equation 6.7 and Equation 6.8 respectively.

$$TPR = \frac{TP}{TP + FN} \tag{6.7}$$

$$FPR = \frac{FP}{FP + TN} \tag{6.8}$$

The rate of unpredicted landslides (FNR, false negative rate) and the rate of correct prediction of no-landslides (TNR, true negative rates) are computed using Equation 6.9 and Equation 6.10.

$$FNR = \frac{FN}{FN + TP} \tag{6.9}$$

$$TNR = \frac{TN}{TN + FP} \tag{6.10}$$

Where TP are true positives or true alarms i.e. outcomes with correctly predicted landslides, FN are false negatives or missed alarms i.e. the number of landslides that occurred in reality but were not predicted, FP are false positives or false alarms i.e. predictions of landslide occurrence while in reality there was no landslide reported, and TN are true negatives i.e. correct predictions of no-landslide occurrence.

Since the ROC curve only indicates all possible thresholds and their relative balance between TPR and FPR, one is free to choose the optimum threshold depending on whether to maximize the TPR or minimize the FPR. However, according to Postance and

Hillier (2017), the optimum threshold is the one that maximizes the TPR while minimizing the FPR. Therefore, that optimum threshold level above which landslides are highly likely to occur have been defined using two statistical metrics i.e. the maximum true skill statistic (TSS) and minimum radial distance (Rad). The TSS is expressed as a balance between the TPR and FPR as indicated in Equation 6.11.

$$TSS = TPR - FPR \quad (6.11)$$

Where the maximum value of TSS indicates the optimum threshold that maximizes the TPR while minimizing the FPR. For a perfect threshold, the TSS reaches a unity indicating a zero false positive rate (FPR). The radial distance (Rad) shows the relative distance from the defined threshold level on the curve to the perfect model or point whose TPR is a unit and zero FPR and is computed Equation 6.12.

$$Rad = \sqrt{FPR^2 + (TPR - 1)^2} \quad (6.12)$$

LANDSLIDE HYDRO-METEOROLOGICAL THRESHOLDS AND WARNING CAPABILITIES

The optimum thresholds defined based on the maximum TSS and or minimum Rad were plotted in 1D threshold space here referred to as single variable threshold line beyond which the probability of landslides is high. We also followed the cause-trigger concept (Bogaard and Greco, 2018) that reflect the hydro-meteorological thresholds and hypothetically plotted the optimum thresholds of the landslide predisposing hydrological variables i.e the antecedent soil moisture on the x-axis and the meteorological triggering variables on the y-axis of a two dimensional 2D space here referred to as bilinear thresholds. The bilinear threshold models made of hydrological and meteorological variables are plotted in x, y pairs i.e antecedent soil moisture versus E/D or R_{DX} . Furthermore, the bilinear threshold from a traditional landslide prediction model event–duration E–D, that exclusively rely on precipitation, has been also defined to serve as a benchmark for comparative performance evaluation.

6.3. RESULTS AND DISCUSSION

6.3.1. PERFORMANCE OF SATELLITE PRECIPITATION PRODUCTS

The suitability of satellite precipitation products in the study region was assessed using three statistical indicators as summarized in Table 6.2, Table 6.3 and illustrated in Figure 6.4. From the statistical measures of fits (RMSE, CC, RB), it is generally observed that IMERG is consistently more suitable while ERA-5 was found to be the least suitable product as compared to other satellite precipitation products. The evaluation based on frequency indicators is summarised in Table 6.3. These indicators give an overview on whether a given satellite product would overestimate or underestimate the observed gauge precipitation based on the predefined threshold indices. IMERG-GPM displays the highest skill to estimate all ranges of rainfall from heavy to extremely heavy rainy days as recorded by the on-site gauges. CHIRPS and TRMM 3B42 v7 provide good estimates of precipitation with quite similar number of rainy days ($RD_0=1256$ days) to gauge-based rainfall ($RD_0=1259$ days). However, these satellites drastically underestimate the number of heavy to extreme heavy rainfall (RD_{20} , RD_{30} and RD_{50}). For example, TRMM and

Table 6.2: Performance of Satellite precipitation products based on statistical metrics

Metrics	TRMM 3B42 v7	CHIRPS	PERSIANN CDR	GLDAS 2.1	CFSv2	IMERG	ERA 5
RMSE (mm)	8.17	8.53	7.42	8.55	10.58	8.18	12.60
CC (-)	0.31	0.27	0.25	0.24	0.17	0.35	0.22
RB (-)	-0.08	-0.01	-0.15	0.03	0.11	0.02	0.29

Table 6.3: Performance of Satellite precipitation products based on rainfall frequency indicators

Indices	Description	Gauge	TRMM 3B42 v7	CHIRPS	PERSIANN CDR	GLDAS 2.1	CFSv2	IMERG	ERA 5
RD ₀	Rainy days >0mm	1259	1691	1256	2732	3086	2835	2842	3520
RD ₁₀	Heavy rainy days >10mm	397	307	424	138	377	617	383	879
RD ₂₀	Very Heavy rainy days >20mm	132	87	101	9	79	199	126	250
RD ₃₀	Even heavier rainfall days >30mm	49	29	25	0	22	84	42	78
RD ₅₀	Extremely heavy rainfall >50mm	9	4	3	0	2	22	6	21

CHIRPS estimated RD₂₀=87 and 101days respectively out of 132 days estimated by rain gauge (Table 6.3).

The suitability of satellite products was also assessed using intensity comparison indicated by the density of the scatter points around 1:1 line as shown in Figure 6.4. The scatter plots compare 30day cumulative rainfall from satellite precipitation products versus rain gauges. The scatter plots reveal that GLDAS, CFSv2 and ERA-5 tend to overestimate rainfall while underestimations are noticed from PERSIANN CDR as compared to the in-situ gauge rainfall. Based on the closeness of scatter points to the 1:1 line, CHIRPS and IMERG exhibit a higher resemblance to gauge data (Pearson correlation R=0.67 and 0.60 respectively) than other satellite products and could thus be used as alternative to gauge-based precipitation.

Overall, IMERG shows rainfall pattern that are most consistent with available gauge observations in Rwanda despite the over estimation of the number of rainy days with less than 10mm (RD₀). According to Kimani et al. (2017), the overestimation of rainfall in areas with elevation >2500m and underestimation in areas with elevation < 2500m was observed before and is attributed to satellite inherent challenges to retrieve orographic rainfall. To overcome this constraint, 10mm/d has been considered as a threshold to define a satellite-based rainy day and thus being relevant for landslide hazard assessment in Rwandan climate conditions. Other researchers in the regions also found CHIRPS and TRMM to be comparable to gauge based precipitation in east Africa (Kimani et al., 2017; Monsieurs et al., 2018c). Monsieurs et al. (2018c) found the areal-averaged TMPA rainfall estimates, the predecessor of IMERG, to be more suitable for assessing landslide hazard threshold than the sparsely distributed gauge data with limited representativeness in the context of high rainfall variability of the east African rift.

6.3.2. MEAN SOIL MOISTURE RESPONSE TO RAINFALL AND LANDSLIDE EVENTS

Figure 6.6 indicates the temporal dynamics of the satellite estimates Se_{top} and the model derived soil moisture time series Se_{root} and Se_{uz} compared to in-situ soil moisture observations from the automatic weather station AWS. Regardless of the difference in measuring depth (5cm, 50cm 2m), the time response to precipitation and overestimation of soil moisture, the satellite Se_{top} and model derived soil moisture time series Se_{root} and Se_{uz} broadly reproduce the most important temporal variation as recorded by in-situ

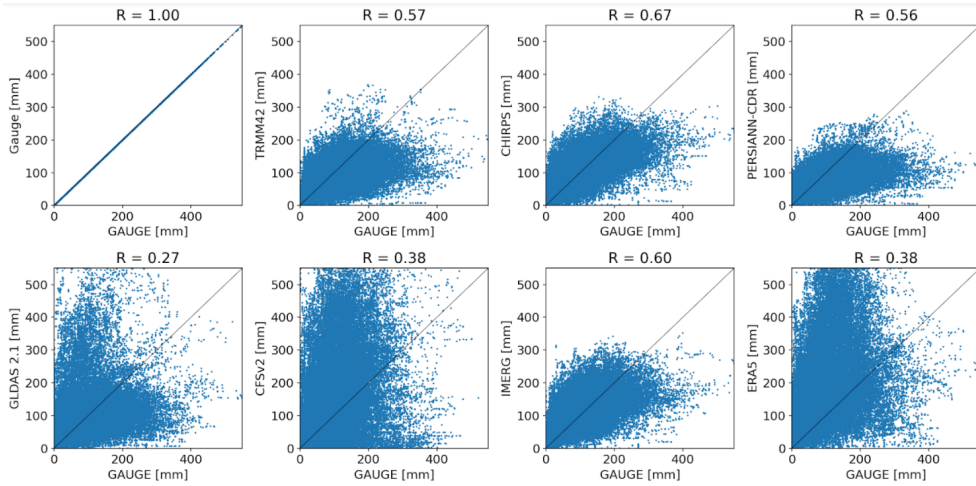


Figure 6.4: Intensity comparison between satellite and gauge based precipitation based on the cumulative 30day rainfall

soil moisture sensors. This indicates their usefulness for landslide hazards assessment as an alternative to the sparse in-situ AWSs.

The spatial averaging of soil moisture across all research areas of interest (ROIs) was undertaken to have an insight on the critical ranges of soil moisture that induce landslides in Rwandan climate conditions. The spatially averaged Se_{top} , Se_{root} and Se_{uz} soil moisture dynamics and the linked landslide occurrence are presented in Figure 6.6. The average Se_{top} , Se_{root} and Se_{uz} of all ROIs, indicate general similarities in terms of landslide predisposing but also reveal systematic differences between response time influenced by the soil moisture recording depth. For example, it is obvious that the Se_{top} (5cm) responds faster than Se_{root} (50cm) and Se_{uz} (2m). It is clear that the majority of landslides occurs when the soil moisture levels positively deviate from the long-term mean up to a critical level (about 0.1) for landslide initiation. It is also evident that the critical level for landslide occurrence is more or less fixed when other geological and geomorphological condition are kept constant and it is reached more or less easily depending on the prior rainfall expressed in terms of antecedent soil moisture and the time lag between the landslide triggering rainfall and hydrological response.

6.3.3. SINGLE VARIABLE LANDSLIDE METEOROLOGICAL AND HYDROLOGICAL THRESHOLDS AND PREDICTION CAPABILITIES

Figure 6.7 and Table 6.4 show the derived landslide meteorological and hydrological thresholds and their predictive capabilities in terms of true positive rate TPR and false positive rate FPR. The discriminatory power of each of the tested variables was evaluated with a receiver operating characteristic (ROC) curve and the area under the curve (AUC) statistical metrics. Among the tested landslide triggering meteorological variables E, D, E/D, R_{D1} , R_{D2} , and R_{D3} , the cumulative 3day rainfall R_{D3} and event rainfall volume E showed the highest discriminatory power with AUC of about 0.72 and hence the highest

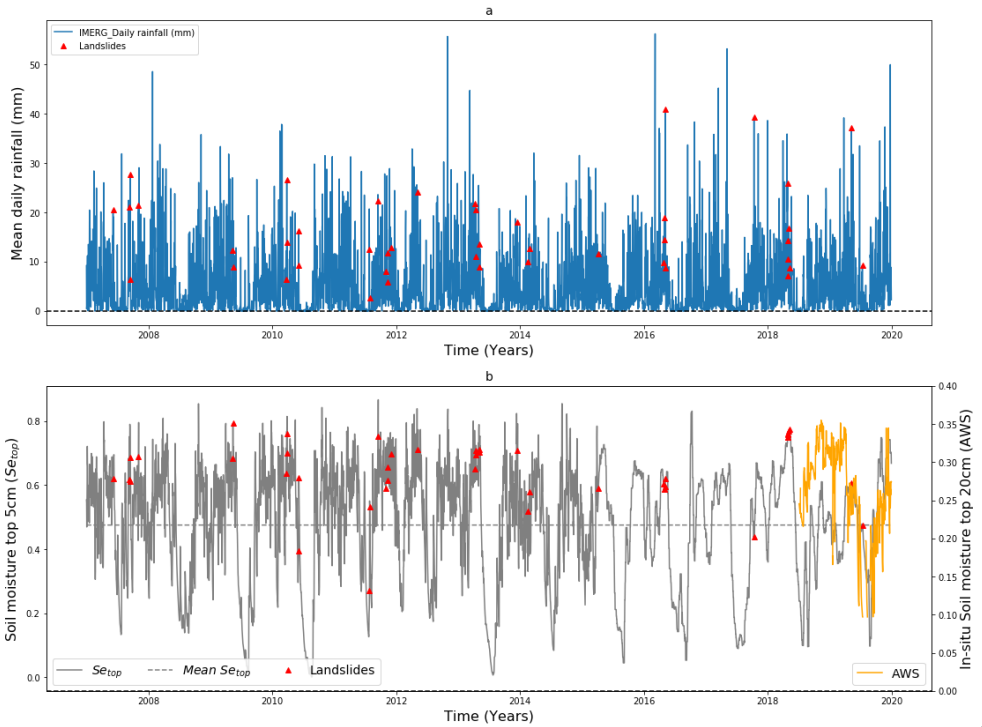


Figure 6.5: Satellite and model derived information and landslide activities a) GPM based IMERG precipitation [mm] spatially averaged over all landslide precipitation foot prints b) satellite derived soil moisture Se_{top} [-] spatially averaged over all landslide ROIs and in-situ soil moisture AWS [-] on secondary y-axis; The dashed horizontal lines represent the long term mean soil moisture and the red triangles stand for the landslide events

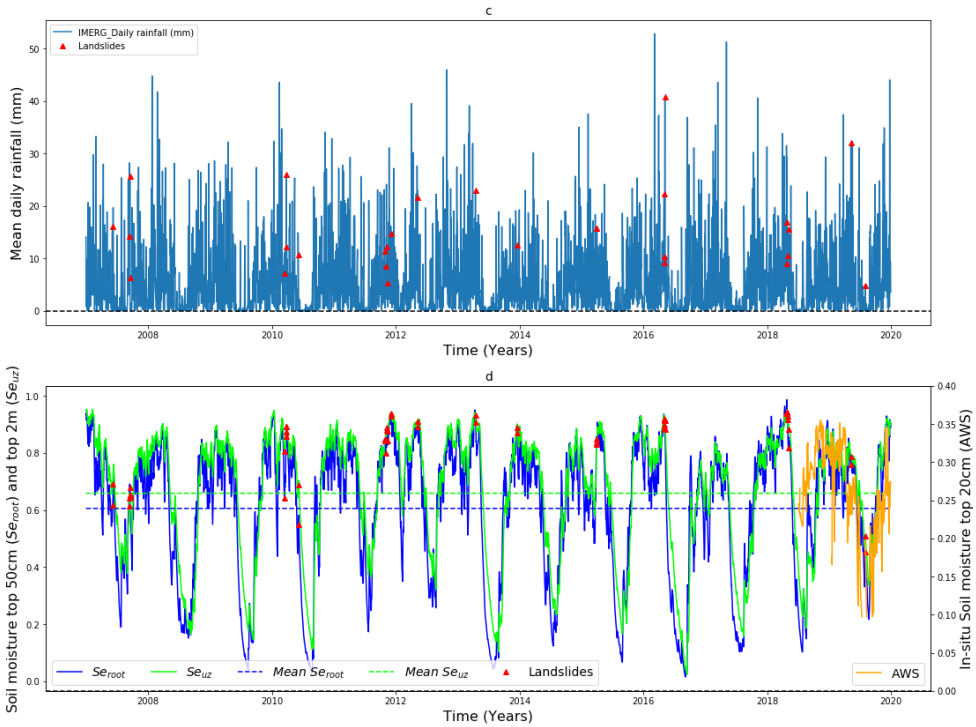


Figure 6.6: Satellite and model derived information and landslide activities c) GPM based IMERG precipitation [mm] spatially averaged over the landslide precipitation foot prints located in the modelled catchments, d) modelled soil moisture at the root zone top 50cm Se_{root} [-], modelled soil moisture top 2m Se_{uz} [-] and in-situ soil moisture AWS [-] on secondary y-axis. The dashed horizontal lines represent the long term mean soil moisture and the red triangles stand for the landslide events

impact on landslide initiation. However, the event rainfall intensity, i.e. E normalised over the event duration D as E/D indicated low capability ($AUC=0.53$) to distinguish landslides from no landslides. This stresses the importance of using the recent cumulative rainfall with a fixed duration and thus highlighting the highest impact of R_{D3} on landslide initiation process and its relevance on landslide hazard assessment and prediction compared to E that need to be normalised.

Contrarily to the gauge-based cumulative rainfall thresholds (Chapter 4), the satellite-based cumulative rainfall on the day of landslide R_{D1} was not impactful to landslide initiation ($AUC=0.35-0.38$). This may not only be due to the inaccuracies between the landslide occurrence and the reporting time but likely the landslides induced by the hydrological responses to rainfall rather than the rainfall itself. Additionally, the satellite revisiting time and or period may introduce inaccuracies in timing. Figure 6.7c and d indicate that the wetness state of soil prior to the cumulative rainfall R_{Dx} have the most significant impact on landslide occurrence as indicated by their $AUC=0.72-0.76$. Contrarily, Figure 6.7a and b show that the wetness state of the soil prior to the landslide triggering event E has no significant impact on landslide occurrence ($AUC=0.66-0.67$). This is to say that the antecedent soil moisture conditions prior to the longer triggering rainfall event E are not relevant for landslide initiation in the study area conditions. Among other factors, the duration of the triggering condition plays a major role in determining the relevance of the antecedent soil moisture on landslide occurrence. The shorter the duration of the triggering conditions, the higher the relevance of the antecedent soil moisture on landslides initiation. Highly permeable soils are less sensitive to antecedent soil moisture conditions because of the high gravity driven drainage and or deep percolation. With a tropical climate, evaporation process may also rapidly take away the antecedent soil moisture content of the top soil due to the longer timescale of the minimum inter-event time IET and the landslide triggering event E .

The thresholds definition metrics, TSS and Rad, resulted in quite comparable landslide thresholds as summarised in Table 6.4. It was noticed that the defined satellite precipitation thresholds are similar to the ones defined using gauge-based precipitation. For example, the optimum landslide threshold event rainfall volume E defined from satellite precipitation varied between 44.9mm and 60.7mm (Table 6.4) while gauge-based threshold E varied from 46mm to 67mm. Similarly but with a quite minor difference, the defined satellite-based E/D thresholds 16-17.5 mmd^{-1} seemed quite similar to gauge-based thresholds 7-13 mmd^{-1} . Nevertheless, the single variable threshold E/D being the most informative, showed quite low prediction capability in terms of TPR (56-60%) with elevated rate of false positive FPR (43-54%) i.e. incorrect predictions of landslide and thus being less effective for a robust early warning system development.

Contrarily, the single variable thresholds defined from the cumulative 3day rainfall R_{D3} outperforms other tested triggering conditions with highest prediction capability in terms of true positive rate TPR=79-81%. The same holds for the soil moisture in the root zone (50cm deep) Se_{root} that consistently showed the highest performance. Nevertheless, despite the high true positive rate from these single variables thresholds, the resulting elevated rate of false positives FPR (36-42%) still constrain their use for the development of a robust landslide early warning system. It has to be noted that the threshold defined from the antecedent soil moisture specifies the critical levels below which

Table 6.4: Event based-variable thresholds and prediction capabilities^{abcdef}

Variables	Maximum True skill statistics (TSS)					Minimum radial distance (Rad)				
	Threshold	TPR	FPR	TSS	Rad	Threshold	TPR	FPR	TSS	Rad
Event E (mm) ^a	53.1	0.54	0.21	0.33	0.51	44.9	0.60	0.27	0.33	0.49
Duration D (d) ^b	2.5	0.56	0.27	0.29	0.52	1.5	0.72	0.43	0.29	0.51
Event/Duration E/D (mmd ⁻¹) ^c	16.1	0.64	0.54	0.10	0.65	17.3	0.56	0.47	0.09	0.65
Se _{top(t-1)}	0.56	0.72	0.44	0.28	0.52	0.57	0.68	0.41	0.27	0.52
Event E (mm) ^d	60.7	0.53	0.17	0.36	0.50	60.7	0.53	0.17	0.36	0.50
Duration D (d) ^e	2.5	0.59	0.28	0.32	0.49	2.5	0.59	0.28	0.32	0.49
Event/Duration E/D (mmd ⁻¹) ^f	16.1	0.69	0.54	0.15	0.62	17.5	0.59	0.46	0.14	0.61
Se _{root(t-1)}	0.56	0.72	0.44	0.28	0.52	0.56	0.72	0.44	0.28	0.52
Se _{uz(t-1)}	0.91	0.53	0.22	0.31	0.52	0.87	0.63	0.34	0.28	0.51

^{abc} Event rainfall volume, duration and intensity defined from all landslides representative precipitation foot prints, ^{def} Event rainfall volume, duration and intensity defined using precipitation foot prints located in the modelled catchments (Kivu, Nyabarongo upper and Mukungwa)

Table 6.5: Short-scaled cumulative rainfall based-variable thresholds and prediction capabilities^{abcdef}

Variables	Maximum True skill statistics (TSS)							Minimum radial distance (Rad)				
	Threshold	TPR	FPR	FNR	TNR	TSS	Rad	Threshold	TPR	FPR	TSS	Rad
R _{D1} (mmd ⁻¹) ^a	10.90	0.35	0.16	0.65	0.84	0.19	0.67	10.90	0.35	0.16	0.19	0.67
R _{D2} (mmd ⁻²) ^b	14.70	0.50	0.20	0.50	0.80	0.30	0.54	10.90	0.54	0.27	0.27	0.53
R _{D3} (mm) ^c	15.05	0.79	0.40	0.21	0.60	0.39	0.45	15.05	0.79	0.40	0.39	0.45
Se _{top(t-1)}	0.53	0.85	0.43	0.15	0.57	0.41	0.46	0.56	0.77	0.37	0.40	0.44
Se _{top(t-2)}	0.57	0.75	0.35	0.25	0.65	0.40	0.43	0.57	0.75	0.35	0.40	0.43
Se _{top(t-3)}	0.56	0.75	0.38	0.25	0.62	0.37	0.50	0.56	0.75	0.38	0.37	0.50
R _{D1} (mmd ⁻¹) ^d	10.90	0.38	0.16	0.62	0.84	0.21	0.64	10.90	0.38	0.16	0.21	0.64
R _{D2} (mmd ⁻²) ^e	14.70	0.59	0.21	0.41	0.79	0.38	0.45	10.90	0.67	0.28	0.38	0.44
R _{D3} (mm) ^f	15.05	0.81	0.42	0.19	0.58	0.40	0.46	35.70	0.63	0.25	0.38	0.45
Se _{root(t-1)}	0.75	0.81	0.38	0.19	0.62	0.43	0.43	0.75	0.81	0.38	0.43	0.43
Se _{root(t-2)}	0.76	0.84	0.36	0.16	0.64	0.49	0.39	0.76	0.84	0.36	0.49	0.39
Se _{root(t-3)}	0.72	0.84	0.41	0.16	0.59	0.43	0.44	0.79	0.72	0.30	0.42	0.41
Se _{uz(t-1)}	0.90	0.66	0.23	0.34	0.77	0.43	0.41	0.90	0.66	0.23	0.43	0.41
Se _{uz(t-2)}	0.89	0.63	0.25	0.37	0.75	0.38	0.45	0.89	0.63	0.25	0.38	0.45
Se _{uz(t-3)}	0.92	0.56	0.18	0.44	0.82	0.38	0.47	0.89	0.63	0.24	0.38	0.45

^{abc} Cumulative 1, 2, and 3day rainfall defined from all landslides representative precipitation foot prints, ^{def} Cumulative 1, 2, and 3day rainfall volume defined using precipitation foot prints located in the model catchments (Kivu, Nyabarongo upper and Mukungwa)

the impact of pre-wetting state of the soil is considered unimportant for landslide occurrence. On the contrary, once these thresholds are exceeded, the pre-wetting state of the soil has significant impact on landslide occurrence and has to be considered while defining the landslide hydro-meteorological threshold models.

6.3.4. LANDSLIDE HYDRO-METEOROLOGICAL THRESHOLDS AND IMPLICATION FOR WARNING

With respect to the high rate of false positives resulting from the single variable thresholds, we have tested whether the incorporation of antecedent soil moisture information to the triggering rainfall conditions improves the landslide prediction capability. The optimum single variable hydrological and meteorological thresholds have been therefore combined into hydro-meteorological thresholds following the cause-trigger concept in a bilinear framework as shown in Figure 6.8 and Figure 6.9. Figure 6.8 illustrates the first

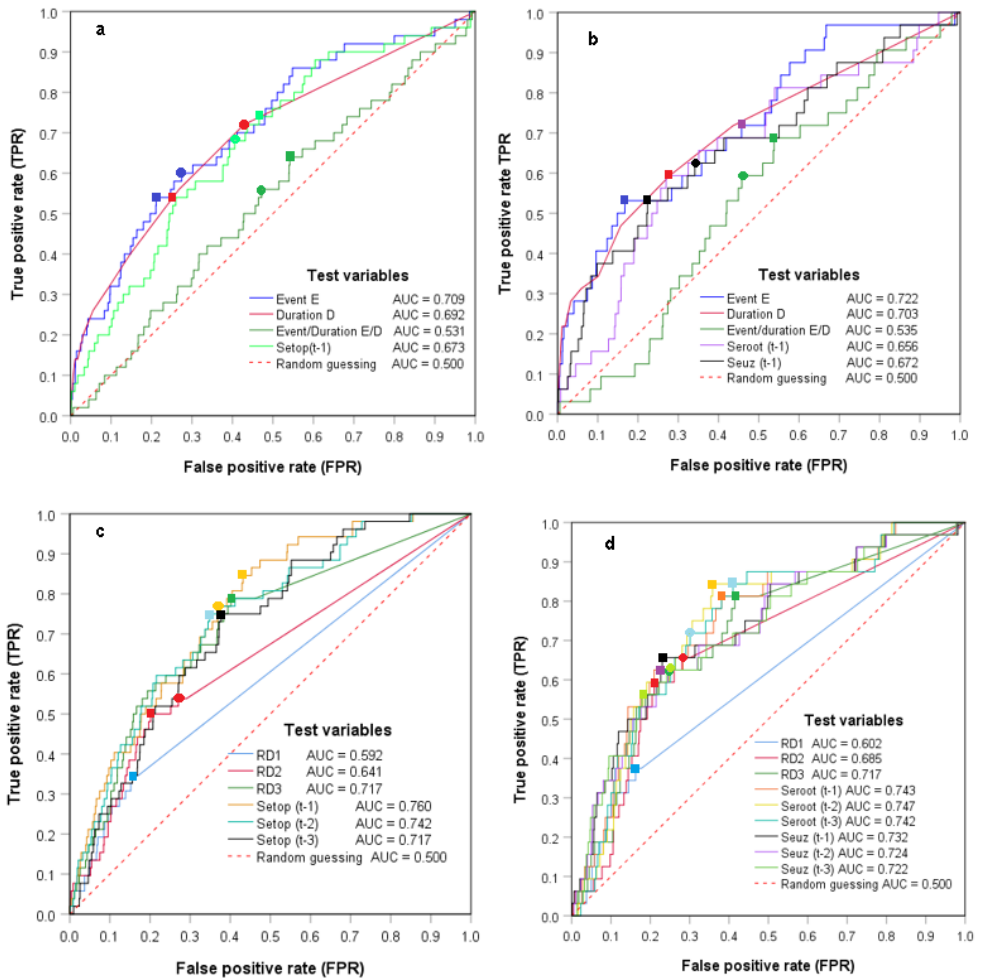


Figure 6.7: Receiver operating characteristics ROC curves, area under the curves AUC and optimum landslide thresholds defined by the true skill statistic TSS (square shaped marker) and radial distance Rad (cycle shaped marker) using: a) Event rainfall and satellite (VdS) based-top 5cm soil moisture Se_{top} from all ROIs b) Event rainfall and modelled root zone soil moisture of the top 50cm Se_{root} and top 2m soil moisture Se_{uz} from ROIs located in the Wflow model catchment c) Cumulative 1, 2 and 3day rainfall (RD) and satellite (VdS) based-top 5cm soil moisture Se_{top} from all ROIs and d) cumulative 1, 2 and 3day rainfall (RD) and modelled root zone soil moisture of the top 50cm Se_{root} and top 2m soil moisture Se_{uz} from ROIs located in the Wflow model catchment

category of landslide hydro-meteorological thresholds defined based on the maximum possible rainfall event E combined with different variables of antecedent soil moisture. The derived thresholds resulted into quite elevated rate of false alarms FPR once used as single variable thresholds (single lines). In contrast to the classical precipitation thresholds, the combination of hydro-meteorological thresholds in a bilinear framework provide an improvement in terms of reduced rate of false alarms by about 30% [$Se_{top(t1)}-E/D$], 13% [$Se_{root(t1)}-E/D$], and 35% [$Se_{uz(t1)}-E/D$] respectively as compared to the ones obtained from the exclusive use of single variable precipitation based E/D thresholds.

The intention of adopting the bilinear hydro-meteorological threshold in spite of precipitation thresholds is to minimize the rate of incorrect prediction of landslides FPR while improving or at least keeping unchanged the rate of true alarms TPR. This was only achieved by using the bilinear hydro-meteorological thresholds defined using antecedent soil moisture at the root zone [$Se_{root(t1)}-E/D$] that performs better (TPR=66%) than the traditional precipitation threshold E-D (TPR=50%). However, this category still suffers from the low landslide warning capability (max TPR=66%) and is thus not satisfactory for a robust early warning system development. The lower performance was attributed to the timescale of the triggering events. Apparently, the effect of the antecedent soil moisture lasts for a limited period of time and subsequently decays towards zero and below. The inter-event time IET and the timescale of the rainfall events E are not constant and vary in duration. They be too long and thus implying the decay of the antecedent soil moisture and thus negligible contribution to landslide initiation. Consequently, the incorporation of the wetness state of the soil prior to the landslide triggering events E did not lead to a significant improvement of the landslide prediction in Rwanda conditions.

We therefore explored other landslide hydro-meteorological thresholds that use the triggering meteorological conditions with short and constant timescale as shown in [Figure 6.9](#). These consider the cumulative one, two and three day rainfall R_{D1} , R_{D2} , and R_{D3} while extending the timescale of the predisposing conditions up to one, two or three days prior to the landslide triggering conditions. [Figure 6.9](#) portrays the optimum bilinear hydro-meteorological threshold models defined from this second category. The 3-day cumulative rainfall R_{D3} was the most impactful trigger of landslide with an optimum threshold of 15.05mm/3days as defined by both TSS Rad and resulted into 79-81% of TPR much higher than predicted by the first category. Similarly, the antecedent soil moisture threshold $Se_{root(t3)}$ was able to predict 84% of landslides. However, this true prediction i.e true alarms is also associated with high rate of false alarms (40-42%). The combination into hydro-meteorological thresholds [$Se_{root(t3)} - R_{D3}$] decreased the rate of false alarms up to 22% with about 72% of true alarms ([Figure 6.9b](#)) and thus being more satisfactory than other hydro-meteorological threshold models and much better than the traditional E-D model (TPR=50%) that exclusively relies on precipitation.

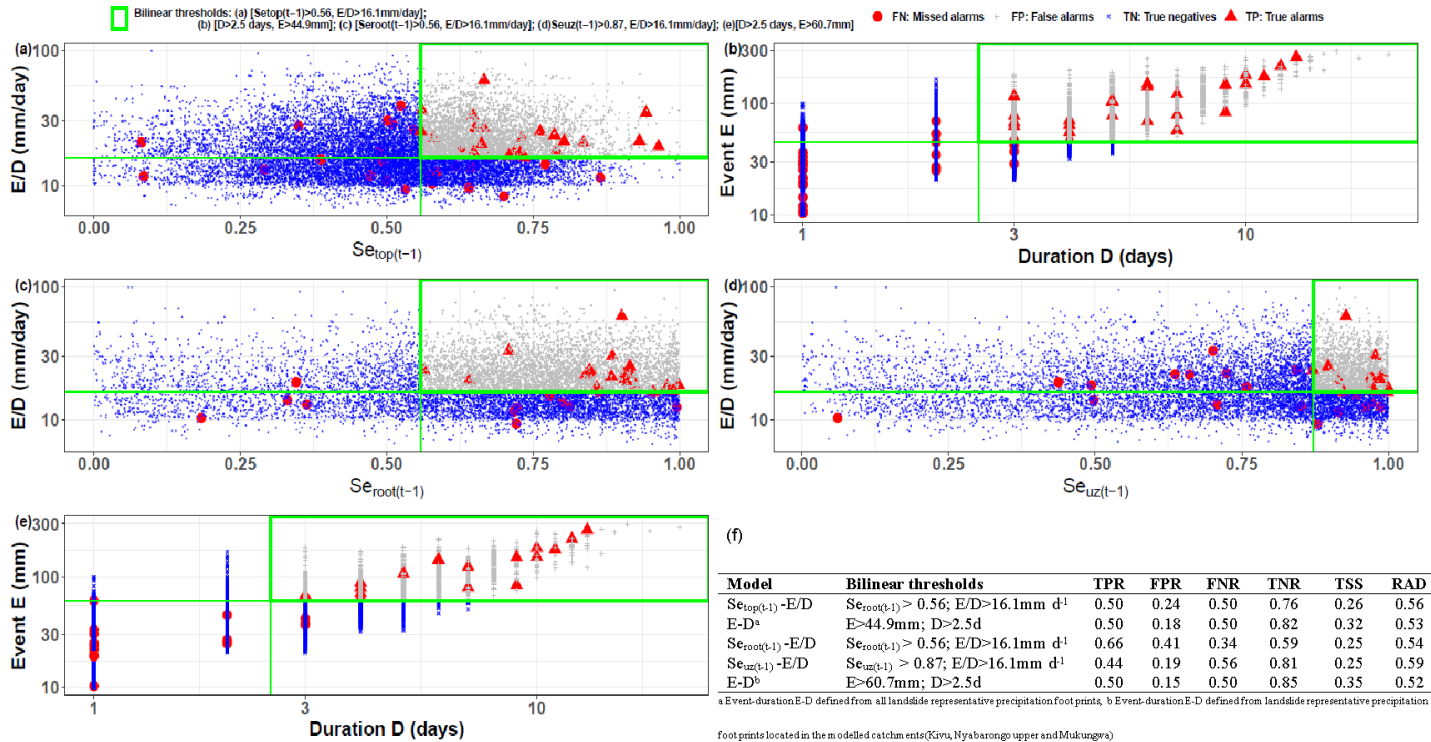


Figure 6.8: Landslide hydro-meteorological thresholds and prediction capabilities: a) Event intensity-Antecedent 5cm top soil moisture thresholds [$Se_{top(t-1)} > 0.56$; $E/D > 16.1 \text{ mm d}^{-1}$] b) Event-duration E-D thresholds [$D > 2.5$ days; $E > 44.9 \text{ mm}$] defined using precipitation foot prints from all landslide locations; c) Event intensity-Antecedent 50cm top soil moisture threshold [$Se_{root(t-1)} > 0.56$ - $E/D > 16.1 \text{ mm}$]; e) Event intensity-Antecedent 2m top soil moisture threshold [$Se_{root(t-1)} > 0.84$; $E/D > 16.1 \text{ mm d}^{-1}$]; e) Event-duration E-D thresholds [$E > 60.7 \text{ mm}$; $D > 2.5$ days] defined using precipitation foot prints and landslides located in Wflow modelled catchments; f) Bilinear threshold values and prediction capabilities

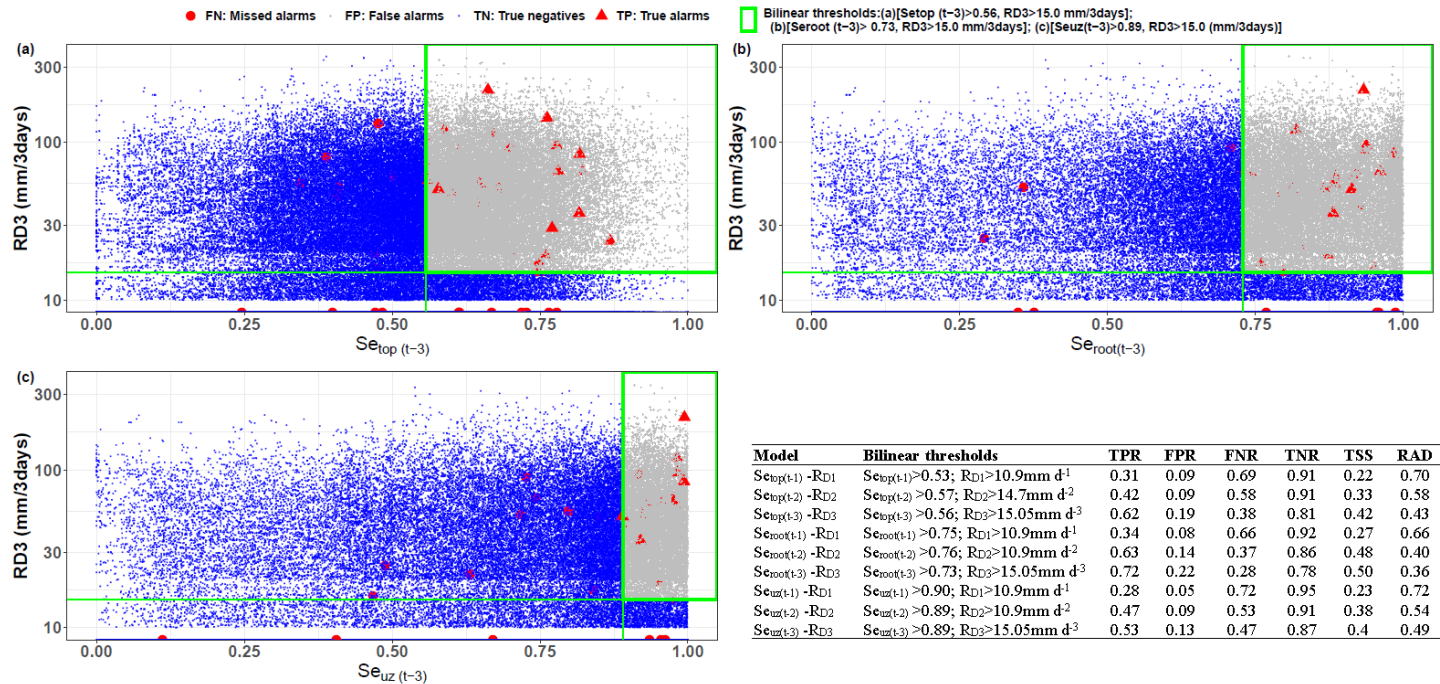


Figure 6.9: Landslide hydro-meteorological thresholds and prediction capabilities: a) Cumulative 3day rainfall R_{D3} and antecedent 5cm top soil moisture $Se_{top(t-1)}$ [$Se_{top(t-3)} > 0.73; R_{D3} > 15.1 \text{ mm d}^{-3}$] defined using precipitation foot prints from all landslide locations; b) Cumulative 3day rainfall R_{D3} and antecedent soil moisture of the root zone $Se_{root(t-3)}$ [$Se_{root(t-3)} > 0.73; R_{D3} > 15.1 \text{ mm d}^{-3}$] c) Cumulative 3day rainfall R_{D3} and antecedent soil moisture of the top 2m $Se_{uz(t-3)}$ [$Se_{uz(t-3)} > 0.89; R_{D3} > 15.1 \text{ mm d}^{-3}$] defined from the Wflow model catchment d) Bilinear hydro-meteorological threshold values and prediction capabilities

6.3.5. PROSPECTIVE OF THE SATELLITE-BASED HYDRO-METEOROLOGICAL THRESHOLDS, ADVANCES AND LIMITATIONS

This chapter reveals the high capability of the NASA GPM-based IMERG product to reproduce rainfall patterns which are consistent with the gauge-based precipitation and thus more suitable for landslide initiation thresholds than sparsely distributed rain gauges in Rwanda. However, it also points out that IMERG satellite-based product overestimates the number of rainy days whose daily rainfall is between 0-10mm and thus the mean annual totals. This may not only lead to differences between satellite- and gauge-based landslide thresholds defined under same locations but also to the statistical bias especially when probabilistic methods are used for landslide threshold definition. To address this constraint and be able to exploit the usefulness of IMERG precipitation in landslide hazards assessment thresholds, we objectively used 10mm as a threshold to define a rainy day for IMERG precipitation data. This threshold was defined based on the frequency indicator metric adopted as one of the techniques of bias evaluation between ground and satellite-based rainfall. For gauge based rainfall, 2 mm is generally considered as a threshold to define a rainy day and have been defined based on the mean daily potential evaporation (Marino et al., 2020; Peres et al., 2017).

Although the threshold definition of a rainy day (10mm) may have led to the omission of some rainfall information and thus shortening the event duration D , this approach improved the similarities between the satellite and gauge-based landslide hazard assessment thresholds. However, the defined satellite-based event/duration E/D thresholds $16-17.5\text{mmd}^{-1}$ were quite higher than previously defined gauge based-thresholds $7-13\text{mmd}^{-1}$. Contrarily the defined thresholds from the recent cumulative 2 and 3day rainfall were much smaller than defined from gauge based data (Chapter 4 and 5). These differences are probably due to the predefined threshold (10mm) that could omit some rainy days. This also led to shortened event duration D and hence slightly higher E/D . Nevertheless, the landslide triggering conditions defined based on the E/D reveals poor discriminatory power to distinguish landslide from no landslides (AUC 0.53) and thus not impactful on landslide initiation. The linked landslide thresholds also underperform in terms of landslide prediction capabilities measured by the resulting low rate of true positives TPR 56-69%. Similarly, the landslide hydro-meteorological thresholds that included the rainfall event E/D as a trigger resulted into poor landslide warning performance TPR max of about 66%.

The poor performance of the rainfall event-based thresholds concept is due to uncertainties from multiple sources. We hypothetically used the rainfall events as landslide triggering conditions, defined as individual periods of continuous rain interrupted by at least two dry day periods referred to as minimum inter-event time (IET). Nevertheless, this definition needs further exploration to be standardised to avoid uncertainties. According to Adams et al. (1987); Hong et al. (2017), the IET is defined as the minimum period of time that separates two consecutive rainfall events and is considered as the period for which the effects of the antecedent soil moisture or precipitation index may last. This is to say that the antecedent soil moisture and or antecedent precipitation index have no significant effect on landslide initiations once the rainfall events and IETs are well defined. However, the IET, the period during which the effect of antecedent soil moisture becomes null, depends on a number of site-specific factors (soil properties,

land use/ land cover, potential evaporation etc.) and is thus difficult to be standardized. Another drawback associated with the use of rainfall event concept may be linked to the transient timescales of the triggering events that bring about difficulties to fix the appropriate time to give an alert or an early landslide warning to the threatened community. Beholding the constraints associated with IET, rainy day and rainfall events definition, we explored the shorter scaled triggering rainfall conditions that include the cumulated rainfall with constant duration 1, 2, 3days (R_{D1} , R_{D2} , R_{D3}). The cumulative 3 days rainfall R_{D3} showed the highest impact on landslide initiation with AUC = 0.72 and true positive alarms TPR 79-81%.

Although the meteorological trigger-based thresholds R_{D3} , have resulted into high rate of true alarms, they lack the concrete physical significance and are also challenging for a robust landslide early warning system due to the linked high level of erroneous alarms i.e false positives FPR 40-42%. To account for the pre-wetting state of the soil, the antecedent soil moisture conditions have been considered. These antecedent soil moisture conditions from the top 5cm, 50cm and 2m, Se_{top} , Se_{root} , Se_{uz} respectively showed significant impact on landslide predisposal AUC=0.71-0.76. Moreover, with exception to the Se_{uz} , the hydrological landslide thresholds 0.56 [Se_{top}], 0.73 [Se_{root}] defined from these soil moisture conditions revealed high landslide warning capability with true alarms TPR = 75-85%. These hydrological thresholds indicate the critical pre-wetting state above which any additional amount of rainfall > 11-15mm is highly likely to trigger landslides. We therefore combined both landslide hydrological predisposing and meteorological triggering conditions following the cause-trigger concept into bilinear hydro-meteorological thresholds framework. This approach improved the landslide prediction capabilities in terms of reduced rate of false alarms (FPR=22%) and increased true alarms (TPR=72%) as compared to the approaches that consider the maximum probable rainfall event (max TPR=66% and FPR=41%). In other words, once combined with the pre-wetting hydrological conditions, the cumulative few days rainfall have significant impact on landslide initiation and warning as compared to the longer and no constant triggering conditions. Furthermore, the incorporation of the antecedent wetness state of the terrain not only improved the landslide warning capabilities but also provide accurate insights into landslide alert time as compared to the use of transient time scale associated with the rainfall event concept.

Among the tested pre-wetting conditions, the incorporation of the antecedent soil moisture modelled at the root zone Se_{root} was the most impactful for landslide initiation and thus the most useful in landslide hazard assessment thresholds in Rwanda. The finer spatial resolution of the hydrological model derived soil moisture together with the consideration of the specific climate and hydrogeological characteristics of the model catchments could be a possible explanation of the positive impact of soil moisture assimilated at the root zone. This could also be explained by the less exposure of the root zone to the solar heat and evaporation processes as compared to the near surface Se_{top} . The probable less prone to the gravity driven drainage and deep percolation due to the soil texture, vegetation and organic matter at the root zone could also be an explanation. Moreover, the soil depth involved in shallow (0.5-2m) and deep landslides(>2m) (Greco et al., 2018) is much thicker than Se_{top} (5cm) currently measured by the satellite based soil moisture technologies and this is more captured by the hydrological modelling approaches

(Wflow). An overestimation of soil moisture by satellite (VdS) and the distributed hydrological model (Wflow) was also noted and attributed to the similar overestimation of satellite-based precipitation, an important element in soil moisture estimation. Therefore, more reliable algorithms that addresses the reliance between the satellite and in-situ based information could thus improve the performance and enhance data accuracy needed for landslide hazard assessment.

The adopted bilinear threshold framework, indicating the distribution of data points in a 2D space, reflects the relationship between the landslide causal and triggering conditions. We objectively used the bilinear thresholds framework because the majority of positive classes were clustered in upper right corner of the 2D threshold space. Although, this format proved to be suitable for landslide hydro-meteorological thresholds definition (Mirus et al., 2018a; Thomas et al., 2019), other formats could also be useful depending on the distribution of the positive classes in the 2D space. The adopted bilinear framework is in line with the goal of the hydro-meteorological cause-trigger based thresholds concept that prioritize the minimization of false alarms while at least keeping unchanged the rate of true alarms. Additionally, in some cases, single variable thresholds lead to high prediction capabilities in terms of elevated rate of true alarms and with quite low rate of false alarms and could be adopted especially for hydrologically based thresholds that consider the long-term wetting process of the soil until the landslide day. Despite the good performance of soil moisture in landslide hydro-meteorological threshold, the incorporation of pre-wetting state of soil in landslide hazard assessment thresholds using groundwater levels, $h_{(t-1)}-E/D$ (TPR=54-64% and FPR=6-11%) (Chapter 5) with low rate of false alarms, performed higher than using root zone soil moisture Seroot(t-1)-E/D (TPR=66% and FPR=44%) due to the elevated rate of false alarms.

Ideally, one would have a landslide inventory of about 200 landslides events in order to have a precise estimation of threshold parameters (Peres and Cancelliere, 2021). However, the landslide inventory used for this study counts for only 32 hazardous landslides. Although, the reliance on this limited sample size is likely to lead to a bias towards the larger landslide events and those with impact to society, this landslide inventory is the most comprehensive currently available in the study area.

6.4. CONCLUSION

This Chapter aimed to evaluate the potential of satellite-based measurements of precipitation and soil moisture as well as hydrological model derived information for landslide initiation thresholds in Rwanda. The GPM-based IMERG rainfall product was found a good spatially distributed source of rainfall data for landslide hazard assessment especially in data scarce areas like Rwanda. The satellite and model derived soil moisture time series broadly reproduce the most important trends of the in-situ soil moisture. Regardless of different depths of data records and slightly overestimation of soil moisture by satellite and model derived techniques, it was concluded that they follow the in-situ observed temporal variation and are thus potentially useful for landslide hazard assessment. The purpose of incorporating the antecedent soil moisture in landslide hazard assessment was to account for the physical effect of the pre-wetness state of soil, responsible for the predisposal of the slopes to near-failure, prior to the landslide triggering conditions. Two categories of landslide triggering conditions have been considered

to assess the potential value of including the antecedent soil moisture information. The category that considers the cumulative 3day rainfall was the most impactful and thus more useful for landslide hazard assessment rather than the rainfall event-based trigger. Although the area under the curve $AUC=0.71-0.76$ statistical metric indicated the significant impact of all tested antecedent soil moisture variables prior to the triggering conditions, the antecedent soil moisture modelled from the root zone Se_{root} performed best. The classical thresholds E-D relying exclusively on rainfall (trigger) performed lower with high rate of missed alarms (50%) and thus less important for a robust early warning system development. Contrary, the hydro-meteorological thresholds that incorporate the antecedent soil moisture Se_{root} and the recent 3day cumulative rainfall R_{D3} [$Se_{root(t3)}-R_{D3}$] outperforms other threshold models with high rate of true alarms (72%) and low rate of false alarms (20%) and thus can be very useful for landslide early warning system development in Rwanda.

7

SYNTHESIS AND CONCLUSIONS

7.1. SYNTHESIS OF RESEARCH FINDINGS

The overarching objective of this thesis was to define the hydro-meteorological thresholds for landslide initiation in Rwanda following the landslide cause-trigger concept in a bilinear framework, as a first step towards the development of landslide early warning system in Rwanda. The specific objectives were to i) understand the key hydro-geological and meteorological processes and the relation thereof for the typical hillslopes prone to landslide in Rwanda; ii) identify precipitation-related variables with the highest landslide explanatory power and warning capability in Rwanda; iii) evaluate the asset that regional groundwater level information may have on landslide initiation thresholds; and iv) assess the potential of satellite and model derived precipitation and soil moisture information for landslide initiation thresholds in Rwanda.

7.1.1. HYDRO-GEOLOGICAL AND METEOROLOGICAL PROCESSES OF THE TYPICAL HILLSLOPES PRONE TO LANDSLIDE IN RWANDA

The key hydro-geological and meteorological processes of the typical landslide prone hillslopes were assessed in Chapter 3. From a geotechnical point of view the Karago hillslope indicated instability conditions. This informs about the expected retrogressive and enlargement processes with high risks on the surrounding infrastructures and community. The Rwaza hillslope shows marginally stable conditions with signs of advancing process with high risks for the downslope local community. The regression analysis indicated the role of rainfall on surface displacement with long lasting low intensity rainfall being more critical than short and high intensity rainfall. A strong correlation between groundwater levels and surface displacement was noticed and thus stressing its consideration in landslide initiation threshold definition and early warning system development.

7.1.2. PRECIPITATION-RELATED VARIABLES WITH THE HIGHEST EXPLANATORY POWER AND WARNING CAPABILITY FOR LANDSLIDE HAZARD IN RWANDA

In chapter 4 we used the landslide and precipitation data in an empirical-statistical approach to define both trigger and trigger-cause based thresholds for landslides initiation and to quantify their predictive performance. The findings indicated the rainfall event volume and the cumulative one day rainfall that coincide with the landslide day as the most informative explanatory variables with the high ability to initiate landslides (trigger). The antecedent precipitation index, 10 days prior to the landslide triggering conditions, showed significant impact on predisposing the slope to near failure (cause). The highest landslide prediction capability (rate of positive alarms) was achieved using a single rainfall variable, so a trigger-based threshold. However, that predictive capability simultaneously resulted in a high rate of false alarms. Constraining the trigger-based threshold with a causal variable in a bilinear framework, improved the overall prediction capacity by reducing the number of false alarms. The findings indicated also that the concept of trigger-cause-based thresholds in bilinear format is not only useful to minimize the rate of false alarms but also to explore the impact of each or combined triggering and causal conditions on landslide occurrence. Despite that however, the resulting

rate of true and false alarms was not sufficient enough to support the development of a robust LEWS and thus requiring further improvement.

7.1.3. ASSET OF REGIONAL GROUNDWATER LEVEL INFORMATION ON LANDSLIDE HAZARD ASSESSMENT THRESHOLDS

In chapter 5 we improved the landslide forecast quality by incorporating the catchment specific groundwater levels as a proxy for catchment water storage. The standardized groundwater levels modelled on a landslide day and the event rainfall volume E were identified as the hydrological and meteorological variables with the most dominant control on landslide occurrence. The single variable threshold model-derived from groundwater levels indicated the highest landslide prediction and/or warning capability in terms of true positive alarms despite the resulting rate of false alarms. Similarly, the single variable threshold models derived from precipitation intensity and event rainfall volume reveal also high landslide predictive skill in terms of true positive alarms associated with quite high rate of false alarms. However, it was noticed that relying on single variable threshold models exclusively derived from precipitation variables considered as landslide triggers could lead to biased results due to the fact that many landslides occur not only due to the trigger itself but a rather combination of both trigger and pre-event hydrological conditions. Contrarily, relying on single variable threshold models exclusively defined using groundwater, lead to unbiased landslide predictions due to their high consideration of long-term antecedent wetness conditions until the day of landslide occurrence. Furthermore, the catchment specific hydro-meteorological threshold models made of groundwater levels and rainfall indicated the best landslide predictive skill in terms of true positive alarms than the classical precipitation thresholds defined at country scale.

7.1.4. POTENTIAL OF SATELLITE AND MODEL DERIVED PRECIPITATION AND SOIL MOISTURE FOR LANDSLIDE INITIATION THRESHOLDS IN RWANDA

To overcome the constraint linked to the coarse spatial resolution of the in-situ gauge and hydrological recording equipment, chapter 6 evaluated the potential of satellite-based measurements of precipitation and soil moisture as well as the hydrological model derived information as alternatives for estimation of landslide initiation thresholds in Rwanda. Based on statistical indicators, the satellite precipitation analysis reveals the NASA GPM-based IMERG to have the highest skill to reproduce the main spatio-temporal precipitation patterns much similar to the recorded gauge-based rainfall and thus a good alternate source of rainfall data for landslide hazard assessment in data scarce areas. The satellite and model derived soil moisture time series broadly reproduce the most important trends of the in-situ soil moisture and was concluded that they potentially are useful for landslide hazard assessment. The incorporation of the satellite and model derived antecedent soil moisture in landslide hazard assessment accounted for the physical effect of the pre-wetness state of soil, responsible for the predisposal of the slopes to near-failure. Despite the significant impact of all tested antecedent soil moisture variables prior to the triggering conditions, their thresholds specified the antecedent soil moisture modelled at the root zone to be the most useful on landslide initiation and warning. Similarly, the hydro-meteorological thresholds that incorporate the same an-

tecedent soil moisture and the recent 3 day cumulative rainfall over performed other thresholds models with high rate of true alarms and low rate of false alarms and thus very useful for landslide initiation and early warning system development in Rwanda.

7.2. COMPARATIVE PERFORMANCE OF THE DEFINED HYDRO-METEOROLOGICAL THRESHOLDS

For a proper comparison of the landslide warning capabilities, the defined landslide hydro-meteorological thresholds have been categorized based on their spatial coverage from national, regional and catchment scales.

7.2.1. LANDSLIDE HYDRO-METEOROLOGICAL THRESHOLDS AT COUNTRY SCALE

At country scale two categories of landslide hydro-meteorological thresholds have been defined. The first category used in-situ meteorological variables as landslide trigger and antecedent precipitation index as a proxy for the pre-wetting state of soil prior to the landslide triggering conditions. In this category the best performing hydro-meteorological thresholds combined the event intensity and antecedent precipitation index 30 day prior to the landslide triggering conditions with 68% of true alarms and 27% of false alarms. The second category used satellite precipitation as an alternative to the in-situ rainfall and replaced the antecedent precipitation by the satellite based top 5 cm soil moisture. The highest warning performance was noted from the hydro-meteorological thresholds that combine the recent cumulative 3 day rainfall and the top soil moisture recorded 3 day prior to the landslide triggering condition with 62% true alarms and 19% false alarms. Despite the low prediction capability from both categories, it was concluded that in-situ rainfall and antecedent precipitation are very useful in landslide hazard assessment threshold at country scale. However, due the frequent coarse resolution of the in-situ gauges, satellite-based precipitation and soil moisture are potential alternatives in data scarce areas like Rwanda.

7.2.2. LANDSLIDE HYDRO-METEOROLOGICAL THRESHOLDS AT REGIONAL SCALE

The landslide hydro-meteorological thresholds defined from satellite base-rainfall and soil moisture from the distributed hydrological model were defined for the north-western region of Rwanda that covers three catchments: Lake Kivu, upper Nyabarongo and Mukungwa. Among the defined thresholds at regional scale, the hydro-meteorological thresholds that combine the short scaled 3 day cumulative rainfall as a trigger and soil moisture modeled at the root zone (50 cm deep) as a pre-wetting state performed higher than other threshold models with 72% of true alarms TPR and 19% of false alarms. The inclusion of soil moisture as a hydrological processes improved the landslide warning capability as compared to the exclusive reliance on precipitation threshold that only predicted 50% of landslides. Furthermore the down scaling of landslide thresholds towards the highly susceptible regions improves the prediction capability in terms of reduced rate of false alarms and increased rate of true alarms.

7.2.3. LANDSLIDE HYDRO-METEOROLOGICAL THRESHOLDS AT CATCHMENT SCALE

The landslide hydro-meteorological thresholds from in-situ rainfall and catchment specific groundwater levels, as a proxy for catchment storage, were defined at each of the studied catchments: Kivu, upper Nyabarongo and Mukungwa. Among the defined thresholds the hydro-meteorological threshold from groundwater levels recorded on a day of landslide and rainfall event intensity performed higher with 65%, 73% and 85% of true alarms with low rate of false alarms 10%, 8% and 15% in the Kivu, upper Nyabarongo and Mukungwa catchments respectively. These prediction capabilities are much higher than predicted once relied exclusively on rainfall using the classical Intensity-Duration thresholds with 36%, 36%, and 77% TPR in the Kivu, upper Nyabarongo and Mukungwa catchments respectively. Overall the landslide hydro-meteorological thresholds that consider the catchment specific rainfall and groundwater as a proxy for catchment storage, were the most important landslide predictors with up to 85% of true alarms and 15% of false alarms and thus potentially useful for a robust landslide early warning system development in Rwanda.

7.3. CAPABILITIES AND LIMITATIONS OF THE DEFINED BILINEAR HYDRO-METEOROLOGICAL THRESHOLDS AND PERSPECTIVE FOR FUTURE RESEARCH

Within the framework of this thesis, the landslide empirical hydro-meteorological thresholds were defined using continuous historical precipitation, groundwater level and soil moisture time series. These time series were derived from in-situ measurements, satellite and hydrological model sources. It was observed that in regions with slow hydrological responding system where rainfall induced shallow landslides prevail, precipitation based thresholds can still practically be useful for landslide prediction and warning. However, the landslide hydro-meteorological thresholds perform best for both shallow and deep seated landslides (Cascini et al., 2010; Corominas et al., 2005a; Duan et al., 2019; Hong and Wan, 2011) and thus, being more powerful than precipitation based thresholds. More studies also confirm the high warning capability of hydro-meteorological thresholds over precipitation-based thresholds after incorporation of either soil moisture or catchment storage (Ciavolella et al., 2016; Mirus et al., 2018b; Prenner et al., 2018; Thomas et al., 2019; Wicki et al., 2020).

One of the constraints of the hydro-meteorological thresholds is indeed that one has to explore a wide range of combinations of landslide explanatory/predictor variables which may be different based on landslide pre-disposing and triggering factors. In this research, a wide range of combinations of landslide explanatory variables that include rainfall, groundwater and soil moisture from in-situ, hydrological model and satellite sources were explored. However, other potential landslide explanatory variables and or predictors can also be explored.

The defined hydro-meteorological threshold models are based on empirical statistical approach with little to no consideration of the physical, and geomorphological characteristic of the terrain and hence classified as black or grey box models. Further inte-

gration of the landslide susceptibility indices defined based on the physical and geomorphological characteristics of the terrain to the defined hydro-meteorological thresholds would enhance their spatial transferability and usability.

Another constraint of the hydro-meteorological threshold definition is linked to the lack of a standardised statistical functional relationship between hydrological and meteorological conditions potentially linked to landslide initiation. In this thesis the bilinear relationship between hydrological and meteorological variables has been adopted based on the fact that the majority of positive cases (landslide conditions) were clustered in the upper right corner of the 2D plane and proved to be efficient. However, one is free to try out other statistical relationship depending on the data points distribution.

Additionally, the conceptual framework of the landslide cause-trigger was to develop a hydro-meteorological threshold that combine the antecedent causal/hydrological conditions and the actual trigger/meteorological conditions potentially linked to landslides initiation. However, there is no clear line indicating the time lag between the hydrological and the triggering rainfall and therefore, constraining the choice of the proper time scale for both landslide causal hydrological and triggering meteorological conditions. This may lead to the violation of the no-collinearity assumption, redundant information and thus suffering from the conceptual limitations related to landslide predictors independence. To overcome this constraint, the triggering rainfall conditions with fixed time scales i.e. cumulated few days rainfall were preferred in spite of the classical event rainfall.

According to [Peres and Cancelliere \(2021\)](#), it is ideal to have a landslide inventory of about 200 landslides events in order to have a precise estimation of threshold parameters. However, the landslide inventory used for this study counts less number than required due to the fact that frequently only hazardous landslides are reported in Rwanda. Although, the reliance on this inventory may likely lead to a bias towards the larger landslide events and those with impact to society, this landslide inventory was the most comprehensive available in Rwanda.

Overall, despite the minor constraints, the defined landslide hydro-meteorological thresholds are potentially useful towards the development of the landslide early warning system in Rwanda.

REFERENCES

- Adams, B.B.J., Asce, M., Fraser, H.G., Hanafy, M.S., 1987. Meteorological data analysis for drainage system design 112, 827–848.
- Aleotti, P., 2004. A warning system for rainfall-induced shallow failures. *Engineering Geology* 73, 247–265. doi:[10.1016/j.enggeo.2004.01.007](https://doi.org/10.1016/j.enggeo.2004.01.007).
- Anderson, M.G., Lloyd, D.M., 1991. Using a combined slope hydrology- stability model to develop cut slope design charts. *ICE Proceedings* 91, 705–718. doi:[10.1680/iicep.1991.17486](https://doi.org/10.1680/iicep.1991.17486).
- Ashouri, H., Hsu, K.L., Sorooshian, S., Braithwaite, D.K., Knapp, K.R., Cecil, L.D., Nelson, B.R., Prat, O.P., 2015. PERSIANN-CDR: Daily precipitation climate data record from multisatellite observations for hydrological and climate studies. *Bulletin of the American Meteorological Society* 96, 69–83.
- Bakker, M., Schaars, F., 2019. Solving Groundwater Flow Problems with Time Series Analysis: You May Not Even Need an other Model 57, 826–833. doi:[10.1111/gwat.12927](https://doi.org/10.1111/gwat.12927).
- Berti, M., Martina, M.L., Franceschini, S., Pignone, S., Simoni, A., Pizzolo, M., 2012. Probabilistic rainfall thresholds for landslide occurrence using a Bayesian approach. *Journal of Geophysical Research: Earth Surface* 117, n/a–n/a. URL: <http://doi.wiley.com/10.1029/2012JF002367>, doi:[10.1029/2012JF002367](https://doi.org/10.1029/2012JF002367).
- Bizimana, H., Sönmez, O., 2015. Landslide Occurrences in The Hilly Areas of Rwanda , Their Causes and Protection Measures 1, 1–7.
- Bogaard, T., Greco, R., 2018. Invited perspectives: Hydrological perspectives on precipitation intensity-duration thresholds for landslide initiation: proposing hydro-meteorological thresholds. *Natural Hazards and Earth System Sciences* 18, 31–39. URL: <https://www.nat-hazards-earth-syst-sci.net/18/31/2018/>, doi:[10.5194/nhess-18-31-2018](https://doi.org/10.5194/nhess-18-31-2018).
- Bordoni, M., Meisina, C., Valentino, R., Lu, N., Bittelli, M., Chersich, S., 2015. Hydrological factors affecting rainfall-induced shallow landslides: From the field monitoring to a simplified slope stability analysis. *Engineering Geology* 193, 19–37. doi:[10.1016/j.enggeo.2015.04.006](https://doi.org/10.1016/j.enggeo.2015.04.006).
- Bouaziz, L.J., Steele-Dunne, S.C., Schellekens, J., Weerts, A.H., Stam, J., Sprokkereef, E., Winsemius, H.H., Savenije, H.H., Hrachowitz, M., 2020. Improved understanding of the link between catchment-scale vegetation accessible storage and satellite-derived soil water index. *Water Resources Research* 56, e2019WR026365.

- Broeckx, J., Vanmaercke, M., Duchateau, R., Poesen, J., 2018. A data-based landslide susceptibility map of africa. *Earth-Science Reviews* 185, 102–121.
- Bronnimann, C.S., 2011. Effect of Groundwater on Landslide Triggering. Ph.D. thesis. École Polytechnique Federale de Lausanne. URL: <https://core.ac.uk/download/pdf/147975151.pdf>.
- Brunetti, M.T., Melillo, M., Peruccacci, S., Ciabatta, L., Brocca, L., 2018. How far are we from the use of satellite rainfall products in landslide forecasting? *Remote Sensing of Environment* 210, 65–75. URL: <https://doi.org/10.1016/j.rse.2018.03.016>, doi:10.1016/j.rse.2018.03.016.
- Brunetti, M.T.P., Peruccacci, S., Rossi, M., Luciani, S., Valigi, D., Guzzetti, F., 2010. Rainfall thresholds for the possible occurrence of landslides in Italy. *Natural Hazards and Earth System Sciences* 10, 447–458.
- Caine, N., 1980. The Rainfall Intensity : Duration Control of Shallow Landslides and Debris Flows. *JSTOR* 62, 23–27. URL: <https://www.jstor.org/stable/pdf/520449.pdf?refreqid=excelsior%3Aa194dd220014eb4f33bd3ea4ff9483cd>.
- Calvello, M., Devoli, G., Freeborough, K., Gariano, S., Guzzetti, F., Kirschbaum, D., Nakaya, H., Robbins, J., Stähli, M., 2020. Landaware: a new international network on landslide early warning systems.
- Casagrande, A., 1948. Classification and identification of soils. *Transactions of the American Society of Civil Engineers* 113, 901–930.
- Cascini, L., Calvello, M., Grimaldi, G.M., 2010. Groundwater Modeling for the Analysis of Active Slow-Moving Landslides. *Journal of Geotechnical and Geoenvironmental Engineering* 136, 1220–1230. doi:10.1061/(asce)gt.1943-5606.0000323.
- Ciavolella, M., Bogaard, T., Gargano, R., Greco, R., 2016. Is there Predictive Power in Hydrological Catchment Information for Regional Landslide Hazard Assessment? *Procedia Earth and Planetary Science* 16, 195–203. URL: <http://linkinghub.elsevier.com/retrieve/pii/S1878522016300212>, doi:10.1016/j.proeps.2016.10.021.
- Collenteur, R.A., Bakker, M., Caljé, R., Klop, S.A., Schaars, F., 2019. Pastas: Open Source Software for the Analysis of Groundwater Time Series. *Groundwater* 57, 877–885. doi:10.1111/gwat.12925.
- Corominas, J., Moya, J., Ledesma, A., Lloret, A., Gili, J.A., 2005a. Prediction of ground displacements and velocities from groundwater level changes at the Vallcebre landslide (Eastern Pyrenees, Spain). *Landslides* 2, 83–96. doi:10.1007/s10346-005-0049-1.
- Corominas, J., Moya, J., Ledesma, A., Lloret, A., Gili, J.A., 2005b. Prediction of ground displacements and velocities from groundwater level changes at the Vallcebre landslide (Eastern Pyrenees, Spain). *Landslides* 2, 83–96. doi:10.1007/s10346-005-0049-1.
- Craig, R., 1997. Soil mechanics. 6 ed., Taylor & Francis e-Library, London and New York.

- Crozier, M.J., 1999. Prediction of rainfall-triggered landslides : a test of the antecedent water status model. *Earth Surf. Process. Landforms* 833, 825–833.
- Cruden, D., Varnes, D., 1996. *Landslide Types and Processes*. Technical Report 247. Special RepTransportation Research Board, National Academy of Sciences. URL: https://www.researchgate.net/publication/269710355_CrudensDM_Varnes_DJ_1996_Landslide_Types_and_Processes
- De Jeu, R.A., Holmes, T.R., Parinussa, R.M., Owe, M., 2014. A spatially coherent global soil moisture product with improved temporal resolution. *Journal of Hydrology* 516, 284–296. URL: <http://dx.doi.org/10.1016/j.jhydrol.2014.02.015>, doi:10.1016/j.jhydrol.2014.02.015.
- Depicker, A., Govers, G., Jacobs, L., Campforts, B., Uwihirwe, J., Dewitte, O., 2021a. Interactions between deforestation , landscape rejuvenation , and shallow landslides in the North Tanganyika – Kivu rift region , Africa , 445–462URL: <https://esurf.copernicus.org/articles/9/445/2021/>, doi:doi.org/10.5194/esurf-9-445-2021.
- Depicker, A., Govers, G., Jacobs, L., Vanmaercke, M., Uwihirwe, J., Campforts, B., Kubwimana, D., Mateso, J.c.M., Bibentyo, T.M., Namihana, L., Smets, B., Dewitte, O., 2021b. Landslide mobilization rates in a changing tropical environment : the North Tanganyika-Kivu Rift region , Africa.
- Depicker, A., Jacobs, L., Delvaux, D., Havenith, H.B., Maki Mateso, J.C., Govers, G., Dewitte, O., 2020. The added value of a regional landslide susceptibility assessment: The western branch of the East African Rift. *Geomorphology* 353, 106886. URL: <https://doi.org/10.1016/j.geomorph.2019.106886>, doi:10.1016/j.geomorph.2019.106886.
- Depicker, A., Jacobs, L., Mboga, N., Smets, B., Van Rompaey, A., Lennert, M., Wolff, E., Kervyn, F., Michellier, C., Dewitte, O., Govers, G., 2021c. Historical dynamics of landslide risk from population and forest-cover changes in the Kivu Rift. *Nature Sustainability* 4, 965–974. doi:10.1038/s41893-021-00757-9.
- Dewitte, O., Depicker, A., Moeyersons, J., Dille, A., 2022. 5.21 - mass movements in tropical climates, in: Shroder, J.J.F. (Ed.), *Treatise on Geomorphology* (Second Edition). second edition ed.. Academic Press, Oxford, pp. 338–349. URL: <https://www.sciencedirect.com/science/article/pii/B9780128182345001188>, doi:<https://doi.org/10.1016/B978-0-12-818234-5.00118-8>.
- Dewitte, O., Dille, A., Depicker, A., Kubwimana, D., Maki Mateso, J.C., Mugaruka Bibentyo, T., Uwihirwe, J., Monsieurs, E., 2021. Constraining landslide timing in a data-scarce context: from recent to very old processes in the tropical environment of the north tanganyika-kivu rift region. *Landslides* 18, 161–177. doi:<https://doi.org/DOI10.1007/s10346-020-01452-0>.
- Duan, G., Chen, D., Niu, R., 2019. Forecasting groundwater level for soil landslide based on a dynamic model and landslide evolution pattern. *Water (Switzerland)* 11. doi:10.3390/w11102163.

- Froude, M.J., Petley, D.N., 2018. Global fatal landslide occurrence from 2004 to 2016. *Natural Hazards and Earth System Sciences* 18, 2161–2181. URL: <https://www.nat-hazards-earth-syst-sci.net/18/2161/2018/>, doi:10.5194/nhess-18-2161-2018.
- Funk, C., Peterson, P., Landsfeld, M., Pedreros, D., Verdin, J., Shukla, S., Husak, G., Rowland, J., Harrison, L., Hoell, A., et al., 2015. The climate hazards infrared precipitation with stations—a new environmental record for monitoring extremes. *Scientific data* 2, 1–21.
- Gariano, S.L., Guzzetti, F., 2016. Landslides in a changing climate. *Earth-Science Reviews* 162, 227–252. URL: <https://www.sciencedirect.com/science/article/pii/S0012825216302458>, doi:10.1016/J.EARSCIREV.2016.08.011.
- Glade, T., 2000. Modelling landslide-triggering rainfalls in different regions of New Zealand - the soil water status model. *Geomorphology* 122, 63–84.
- Glerum, A., Brune, S., Stamps, D.S., Strecker, M.R., 2020. Victoria continental microplate dynamics controlled by the lithospheric strength distribution of the East African Rift. *Nature Communications* 11, 1–15. URL: <http://dx.doi.org/10.1038/s41467-020-16176-x>, doi:10.1038/s41467-020-16176-x.
- Greco, R., Marino, P., Santonastaso, G.F., Damiano, E., 2018. Interaction between perched epikarst aquifer and unsaturated soil cover in the initiation of shallow landslides in pyroclastic soils. *Water* 10, 948.
- Greenwood, J.R., Norris, J.E., Wint, J., 2004. ASSESSING THE CONTRIBUTION OF VEGETATION TO SLOPE STABILITY. *Geotechnical Engineering* , 1–34.
- Guzzetti, F., Gariano, S.L., Peruccacci, S., Brunetti, M.T., Marchesini, I., Rossi, M., Melillo, M., 2020. Geographical landslide early warning systems. *Earth-Science Reviews* 200, 102973. URL: <https://doi.org/10.1016/j.earscirev.2019.102973>, doi:10.1016/j.earscirev.2019.102973.
- Guzzetti, F., Peruccacci, S., Rossi, M., Stark, C.P., 2007. Rainfall thresholds for the initiation of landslides in central and southern Europe. *Meteorology and Atmospheric Physics* 98, 239–267. doi:10.1007/s00703-007-0262-7.
- Guzzetti, F., Peruccacci, S., Rossi, M., Stark, C.P., 2008. The rainfall intensity-duration control of shallow landslides and debris flows: An update. *Landslides* 5, 3–17. doi:10.1007/s10346-007-0112-1.
- Haque, U., Blum, P., da Silva, P.F., Andersen, P., Pilz, J., Chalov, S.R., Malet, J.P., Auflič, M.J., Andres, N., Poyiadji, E., Lamas, P.C., Zhang, W., Peshevski, I., Pétursson, H.G., Kurt, T., Dobrev, N., García-Davalillo, J.C., Halkia, M., Ferri, S., Gaprindashvili, G., Engström, J., Keellings, D., 2016. Fatal landslides in Europe. *Landslides* 13, 1545–1554. doi:10.1007/s10346-016-0689-3.

- Hersbach, H., Bell, B., Berrisford, P., Hirahara, S., Horányi, A., Muñoz-Sabater, J., Nicolas, J., Peubey, C., Radu, R., Schepers, D., et al., 2020. The era5 global reanalysis. *Quarterly Journal of the Royal Meteorological Society* 146, 1999–2049.
- Hong, M., Kim, J., Jeong, S., 2017. Rainfall intensity-duration thresholds for landslide prediction in South Korea by considering the effects of antecedent rainfall. *Landslides* 10.1007/s1. doi:10.1007/s10346-017-0892-x.
- Hong, Y., Alder, R., Huffman, G., 2006. Evaluation of the potential of NASA multi-satellite precipitation analysis in global landslide hazard assessment. *Geophysical Research Letters* 33, 1–5. doi:10.1029/2006GL028010.
- Hong, Y.M., Wan, S., 2011. Forecasting groundwater level fluctuations for rainfall-induced landslide. *Natural Hazards* 57, 167–184. doi:10.1007/s11069-010-9603-9.
- Huffman, G.J., Adler, R.F., Bolvin, D.T., Nelkin, E.J., 2010. The trmm multi-satellite precipitation analysis (tumpa), in: *Satellite rainfall applications for surface hydrology*. Springer, pp. 3–22.
- Huffman, G.J., Bolvin, D.T., Braithwaite, D., Hsu, K., Joyce, R., Xie, P., Yoo, S.H., 2015. Nasa global precipitation measurement (gpm) integrated multi-satellite retrievals for gpm (imerg). *Algorithm Theoretical Basis Document (ATBD) Version 4*, 26.
- Hungr, O., Leroueil, S., Picarelli, L., 2014. The Varnes classification of landslide types, an update. *Landslides* 11, 167–194. doi:10.1007/s10346-013-0436-y.
- Imasiku, K., Ntagwirumugara, E., 2020. An impact analysis of population growth on energy-water-food-land nexus for ecological sustainable development in Rwanda. *Food and Energy Security* 9, 1–17. doi:10.1002/fes3.185.
- Imhoff, R.O., van Verseveld, W.J., van Osnabrugge, B., Weerts, A.H., 2020. Scaling Point-Scale (Pedo) transfer Functions to Seamless Large-Domain Parameter Estimates for High-Resolution Distributed Hydrologic Modeling : An Example for the Rhine River. *Water Resources Research* , 1–28doi:10.1029/2019WR026807.
- Joshi, S., Kumar, K., Joshi, V., Pande, B., 2014. Rainfall variability and indices of extreme rainfall-analysis and perception study for two stations over Central Himalaya, India. *Natural Hazards* 72, 361–374. doi:10.1007/s11069-013-1012-4.
- Kim, D., Ha, S., 2014. Effects of Particle Size on the Shear Behavior of Coarse Grained Soils Reinforced with Geogrid. volume c. doi:10.3390/ma7020963.
- Kimani, M.W., Hoedjes, J.C., Su, Z., 2017. An assessment of satellite-derived rainfall products relative to ground observations over East Africa. *Remote Sensing* 9. doi:10.3390/rs9050430.
- Kirschbaum, D., Adler, R., Adler, D., Peters-Lidard, C., Huffman, G., 2012. Global Distribution of Extreme Precipitation and High-Impact Landslides in 2010 Relative to Previous Years. *Hydrometeorology* 3, 1536–1551. URL: <http://blogs.agu.org/landslideblog/>, doi:10.1175/JHM-D-12-02.1.

- Kirschbaum, D., Stanley, T., Zhou, Y., 2015. Spatial and temporal analysis of a global landslide catalog. *Geomorphology* 249, 4–15. URL: <http://dx.doi.org/10.1016/j.geomorph.2015.03.016>, doi:10.1016/j.geomorph.2015.03.016.
- Kirschbaum, D.B., Adler, R., Hong, Y., Lerner-Lam, A., 2009. Evaluation of a preliminary satellite-based landslide hazard algorithm using global landslide inventories. *Natural Hazards and Earth System Science* 9, 673–686. doi:10.5194/nhess-9-673-2009.
- Kirschbaum, D.B., Adler, R., Yang, A.E., Ae, H., Ae, S.H., Lerner-Lam, A., Kirschbaum, D.B., Lerner-Lam, A., Adler, R., Hong, Y., Hill, S., 2010. A global landslide catalog for hazard applications: method, results, and limitations 52, 561–575. URL: <https://link.springer.com/content/pdf/10.1007/2Fs11069-009-9401-4.pdf>, doi:10.1007/s11069-009-9401-4.
- Kirschbaum, D.B., Huffman, G.J., Adler, R.E., Braun, S., Garrett, K., Jones, E., McNally, A., Skofronick-Jackson, G., Stocker, E., Wu, H., Zaitchik, B.F., 2017. NASA'S remotely sensed precipitation: A reservoir for applications users. *Bulletin of the American Meteorological Society* 98, 1169–1184. doi:10.1175/BAMS-D-15-00296.1.
- Kuriakose, S.L., van Beek, L.P.H., van Westen, C.J., 2009. Parameterizing a physically based shallow landslide model in a data poor region. *Earth Surf. Process. Landforms* 34, 867–881. doi:10.1002/esp.
- Ma, C., van Westen, C., Jetten, V., Mavrouli, O., 2018. COMPARING AND EVALUATING TWO PHYSICALLY-BASED MODELS: OPENLISEM AND SCOOPS3D, FOR LANDSLIDE VOLUME PREDICTION. Ph.D. thesis. University of Twente, Enschede, The Netherlands.
- Ma, T., Li, C., Lu, Z., Bao, Q., 2015. Rainfall intensity–duration thresholds for the initiation of landslides in Zhejiang Province, China. *Geomorphology* 245, 193–206. URL: <http://linkinghub.elsevier.com/retrieve/pii/S0169555X15002706>, doi:10.1016/j.geomorph.2015.05.016.
- Marino, P., Peres, D.J., Cancelliere, A., Greco, R., Bogaard, T.A., 2020. Soil moisture information can improve shallow landslide forecasting using the hydrometeorological threshold approach. *Landslides* doi:10.1007/s10346-020-01420-8.
- Martelloni, G., Segoni, S., Fanti, R., Catani, F., 2012. Rainfall thresholds for the forecasting of landslide occurrence at regional scale. *Landslides* 9, 485–495. doi:10.1007/s10346-011-0308-2.
- Melillo, M., Brunetti, M.T., Peruccacci, S., Gariano, S.L., Roccati, A., Guzzetti, F., 2018. A tool for the automatic calculation of rainfall thresholds for landslide occurrence. *Environmental Modelling and Software* 105, 230–243. URL: <https://doi.org/10.1016/j.envsoft.2018.03.024>, doi:10.1016/j.envsoft.2018.03.024.
- MIDIMAR, 2012. Identification of disaster higher risk zones on floods and landslides. Technical Report March. MINISTRY OF DISASTER MANAGEMENT AND REFUGEE AFFAIRS. Kigali-RWANDA.

- MIDIMAR, 2014. National Contingency Plan for Floods and landslides. Technical Report. MINISTRY OF DISASTER MANAGEMENT AND REFUGEE AFFAIRS. Kigali-RWANDA.
- MIDIMAR, 2015. The National Risk Atlas of Rwanda. Technical Report. MINISTRY OF DISASTER MANAGEMENT AND REFUGEE AFFAIRS. Kigali-RWANDA.
- Mirus, B., Morphew, M., Smith, J., 2018a. Developing Hydro-Meteorological Thresholds for Shallow Landslide Initiation and Early Warning. *Water* 10, 1274. doi:[10.3390/w10091274](https://doi.org/10.3390/w10091274).
- Mirus, B.B., Becker, R.E., Baum, R.L., Smith, J.B., 2018b. Integrating real-time subsurface hydrologic monitoring with empirical rainfall thresholds to improve landslide early warning. *Landslides* 15, 1909–1919. doi:[10.1007/s10346-018-0995-z](https://doi.org/10.1007/s10346-018-0995-z).
- Mirus, B.B., Perkins, K.S., 2012. Practical estimates of field-saturated hydraulic conductivity of bedrock outcrops using a modified bottomless bucket method. *Water Resources Research* 48. doi:[10.1029/2012WR012053](https://doi.org/10.1029/2012WR012053).
- Moeyersons, J., 1989. A possible causal relationship between creep and sliding on Rwaza Hill, southern Rwanda. *Earth Surface Processes and Landforms* 14, 597–614. doi:[10.1002/esp.3290140615](https://doi.org/10.1002/esp.3290140615).
- Monsieurs, E., Dewitte, O., Demoulin, A., 2018a. A susceptibility-based rainfall threshold approach for landslide occurrence. *Natural Hazards and Earth System Sciences Discussions*, 1–25doi:[10.5194/nhess-2018-316](https://doi.org/10.5194/nhess-2018-316).
- Monsieurs, E., Dewitte, O., Depicker, A., Demoulin, A., 2019. Towards a Transferable Antecedent Rainfall—Susceptibility Threshold Approach for Landsliding. *Water* 2019, Vol. 11, Page 2202 11, 2202. URL: <https://www.mdpi.com/2073-4441/11/11/2202>, doi:[10.3390/W11112202](https://doi.org/10.3390/W11112202).
- Monsieurs, E., Kirschbaum, D.B., Tan, J., Maki Mateso, J.C., Jacobs, L., Plisnier, P.D., Thiery, W., Umutoni, A., Musoni, D., Bibentyo, T.M., Ganza, G.B., Mawe, G.I., Bagalwa, L., Kankurize, C., Michellier, C., Stanley, T., Kervyn, F., Kervyn, M., Demoulin, A., Dewitte, O., 2018b. Evaluating TMPA Rainfall over the Sparsely Gauged East African Rift. *Journal of Hydrometeorology* 19. doi:[10.1175/JHM-D-18-0103.1](https://doi.org/10.1175/JHM-D-18-0103.1).
- Monsieurs, E., Liesbet, J., Michellier, C., Tchangabo, B.J., Ganza, B.G., Bibentyo, M.T., Kervyn, M., Mateso, M.J.C., Nkurunziza, P., Ndayisenga, A., Buzera, K.C., Nahimana, L., Wim, T., Demoulin, A., Kervyn, M., Dewitte, O., 2018c. Landslide inventory for hazard assessment in a data-poor context : a regional-scale approach in a tropical African environment. *Landslides* DOI 10.100. doi:[10.1007/s10346-018-1008-y](https://doi.org/10.1007/s10346-018-1008-y).
- Montgomery, D.R., Dietrich, W.E., 1994. A physically based model for the topographic control on shallow landsliding. *WATER RESOURCES RESEARCH* 30, 1153–1171.
- Mostbauer, K., Kaitna, R., Prenner, D., Hrachowitz, M., 2018. The temporally varying roles of rainfall, snowmelt and soil moisture for debris flow initiation in a snow-dominated system. *Hydrology and Earth System Sciences* 22, 3493–3513. doi:[10.5194/hess-22-3493-2018](https://doi.org/10.5194/hess-22-3493-2018).

- Nahayo, L., Mupenzi, C., 2017. Early alert and community involvement : approach for disaster risk reduction in Rwanda. *Natural Hazards* 86, 505–517. doi:[10.1007/s11069-016-2702-5](https://doi.org/10.1007/s11069-016-2702-5).
- Nambajimana, J.d.D., He, X., Zhou, J., Justine, M.F., Li, J., Khurram, D., Mind'je, R., Nsabi-
mana, G., 2020. Land use change impacts on water erosion in Rwanda. *Sustainability*
(Switzerland) 12, 1–23. doi:[10.3390/SU12010050](https://doi.org/10.3390/SU12010050).
- Ngarukiyimana, J.P., Fu, Y., Yang, Y., Ogwang, A., 2017. Dominant atmospheric circulation patterns associated with abnormal rainfall events over Rwanda , East Africa. *INTERNATIONAL JOURNAL OF CLIMATOLOGY* doi:[10.1002/joc.5169](https://doi.org/10.1002/joc.5169).
- Nicholson, S.E., 2017. Climate and climatic variability of rainfall over eastern Africa. *Reviews of Geophysics* 55, 590–635. doi:[10.1002/2016RG000544](https://doi.org/10.1002/2016RG000544).
- Nieuwenhuis, R., Taylor, E., Nieuwenhuis, R., Mugunga, R., Mahirwe, B., 2019. IWRM Programme Rwanda. Technical Report April. Water for growth Rwanda. Netherlands. URL: https://waterportal.rwb.rw/sites/default/files/2019-07/CatchmentPlanManual_v6_complete.pdf.
- Nsengiyumva, J.B., Luo, G., Nahayo, L., Huang, X., Cai, P., 2018. Landslide susceptibility assessment using spatial multi-criteria evaluation model in Rwanda. *International Journal of Environmental Research and Public Health* 15. doi:[10.3390/ijerph15020243](https://doi.org/10.3390/ijerph15020243).
- Nsengiyumva, J.B., Valentino, R., 2020. Predicting landslide susceptibility and risks using GIS-based machine learning simulations, case of upper Nyabarongo catchment. *Geomatics, Natural Hazards and Risk* 11, 1250–1277. URL: <https://doi.org/10.1080/19475705.2020.1785555>, doi:[10.1080/19475705.2020.1785555](https://doi.org/10.1080/19475705.2020.1785555).
- Owe, M., De Jeu, R., Walker, J., 2001. A methodology for surface soil moisture and vegetation optical depth retrieval using the microwave polarization difference index. *IEEE Transactions on Geoscience and Remote Sensing* 39, 1643–1654. doi:[10.1109/36.942542](https://doi.org/10.1109/36.942542).
- Owe, M., de Jeu, R., Holmes, T., 2008. Multisensor historical climatology of satellite-derived global land surface moisture. *Journal of Geophysical Research: Earth Surface* 113, 1–17. doi:[10.1029/2007JF000769](https://doi.org/10.1029/2007JF000769).
- Pavez, A.R., 2021. The Potential of Satellite and Model Derived Variables for Rainfall-Induced Landslide Initiation Thresholds in Rwanda. Ph.D. thesis. Delft University of Technology. URL: <http://resolver.tudelft.nl/uuid:f0c57c4f-2597-44a6-a41a-1b6a5d75d155>.
- Peres, D.J., Cancelliere, A., 2021. Comparing methods for determining landslide early warning thresholds: potential use of non-triggering rainfall for locations with scarce landslide data availability. *Landslides* 18, 3135–3147.

- Peres, D.J., Cancelliere, A., Greco, R., Bogaard, T.A., 2017. Influence of uncertain identification of triggering rainfall on the assessment of landslide early warning thresholds. *Natural Hazards and Earth System Sciences Discussions*, 1–28 URL: <https://www.nat-hazards-earth-syst-sci-discuss.net/nhess-2017-328/>, doi:10.5194/nhess-2017-328.
- Peruccacci, S., Brunetti, M.T., Gariano, S.L., Melillo, M., Rossi, M., Guzzetti, F., 2017. Rainfall thresholds for possible landslide occurrence in Italy. *Geomorphology* 290, 39–57. URL: <http://dx.doi.org/10.1016/j.geomorph.2017.03.031>, doi:10.1016/j.geomorph.2017.03.031.
- Petley, D., 2012. Global patterns of loss of life from landslides. *Geology* 40, 927–930. URL: <http://pubs.geoscienceworld.org/geology/article/40/10/927/130722/Global-patterns-of-loss-of-life-from-landslides>, doi:10.1130/G33217.1.
- Piciullo, L., Calvello, M., Cepeda, J.M., 2018. Territorial early warning systems for rainfall-induced landslides. *Earth-Science Reviews* 179, 228–247. URL: <https://doi.org/10.1016/j.earscirev.2018.02.013>, doi:10.1016/j.earscirev.2018.02.013.
- Postance, B., Hillier, J., 2017. Comparing threshold definition techniques for rainfall-induced landslides : A national assessment using radar rainfall. *Earth Surface Processes and Landforms* 560, 553–560. doi:10.1002/esp.4202.
- Prenner, D., Hrachowitz, M., Kaitna, R., 2019. Trigger characteristics of torrential flows from high to low alpine regions in Austria. *Science of the Total Environment* 658, 958–972. URL: <https://doi.org/10.1016/j.scitotenv.2018.12.206>, doi:10.1016/j.scitotenv.2018.12.206.
- Prenner, D., Kaitna, R., Mostbauer, K., Hrachowitz, M., 2018. The Value of Using Multiple Hydrometeorological Variables to Predict Temporal Debris Flow Susceptibility in an Alpine Environment. *Water Resources Research* 54, 6822–6843. doi:10.1029/2018WR022985.
- Robbins, J.C., 2016. A probabilistic approach for assessing landslide-triggering event rainfall in Papua New Guinea, using TRMM satellite precipitation estimates. *Journal of Hydrology* 541, 296–309. URL: <http://dx.doi.org/10.1016/j.jhydrol.2016.06.052>, doi:10.1016/j.jhydrol.2016.06.052.
- Roccati, A., Faccini, F., Luino, F., Turconi, L., Guzzetti, F., 2018. Rainfall events with shallow landslides in the Entella catchment , Liguria , northern Italy. *Nat. Hazards Earth Syst. Sci.* 18, 2367–2386. doi:<https://doi.org/10.5194/nhess-18-2367-2018>.
- Rodell, M., Houser, P., Jambor, U., Gottschalck, J., Mitchell, K., Meng, C.J., Arsenault, K., Cosgrove, B., Radakovich, J., Bosilovich, M., et al., 2004. The global land data assimilation system. *Bulletin of the American Meteorological society* 85, 381–394.
- Rosi, A., Peternel, T., Jemec-Auflič, M., Komac, M., Segoni, S., Casagli, N., 2016. Rainfall thresholds for rainfall-induced landslides in Slovenia. *Landslides* 13, 1571–1577. doi:10.1007/s10346-016-0733-3.

- Rosso, R., Rulli, M.C., Vannucchi, G., 2006. A physically based model for the hydrologic control on shallow landsliding. *Water Resources Research* 42, 1–16. doi:[10.1029/2005WR004369](https://doi.org/10.1029/2005WR004369).
- Saha, S., Moorthi, S., Wu, X., Wang, J., Nadiga, S., Tripp, P., Behringer, D., Hou, Y.T., Chuang, H.y., Iredell, M., et al., 2014. The ncep climate forecast system version 2. *Journal of climate* 27, 2185–2208.
- Sekaranom, A.B., Suarma, U., Nurjani, E., 2020. Climate extremes over the maritime continent and their associations with Madden-Julian Oscillation. *IOP Conference Series: Earth and Environmental Science* 451. doi:[10.1088/1755-1315/451/1/012006](https://doi.org/10.1088/1755-1315/451/1/012006).
- Sidle, R.C., Greco, R., Bogaard, T., 2019. Overview of landslide hydrology. *Water (Switzerland)* 11, 11–13. doi:[10.3390/w11010148](https://doi.org/10.3390/w11010148).
- Talebi, A., Uijlenhoet, R., Troch, P.A., 2007. Soil moisture storage and hillslope stability. *Natural Hazards and Earth System Sciences* , 523–534.
- Tank, A., Zwiers, F., Zhang, X., 2009. Guidelines on Analysis of extremes in a changing climate. World Meteorological Organization URL: http://www.wmo.int/pages/prog/wcp/wcdmp/wcdmp_series/documents/WCDMP_72_TD_1500_en__1.pdf.
- Thomas, M.A., Collins, B.D., Mirus, B.B., 2019. Assessing the Feasibility of Satellite-Based Thresholds for Hydrologically Driven Landsliding. *Water Resources Research* 55, 9006–9023. doi:[10.1029/2019WR025577](https://doi.org/10.1029/2019WR025577).
- Thornthwaite, C., 1948. An approach toward a rational classification of climate. *American Geographical Society* 38, 55–94. URL: <https://www.jstor.org/stable/pdf/210739.pdf?refreqid=excelsior%3A568a8e19eb0e98b20b95b0a0e1dac1f4>.
- Trigo, R.M., Zêzere, J.L., Rodrigues, M.L., Trigo, I.F., 2005. The Influence of the North Atlantic Oscillation on rainfall triggering of landslides near Lisbon. *Natural Hazards* 36, 331–354. doi:[10.1007/s11069-005-1709-0](https://doi.org/10.1007/s11069-005-1709-0).
- UNISDR, 2009. Unisdr terminology on disaster risk reduction. United Nations Office for Disaster Risk Reduction, Report .
- Uwihirwe, J., 2021. Data underlying the research of Integration of observed and model derived groundwater levels in landslide threshold models in Rwanda URL: https://data.4tu.nl/articles/dataset/Data_underlying_the_research_of_Integration_of_observed_and_model_derived_groundwater_levels_in_landslide_threshold_models_in_Rwanda/15040446, doi:[10.4121/15040446.v1](https://doi.org/10.4121/15040446.v1).
- Uwihirwe, J., Hrachowitz, M., Bogaard, T.A., 2020. Landslide precipitation thresholds in Rwanda. *Landslides* doi:[10.1007/s10346-020-01457-9](https://doi.org/10.1007/s10346-020-01457-9).
- Valentino, R., Sobio, Y., Mizero, J., Nsengiyumva, F., 2021. Unstable road cut slopes and design of retaining structures in the Rwandan context. *Arabian Journal of Geosciences* .

- Van Asch, T.W.J., Buma, J., Van Beek, L.P.H., 1999. A view on some hydrological triggering systems in landslides. *Geomorphology* 30, 25–32. doi:[10.1016/S0169-555X\(99\)00042-2](https://doi.org/10.1016/S0169-555X(99)00042-2).
- Van Beek, L.P., Van Asch, T.W., 2004. Regional assessment of the effects of land-use change on landslide hazard by means of physically based modelling. *Natural Hazards* 31, 289–304. doi:[10.1023/B:NHAZ.0000020267.39691.39](https://doi.org/10.1023/B:NHAZ.0000020267.39691.39).
- Van Beek, R., 2002. Assessment of the influence of changes in land use and climate on landslide activity in a Mediterranean environment. Ph.D. thesis. Universiteit Utrecht, Netherlands.
- Walraven, B.J., 2018. An analysis of hydrological and geotechnical parameters of rotational landslides in pegmatite lithology in North Western Rwanda. URL: <http://resolver.tudelft.nl/uuid:786cf433-400e-4757-adbc-586ac988b12d>.
- Wang, S., Zhang, K., van Beek, L.P., Tian, X., Bogaard, T.A., 2019. Physically-based landslide prediction over a large region: Scaling low-resolution hydrological model results for high-resolution slope stability assessment. *Environmental Modelling & Software* 1675, 104607. URL: <https://linkinghub.elsevier.com/retrieve/pii/S1364815219308886>, doi:[10.1016/j.envsoft.2019.104607](https://doi.org/10.1016/j.envsoft.2019.104607).
- Wicki, A., Lehmann, P., Hauck, C., Seneviratne, S.I., Waldner, P., Stähli, M., 2020. Assessing the potential of soil moisture measurements for regional landslide early warning. *Landslides* 17, 1881–1896. doi:[10.1007/s10346-020-01400-y](https://doi.org/10.1007/s10346-020-01400-y).
- Zhao, B., Dai, Q., Han, D., Zhang, J., Zhuo, L., Berti, M., 2020. Application of hydrological model simulations in landslide predictions. *Landslides* 17, 877–891. doi:[10.1007/s10346-019-01296-3](https://doi.org/10.1007/s10346-019-01296-3).
- Zhao, Y., Li, Y., Zhang, L., Wang, Q., 2016. Groundwater level prediction of landslide based on classification and regression tree. *Geodesy and Geodynamics* 7, 348–355. URL: <http://dx.doi.org/10.1016/j.geog.2016.07.005>, doi:[10.1016/j.geog.2016.07.005](https://doi.org/10.1016/j.geog.2016.07.005).
- Zhuo, L., Dai, Q., Han, D., Chen, N., Zhao, B., Berti, M., 2019. Evaluation of Remotely Sensed Soil Moisture for Landslide Hazard Assessment. *IEEE Journal of Selected Topics in Applied Earth Observations and Remote Sensing* 12, 162–173. doi:[10.1109/JSTARS.2018.2883361](https://doi.org/10.1109/JSTARS.2018.2883361).

ACKNOWLEDGEMENTS

The Doctoral research is a journey where one needs to either swim or sink. I am grateful that my swimming journey has always been tough and challenging but survived thanks to the rescue from many people.

I would like to thank Prof. Nick van de Giesen and Dr. Ir. Maurits W. Ertsen for pre-selecting and offering me the opportunity to do my PhD studies in this world-renown University.

My sincere gratitude goes to my Promotors Dr. Thom A. Bogaard and Dr. Markus Hrachowitz. Thank you for introducing me to the scientific world of landslides, for your patience to listen to my less scientific ideas, endless corrections and polishing of my work. Thank you once again Dr. Thom A. Bogaard for guiding me through the field and laboratory work, and introducing me to the landslide network groups. Referring to the field, laboratory work and data collection, I would like to give my special thanks to Ir. Bas Walraven for his assistance during field equipment installation and data collection. I thank also Ir. Alessia Riveros Pavez for satellite data acquisition and cleaning.

I am very thankful to the Secretaries of Water Resources for all the support since the start to the end of this PhD journey.

My heartfelt thanks to my colleagues and friends in room 4.97 and 4.74 for the lovely and multicultural moment shared: Dr. Yang Lu, Dr. Changrang Zhou, Dr. Banerjee Indushree, Alexandra Urgilez Vinueza, Saeed Khabbazan, Anjana Ekka and Dr. Singirankabo Uwacu Alban. Without you all, this PhD journey wouldn't have been enjoyable and pleasant.

I am deeply grateful to my beloved Father Edouard Nzagirukwayo and Mother Donatrise Nyirabakiga for all the moral and physical supports. I am thankful to my brothers and sisters and hope I have made you all proud. I am grateful to Dr. Bonaventure Nizeyimana for taking me as a member of his family in the Netherlands and the endless motivation during my worry periods of the research.

Most importantly, I wish to express my heartfelt gratitude to my Husband Ir. Pierre Celestin Uwamahoro. Thank you for the motivational messages and all the supports. Thank you my sister in law Mrs. Annemarie Mukaminega for taking care of my children "Impano Divine and Iganze Drice Eloi". I wouldn't imagine my life without you my Angels. I love you unconditionally.

Judith Uwihirwe

CURRICULUM VITAE

Judith Uwihirwe

Judith Uwihirwe was born on 2nd January 1982 in Muhanga district of Rwanda. She completed her PhD in January 2023 in Water Management department, Faculty of Civil Engineering and Geosciences at Delft University of Technology, The Netherlands. She conducted her PhD research on “Landslide hazard assessment: Landslide hydro-meteorological thresholds in Rwanda”. In September 2014, she completed her inter-university Master’s in Physical Land Resources, option of Land Resources Engineering under the department of Hydrology and hydraulic Engineering, faculty of Engineering at Vrije Universiteit Brussel and Ghent University, Belgium. In 2008, she completed the undergraduate study in Soil and Water Management department, Faculty of Agricultural Engineering and Environmental Sciences at the Higher Institute of Agriculture and Animal Husbandry (ISAE-Busogo), in Musanze district, Rwanda. After her undergraduate school, from 2009, she worked as an Assistant Lecturer at the former ISAE-Busogo, the current College of Agriculture, Animal Sciences and Veterinary Medicine of the University of Rwanda. The findings of her PhD research have been presented in numerous international conferences: the European Geoscience Union EGU 2021; the Fifth World Landslide Forum WLF 5 in 2021. The findings of her PhD resulted into publications in peer review journals and conference abstracts. One of her publications "Integration of observed and model derived groundwater levels in landslide threshold models in Rwanda" won "The best paper award runner up" offered by the TU Delft Water For Impact in Water Summit for Global Development 2022.

LIST OF PUBLICATIONS

6. **Uwihirwe, J.**, Pavez R. A., Wanjala, H., Schellekens, J., Weiland, S.F, Markus Hrachowitz, M., and Bogaard, T. (2022). *The potential of satellite derived hydro-meteorological information for landslide initiation thresholds in Rwanda*. Nat. Hazards Earth Syst. Sci. <https://doi.org/10.5194/egusphere-2022-596>.
5. **Uwihirwe, J.**, Hrachowitz, M., and Bogaard, T. (2022). *Integration of observed and model derived groundwater levels in landslide threshold models in Rwanda*. Nat. Hazards Earth Syst. Sci., 22, 1723–1742, <https://doi.org/10.5194/nhess-22-1723-2022>.
4. Depicker, A., Govers, G. Jacobs, L., Campforts, B., **Uwihirwe, J.**, and Dewitte, O. (2015). *Interactions between deforestation, landscape rejuvenation, and shallow landslides in the North Tanganyika–Kivu rift region, Africa*. Earth Surf. Dynam., 9, 445–462, <https://doi.org/10.5194/esurf-9-445-2021>.
3. **Uwihirwe, J.**, Hrachowitz, M., and Bogaard, T. (2020). *Landslide precipitation thresholds in Rwanda*. Landslides 17, 2469–2481, <https://doi.org/10.1007/s10346-020-01457-9>
2. Dewitte, O., Dille, A., Depicker, A., Kubwimana, D., Maki Mateso, J.C., Bibentyo, M.T., **Uwihirwe, J.**, and Monsieurs, E. (2021). *Constraining landslide timing in a data-scarce context: from recent to very old processes in the tropical environment of the North Tanganyika-Kivu Rift region*. Landslides 18, 161–177, <https://doi.org/10.1007/s10346-020-01452-0>.
1. Karemangingo, C., Fashaho, A., and **Uwihirwe, J.** (2019). *Comparison of bioslurry to common nitrogen sources on potato (*Solanum tuberosum* L.) yield and yield components in andisols and oxisols of Northern Rwanda*. AJAR2018.13617, Vol.14(6), pp. 335-344, <https://doi.org/10.5897/AJAR2018.13617/>.

